DESY-97-056
TUIMP-TH-97/84
MSUHEP-70105

March, 1997
hep-ph/9704276

DESY-97-056
TUIMP-TH-97/84
MSUHEP-70105

Global Analysis for Probing Electroweak Symmetry Breaking Mechanism at High Energy Colliders *

Hong-Jian He [a], Yu-Ping Kuang [b], C.–P. Yuan [c]

[a] *Theory Division, Deutsches Elektronen-Synchrotron DESY D-22603 Hamburg , Germany*

[b] *CCAST (World Laboratory), P.O.Box 8730, Beijing 100080, China*
Institute of Modern Physics, Tsinghua University, Beijing 100084, China

[c] *Department of Physics and Astronomy, Michigan State University East Lansing, Michigan 48824, USA*

hep-ph/9704276 9 Apr 1997

Abstract

We review our recent global analysis for probing the electroweak symmetry breaking (EWSB) mechanism by the universal effective Lagrangian description. After summarizing and commenting upon the current bounds for the EWSB parameters, we focus on testing them at the forthcoming high energy colliders such as the CERN LHC and the future linear colliders. We develop a precise electroweak power counting method (à la Weinberg) and formulate the longitudinal-Goldstone boson equivalence as a necessary criterion for sensitively probing the EWSB sector. Armed with these, we systematically estimate and classify the contributions of *all* next-to-leading order (NLO) bosonic operators to various scattering processes at the high energy colliders. The experimental signatures at these colliders are also analyzed. Furthermore, the *complementarity* of different scattering processes via different colliders for a complete probe of all these NLO effective operators is demonstrated.

PACS number(s): 11.30.Qc, 11.15.Ex, 12.15.Ji, 14.70.–e

---

* Lectures given by C.–P. Yuan at the CCAST Workshop on " *Physics at TeV Energy Scale* ", July 15-26, 1996, Beijing, China.

Contents: Pages

1. Introduction 3

2. Effective Lagrangians for Strongly Interacting EWSB Sector 4

3. Current Bounds on the EWSB Parameters 7

4. Precise Electroweak Power Counting Method 13

4.1. Generalizing Weinberg's power counting rule to SSB gauge theories 13
4.2. Constructing the precise electroweak power counting method 15
4.2.1. Non-decoupling scenario (without Higgs boson) 15
4.2.2. Decoupling scenario (with Higgs boson) 18

5. Longitudinal-Goldstone Boson Equivalence Theorem: from mathematical formulation to its physical content for probing EWSB 22

5.1. ET and the Higgs mechanism 22
5.2. ET and its multiplicative modifications 27
5.3. ET and its additive modifications 34
5.3.1. The Longitudinal-transverse ambiguity and the precise formulation of the ET 34
5.3.2. On the kinematic singularity 37
5.4. Formulating the ET as a Criterion for probing the EWSB 42

6. Global Classification for the S-matrix Elements 45

6.1. Power Counting Hierarchy 45
6.2. Classifications for VV-fusions and $f\bar{f}'$-annihilations 48
6.3. A comparative analysis for the LHC and LCs 50

7. Global Analysis at the Event Rate Level 54

7.1. Effective-W approximation 54
7.2. At the LHC 57
7.2.1. Preliminaries 57
7.2.2. Analyzing the model-independent contributions to the event rates 59
7.2.3. Estimating the sensitivities for probing the model-dependent operators 60
7.3. At the LCs 63

(Continued) Pages

8. How to Study TeV $W_LW_L \to W_LW_L$ Interactions Experimentally 64

8.1. Signal 64
8.2. Backgrounds 65
8.3. How to distinguish signal from backgrounds 68
8.4. Various models 72
8.4.1. A TeV scalar resonance 72
8.4.2. A TeV vector resonance 74
8.4.3. No resonance 74

9. Conclusion 76

Acknowledgments 79

References 80

Table Captions 87
Figure Captions 89
Table I-VII 91-99
Figure 1-12 100-115

1. Introduction

The Standard Model (SM) has successfully passed all available experimental tests with high precisions, but still leaves its electroweak symmetry breaking (EWSB) sector undetermined. Due to Veltman's screening theorem [1], the current data, allowing the SM Higgs boson mass to range from 65.2 GeV to about $O(1)$ TeV [2], tell us little about the EWSB mechanism. The light resonance(s) originating from the EWSB sector with mass(es) well below the TeV scale can exist possibly in the SM and necessarily in its supersymmetric extensions. In such cases, these particles should be detected [3, 4, 5] at the high energy colliders such as the CERN Large Hadron Collider (LHC), a proton-proton collider, and the future electron (and photon) Linear Colliders (LC) [6], even though the current direct experimental searches so far are all negative. If the EWSB is, however, driven by strong interactions with no new resonance well below the TeV scale, then it will be a *greater challenge* to future colliders to decisively probe the EWSB mechanism. This latter case is what our present global analysis will focus on.

At the scale below new heavy resonances, the EWSB sector can be parametrized by means of the electroweak chiral Lagrangian (EWCL) in which the $SU(2)_L \otimes U(1)_Y$ gauge symmetry is nonlinearly realized. Without experimental observation of any new light resonance in the EWSB sector, this effective field theory approach provides the most economic description of the possible new physics effects and is thus *complementary* to those specific model buildings [7]. In the present analysis, taking this general EWCL approach, we shall concentrate on studying the effective bosonic operators among which the leading order operators are universal and the next-to-leading-order (NLO) operators describe the model-dependent new effects.

In performing such a global analysis, in contrast to just studying a few operators in the literature, we need to estimate the contributions of all the NLO operators to various high energy scattering processes. For this purpose, we construct a precise electroweak power counting rule for the EWCL formalism through a natural generalization of Weinberg's counting method for non-linear sigma model [8]. This simple power counting rule proves to be extremely convenient and useful for our global analysis [9, 10].

Furthermore, we analyze how the longitudinal-Goldstone boson equivalence theorem

(ET) is deeply rooted in the underlying (elementary or dynamical) Higgs mechanism and demonstrate under what conditions this *equivalence* can be manifest in the physical processes. The intrinsic connection of the longitudinal-Goldstone boson *equivalence* to probing the EWSB sector is thus revealed [11]. We theoretically formulate this *equivalence* as a *necessary criterion* for sensitively probing the EWSB sector. Armed with these, we globally analyze and classify the sensitivities of all the effective operators for probing the EWSB mechanism at the high energy colliders [11, 9, 10]. This global classification will be performed at both the S-matrix element and event-rate levels. We note that at the event-rate level the sensitivity of a collider will also depend on the detection efficiency for suppressing the backgrounds to observe the specific decay mode of the final state for each given process (cf. Ref. [4]). Some general features of the event structure in the experimental signals and backgrounds will be discussed and summarized (cf. Sec. 8).

2. Effective Lagrangians for Strongly Interacting EWSB Sector

The electroweak chiral Lagrangian (EWCL) gives the most economical description of the EWSB sector below the scale of new heavy resonance and can be constructed as follows [12, 13]:

$$\mathcal{L}_{\rm eff} = \sum_n \ell_n \frac{f_\pi{}^{r_n}}{\Lambda^{a_n}} \mathcal{O}_n(\mathbf{W}_{\mu\nu}, \mathbf{B}_{\mu\nu}, D_\mu U, U, f, \bar{f}) = \mathcal{L}_{\rm G} + \mathcal{L}_{\rm S} + \mathcal{L}_{\rm F} \tag{2.1}$$

where

$$\begin{aligned}
&D_\mu U = \partial_\mu U + ig\mathbf{W}_\mu U - ig' U \mathbf{B}_\mu \ , \\
&U = \exp[i\tau^a \pi^a / f_\pi] \ , \quad \mathbf{W}_\mu \equiv W_\mu^a \frac{\tau^a}{2} \ , \quad \mathbf{B}_\mu \equiv B_\mu \frac{\tau^3}{2} \ , \\
&\mathbf{W}_{\mu\nu} = \partial_\mu \mathbf{W}_\nu - \partial_\nu \mathbf{W}_\mu + ig[\mathbf{W}_\mu, \mathbf{W}_\nu] \ , \\
&B_{\mu\nu} = \partial_\mu B_\nu - \partial_\nu B_\mu \ ,
\end{aligned}$$

π^a is the would-be Goldstone boson (GB) field and $f(\bar{f})$ is the SM fermion with mass $m_f \leq O(m_t) \simeq O(M_W)$. $\mathcal{L}_{\rm G}$, $\mathcal{L}_{\rm S}$ and $\mathcal{L}_{\rm F}$ denote gauge boson kinetic terms, scalar boson interaction terms (containing GB self-interactions and gauge-boson-GB interactions), and fermion interaction terms, respectively. Here we concentrate on probing new physics from all possible bosonic operators so that we shall not include the next-to-leading order

fermionic operators in $\mathcal{L}_F$. For clearness, we have factorized out the dimensionful parameters f_π and Λ in the coefficients so that the dimensionless factor ℓ_n is of $O(1)$. This makes our definitions of the ℓ_n's different from the α_i's in Ref. [12] by a factor of $(f_\pi/\Lambda)^2$. We note that f_π and Λ are the two essential scales in any effective Lagrangian that describes the spontaneously broken symmetry. The former determines the symmetry breaking scale while the latter determines the scale at which new resonance(s) besides the light fields (such as the SM weak bosons, would-be Goldstone bosons and fermions) may appear. In the non-decoupling scenario, the effective cutoff scale Λ cannot be arbitrarily large: $\Lambda = \min(M_{SB}, \Lambda_0) \leq \Lambda_0$ [14], where $\Lambda_0 \equiv 4\pi f_\pi \simeq 3.1$ TeV and M_{SB} is the mass of the lightest new resonance in the EWSB sector. In (2.1), $r_n = 4 + a_n - D_{\mathcal{O}_n}$, where $D_{\mathcal{O}_n} = \dim(\mathcal{O}_n)$. The power factor Λ^{a_n} associated with each operator $\mathcal{O}_n$ can be counted by the naive dimensional analysis (NDA) [14][1]. For the bosonic part of EWCL, we have [12]:

$$
\begin{aligned}
\mathcal{L}_{\rm G} &= -\tfrac{1}{2}{\rm Tr}(\mathbf{W}_{\mu\nu}\mathbf{W}^{\mu\nu}) - \tfrac{1}{4}B_{\mu\nu}B^{\mu\nu} \quad , \\
\mathcal{L}_{\rm S} &= \mathcal{L}^{(2)} + \mathcal{L}^{(2)\prime} + \sum_{n=1}^{14}\mathcal{L}_n \quad , \\
\mathcal{L}^{(2)} &= \tfrac{f_\pi^2}{4}{\rm Tr}[(D_\mu U)^\dagger (D^\mu U)] \quad , \\
\mathcal{L}^{(2)\prime} &= \ell_0(\tfrac{f_\pi}{\Lambda})^2 \ \tfrac{f_\pi^2}{4}[{\rm Tr}(\mathcal{T}\mathcal{V}_\mu)]^2 \quad , \\
\mathcal{L}_1 &= \ell_1(\tfrac{f_\pi}{\Lambda})^2 \ \tfrac{gg'}{2}B_{\mu\nu}{\rm Tr}(\mathcal{T}\mathbf{W}^{\mu\nu}) \quad , \\
\mathcal{L}_2 &= \ell_2(\tfrac{f_\pi}{\Lambda})^2 \ \tfrac{ig'}{2}B_{\mu\nu}{\rm Tr}(\mathcal{T}[\mathcal{V}^\mu, \mathcal{V}^\nu]) \quad , \\
\mathcal{L}_3 &= \ell_3(\tfrac{f_\pi}{\Lambda})^2 \ ig{\rm Tr}(\mathbf{W}_{\mu\nu}[\mathcal{V}^\mu, \mathcal{V}^\nu]) \quad , \\
\mathcal{L}_4 &= \ell_4(\tfrac{f_\pi}{\Lambda})^2[{\rm Tr}(\mathcal{V}_\mu\mathcal{V}_\nu)]^2 \quad , \\
\mathcal{L}_5 &= \ell_5(\tfrac{f_\pi}{\Lambda})^2[{\rm Tr}(\mathcal{V}_\mu\mathcal{V}^\mu)]^2 \quad , \\
\mathcal{L}_6 &= \ell_6(\tfrac{f_\pi}{\Lambda})^2[{\rm Tr}(\mathcal{V}_\mu\mathcal{V}_\nu)]{\rm Tr}(\mathcal{T}\mathcal{V}^\mu){\rm Tr}(\mathcal{T}\mathcal{V}^\nu) \quad , \\
\mathcal{L}_7 &= \ell_7(\tfrac{f_\pi}{\Lambda})^2[{\rm Tr}(\mathcal{V}_\mu\mathcal{V}^\mu)]{\rm Tr}(\mathcal{T}\mathcal{V}_\nu){\rm Tr}(\mathcal{T}\mathcal{V}^\nu) \quad , \\
\mathcal{L}_8 &= \ell_8(\tfrac{f_\pi}{\Lambda})^2 \ \tfrac{g^2}{4}[{\rm Tr}(\mathcal{T}\mathbf{W}_{\mu\nu})]^2 \quad ,
\end{aligned}
$$

[1] In this paper, the NDA is only used to count the Λ-powers (Λ^{a_n}) associated with the operators $\mathcal{O}_n$'s in the chiral Lagrangian (2.1). This is irrelevant to the derivation of the power counting rule for D_E in the following (3.2.4).

$$
\begin{aligned}
\mathcal{L}_9 &= \ell_9(\tfrac{f_\pi}{\Lambda})^2\ \tfrac{ig}{2}\mathrm{Tr}(\mathcal{T}\mathbf{W}_{\mu\nu})\mathrm{Tr}(\mathcal{T}[\mathcal{V}^\mu,\mathcal{V}^\nu])\ \ , \\
\mathcal{L}_{10} &= \ell_{10}(\tfrac{f_\pi}{\Lambda})^2\tfrac{1}{2}[\mathrm{Tr}(\mathcal{T}\mathcal{V}^\mu)\mathrm{Tr}(\mathcal{T}\mathcal{V}^\nu)]^2\ \ , \\
\mathcal{L}_{11} &= \ell_{11}(\tfrac{f_\pi}{\Lambda})^2\ g\epsilon^{\mu\nu\rho\lambda}\mathrm{Tr}(\mathcal{T}\mathcal{V}_\mu)\mathrm{Tr}(\mathcal{V}_\nu\mathbf{W}_{\rho\lambda})\ \ , \\
\mathcal{L}_{12} &= \ell_{12}(\tfrac{f_\pi}{\Lambda})^2\ 2g\mathrm{Tr}(\mathcal{T}\mathcal{V}_\mu)\mathrm{Tr}(\mathcal{V}_\nu\mathbf{W}^{\mu\nu})\ \ , \\
\mathcal{L}_{13} &= \ell_{13}(\tfrac{f_\pi}{\Lambda})^2\ \tfrac{gg'}{4}\epsilon^{\mu\nu\rho\lambda}B_{\mu\nu}\mathrm{Tr}(\mathcal{T}\mathbf{W}_{\rho\lambda})\ \ , \\
\mathcal{L}_{14} &= \ell_{14}(\tfrac{f_\pi}{\Lambda})^2\ \tfrac{g^2}{8}\epsilon^{\mu\nu\rho\lambda}\mathrm{Tr}(\mathcal{T}\mathbf{W}_{\mu\nu})\mathrm{Tr}(\mathcal{T}\mathbf{W}_{\rho\lambda})\ \ ,
\end{aligned}
\tag{2.2}
$$

where $\mathcal{V}_\mu \equiv (D_\mu U)U^\dagger$, and $\mathcal{T} \equiv U\tau_3 U^\dagger$. There is certain arbitrariness in choosing the complete set of operators which can be related to another set after applying the equation of motion, but this will not affect the physical results [15]. Eq. (2.2) contains fifteen bosonic NLO effective operators among which there are twelve CP-conserving operators ($\mathcal{L}^{(2)\prime}, \mathcal{L}_{1\sim 11}$) and three CP-violating operators ($\mathcal{L}_{12\sim 14}$). Furthermore, the operators $\mathcal{L}_{6,7,10}$ violate custodial $SU(2)_C$ symmetry (even after g' being turned off) in contrary to $\mathcal{L}_{4,5}$ which contain $SU(2)_C$-invariant pure GB interactions. The coefficients (ℓ_n's) of all the above operators are model-dependent and carry information about possible new physics beyond the SM. The dimension-2 custodial $SU(2)_C$-violating operator $\mathcal{L}^{(2)\prime}$ has a coefficient at most of $O(f_\pi^2/\Lambda^2)$ since it is proportional to $\delta\rho \approx O(m_t^2/(16\pi^2 f_\pi^2)) \approx O(f_\pi^2/\Lambda^2)$ for the top Yukawa coupling being of $O(1)$.

In the non-decoupling scenario [14, 16], the coefficients for all NLO dimension-4 operators are suppressed by a factor $(f_\pi/\Lambda)^2 \approx 1/(16\pi^2)$ relative to that of the universal dimension-2 operator $\mathcal{L}^{(2)}$, because of the derivative expansion in terms of $(D_\mu/\Lambda)^2$. If we ignore the small CP-violating effects from the Cabibbo-Kobayashi-Maskawa mixings in the lowest order fermionic Lagrangian $\mathcal{L}_{\rm F}$, all the one-loop level new divergences generated from $\mathcal{L}_{\rm G} + \mathcal{L}_{\rm F} + \mathcal{L}^{(2)}$ are thus CP-invariant. Therefore, the CP-violating operators $\mathcal{L}_{12\sim 14}$ are actually *decoupled* at this level, and their coefficients can have values significantly larger or smaller than that from the naive dimensional analysis [14]. Since the true mechanism for CP-violation remains un-revealed, we shall consider in this paper the coefficients $\ell_{12\sim 14}$ to be around of $O(1)$.

3. Current Bounds on the EWSB Parameters

Before proceeding further, we analyze the current constraints on these EWCL parameters in this section which is useful for our study on future high energy colliders. First, the coefficients $\ell_{0,1,8}$ are related to the low energy S, T, U parameters [17] through the oblique corrections:

$$\begin{aligned}
\ell_0 &= \left(\frac{\Lambda}{\Lambda_0}\right)^2 8\pi^2 \alpha T = \left(\frac{\Lambda}{\Lambda_0}\right)^2 8\pi^2 \delta\rho = \left(\frac{\Lambda}{\Lambda_0}\right)^2 \frac{32\pi^3\alpha}{c_{\rm w}^2 s_{\rm w}^2 M_Z^2}[\Pi_{11}^{\rm new}(0) - \Pi_{33}^{\rm new}(0)] \ , \\
\ell_1 &= -\left(\frac{\Lambda}{\Lambda_0}\right)^2 \pi S = \left(\frac{\Lambda}{\Lambda_0}\right)^2 8\pi^2 \Pi_{3Y}^{\rm new\ \prime}(0) \ , \\
\ell_8 &= -\left(\frac{\Lambda}{\Lambda_0}\right)^2 \pi U = \left(\frac{\Lambda}{\Lambda_0}\right)^2 16\pi^2 [\Pi_{33}^{\rm new\ \prime}(0) - \Pi_{11}^{\rm new\ \prime}(0)] \ ,
\end{aligned} \tag{3.1}$$

where $\Lambda_0 \equiv 4\pi f_\pi \simeq 3.1$ TeV, and $s_{\rm w} = \sin\theta_{\rm W}$, $c_{\rm w} = \cos\theta_{\rm W}$, $\alpha = \frac{e^2}{4\pi}$ are measured at Z-pole in the $\overline{\rm MS}$ scheme. The factor $\left(\frac{\Lambda}{\Lambda_0}\right)^2$ in (3.1) reduces to one for the case $\Lambda = \Lambda_0$. The newest updated global fit to the low energy data gives [18]:

$$\begin{aligned}
S &= -0.26 \pm 0.16 \ , \\
T &= \ \ 0.13 \pm 0.20 \ , \\
U &= \ \ 0.07 \pm 0.42 \ ,
\end{aligned} \tag{3.2}$$

for $s_{\rm w}^2 = 0.2314 \pm 0.0002$ and $m_t = 173 \pm 6$ GeV. For the present analysis, we have specified the reference value of the SM Higgs mass as $m_H = 1$ TeV. Results for other values of m_H can be found in Ref. [18]. The inclusion or exclusion of $\delta R_b^{\rm new}$ in the global fit affects (3.2) very little [18]. Since the experimental errors in (3.4) are still quite large, the parameters T and U (ℓ_0 and ℓ_8) can be either positive or negative within 1σ error. The parameter S (ℓ_1) is only about -1.63σ below the SM value. This is even smaller than the present R_b anomaly which is $+1.86\sigma$ above the SM value [18]. (Another recent global fit [19] gives $+1.75\sigma$ for the R_b anomaly.)

From (3.1) and (3.2), for $\Lambda \simeq 3.1$ TeV, we get the following 2σ (95.5% C.L.) constraints on $\ell_{0,1,8}$ at the scale $\mu = M_Z$:

$$\begin{aligned}
-0.17 \ &\leq \ \ell_0 \ \leq \ 0.32 \ , \\
-0.19 \ &\leq \ \ell_1 \ \leq \ 1.82 \ , \\
-2.86 \ &\leq \ \ell_8 \ \leq \ 2.42 \ ,
\end{aligned} \tag{3.3}$$

which allow $\ell_{0,1,8}$ to be either positive or negative around of $O(1)$. We can further deduce the bounds at the TeV scale (*e.g.*, $\mu = 1$ TeV) by incorporating the running effects from the renormalization log-terms. By the one-loop renormalization calculation [20], we find, for instance, the coefficients $\ell_{0,1,8}$ are running as:

$$\begin{cases} \ell_0(\mu) = \ell_0^b - \left(\dfrac{\Lambda}{\Lambda_0}\right)^2 \dfrac{3}{4}(g')^2 \left(\dfrac{1}{\hat{\epsilon}} + c_0\right) \ , \\ \ell_1(\mu) = \ell_1^b - \left(\dfrac{\Lambda}{\Lambda_0}\right)^2 \dfrac{1}{6} \left(\dfrac{1}{\hat{\epsilon}} + c_1\right) \ , \\ \ell_8(\mu) = \ell_8^b - \left(\dfrac{\Lambda}{\Lambda_0}\right)^2 c_8 \ ; \end{cases} \quad \Longrightarrow \quad \begin{cases} \ell_0(\mu') = \ell_0(\mu) + \left(\dfrac{\Lambda}{\Lambda_0}\right)^2 \dfrac{3}{4}(g')^2 \ln \dfrac{\mu'}{\mu} \ , \\ \ell_1(\mu') = \ell_1(\mu) + \left(\dfrac{\Lambda}{\Lambda_0}\right)^2 \dfrac{1}{6} \ln \dfrac{\mu'}{\mu} \ , \\ \ell_8(\mu') = \ell_8(\mu) \ ; \end{cases} \tag{3.4}$$

where $\dfrac{1}{\hat{\epsilon}} \equiv \dfrac{1}{4-n} - \ln \mu$ and the superscript " ^{b} " denotes the bare quantity. In (3.4), the c_i 's are finite constants which depend on the subtraction scheme and are irrelevant to the running of $\ell_n(\mu)$'s. From (3.3) and (3.4) we can deduce the 2σ bounds at other scales, *e.g.*, at $\mu = 1$ TeV for $\Lambda = \Lambda_0 = 3.1$ TeV,

$$\begin{array}{rcl} -0.06 \ \leq \ \ell_0(1 \text{ TeV}) \ \leq \ 0.55 \ , \\ 0.21 \ \leq \ \ell_1(1 \text{ TeV}) \ \leq \ 2.22 \ , \\ -2.86 \ \leq \ \ell_8(1 \text{ TeV}) \ \leq \ 2.42 \ , \end{array} \tag{3.5}$$

where the ranges for $\ell_{0,1}$ are slightly moved toward positive direction due to the running effects. (3.5) shows that $\ell_{0,1,8}$ are allowed to be around of $O(1)$ except that the parameter space for ℓ_0 is about a factor of $4 \sim 5$ smaller than the others. All those NLO coefficients ℓ_n's in (2.2) varies for different underlying theories and thus must be *independently tested* since the real underlying theory is unknown and these operators are inequivalent by the equation of motion. For example, the $SU(2)_C$-violating operator $\mathcal{L}^{(2)\prime}$ (containing two $\mathcal{T} = U\tau_3 U^\dagger$'s) is constrained to be slightly below $O(1)$ within 2σ bound [cf. (3.3)(3.5)], while the updated data still allow the coefficients of other $SU(2)_C$-violating operators such as $\mathcal{L}_1$ (containing one $\mathcal{T}$ operator) and $\mathcal{L}_8$ (containing two $\mathcal{T}$ operators) to be around of $O(1)$ [cf. (3.3) and (3.5)].

Besides the bounds from the oblique corrections, the tests on triple gauge boson couplings (TGCs) at LEP and Tevatron [21] impose further constraints on more operators at

the tree level. In the conventional notation [21, 22], the TGCs are parameterized as

$$\begin{aligned}\frac{\mathcal{L}_{WWV}}{g_{WWV}} = \; & ig_1^V[W^+_{\mu\nu}W^{-\mu}V^\nu - W^-_{\mu\nu}W^+_\mu V^\nu] + i\kappa_V W^+_\mu W^-_\nu V^{\mu\nu} + \tfrac{i\lambda_V}{\Lambda^2}W^+_{\mu\nu}W^{-\nu}_{\ \ \rho}V^{\rho\mu} \\ & -g_4^V W^+_\mu W^-_\nu[\partial^\mu V^\nu + \partial^\nu V^\mu] + g_5^V\epsilon^{\mu\nu\rho\lambda}[W^+_\mu\partial_\rho W^-_\nu - W^-_\nu\partial_\rho W^+_\mu]V_\lambda \\ & +i\tilde{\kappa}_V W^+_\mu W^-_\nu\tilde{V}^{\mu\nu} + i\tfrac{\tilde{\lambda}_V}{\Lambda^2}W^+_{\mu\nu}W^{-\nu}_{\ \ \rho}\tilde{V}^{\rho\mu} \quad , \\ & V = Z, \text{ or } \gamma \ , \quad W^\pm_{\mu\nu} = \partial_\mu W^\pm_\nu - \partial_\nu W^\pm_\mu \ , \quad \tilde{V}_{\mu\nu} = \tfrac{1}{2}\epsilon_{\mu\nu\rho\lambda}V^{\rho\lambda} \ .\end{aligned} \tag{3.6}$$

We summarize the tree level contributions from all 15 NLO order operators listed in (2.2) to the TGCs defined in (3.6) as follows:

$$\begin{aligned} & g_1^Z - 1 \equiv \Delta g_1^Z = \frac{f_\pi^2}{\Lambda^2}\left[\frac{1}{c^2-s^2}\ell_0 + \frac{e^2}{c^2(c^2-s^2)}\ell_1 + \frac{e^2}{s^2c^2}\ell_3\right] \quad , \quad g_1^\gamma - 1 = 0 \quad , \\ & g_4^Z = -\frac{f_\pi^2}{\Lambda^2}\frac{e^2}{\mathrm{s_w^2 c_w^2}}\ell_{12} \quad , \quad g_4^\gamma = 0 \quad , \\ & g_5^Z = \frac{f_\pi^2}{\Lambda^2}\frac{e^2}{s^2c^2}\ell_{11} \quad , \quad g_5^\gamma = 0 \quad , \\ & \kappa_Z - 1 \equiv \Delta\kappa_Z = \frac{f_\pi^2}{\Lambda^2}\left[\frac{1}{c^2-s^2}\ell_0 + \frac{2e^2}{c^2-s^2}\ell_1 - \frac{e^2}{c^2}\ell_2 + \frac{e^2}{s^2}(\ell_3 - \ell_8 + \ell_9)\right] \quad , \\ & \kappa_\gamma - 1 \equiv \Delta\kappa_\gamma = \frac{f_\pi^2}{\Lambda^2}\frac{e^2}{s^2}[-\ell_1 + \ell_2 + \ell_3 - \ell_8 + \ell_9] \quad , \\ & \tilde{\kappa}_Z = \frac{f_\pi^2}{\Lambda^2}\left[\frac{e^2}{\mathrm{c_w^2}}\ell_{13} - \frac{e^2}{\mathrm{s_w^2}}\ell_{14}\right] \quad , \quad \tilde{\kappa}_\gamma = -\frac{f_\pi^2}{\Lambda^2}\frac{e^2}{\mathrm{s_w^2}}[\ell_{13} + \ell_{14}] \quad , \end{aligned} \tag{3.7}$$

which coincide with Ref. [23] after taking into account the difference in defining the coefficients. (3.7) shows that, at the first non-trivial order [i.e., $O\left(\frac{f_\pi^2}{\Lambda^2}\right)$], only operators $\mathcal{L}^{(2)\prime}$ and $\mathcal{L}_{1,2,3,8,9,11\sim14}$ can contribute to anomalous triple gauge couplings while $\mathcal{L}^{(4)}_{4,5,6,7,10}$ do not. Among $\mathcal{L}^{(2)\prime}$ and $\mathcal{L}_{1,2,3,8,9,11\sim14}$, $\mathcal{L}^{(2)\prime}$ and $\mathcal{L}_{1,8}$ can be constrained by the oblique corrections [cf. (2.5) and (2.7)] so that we are left with seven operators $\mathcal{L}^{(4)}_{2,3,9,11,12,13,14}$. There are just seven independent relations in (3.7) by which the coefficients $\ell_{2,3,9,11,12,13,14}$ can be independently determined in principle if the seven TGC parameters $g^Z_{1,4,5}$ and

$\kappa^{Z,\gamma}$, $\tilde{\kappa}^{Z,\gamma}$ can all be measured. From (3.7), we derive

$$\begin{aligned}
\ell_2 &= \frac{1}{e^2}\frac{s_{\rm w}^2 c_{\rm w}^2}{c_{\rm w}^2 - s_{\rm w}^2}\ell_0 + \frac{c_{\rm w}^2}{c_{\rm w}^2 - s_{\rm w}^2}\ell_1 + \frac{\Lambda^2}{f_\pi^2}\frac{s_{\rm w}^2 c_{\rm w}^2}{e^2}(\Delta\kappa_\gamma - \Delta\kappa_Z) \quad , \\
\ell_3 &= -\frac{1}{e^2}\frac{s_{\rm w}^2 c_{\rm w}^2}{c_{\rm w}^2 - s_{\rm w}^2}\ell_0 - \frac{c_{\rm w}^2}{c_{\rm w}^2 - s_{\rm w}^2}\ell_1 + \frac{\Lambda^2}{f_\pi^2}\frac{s_{\rm w}^2 c_{\rm w}^2}{e^2}\Delta g_1^Z \quad , \\
\ell_9 &= \ell_8 + \frac{\Lambda^2}{f_\pi^2}\frac{s_{\rm w}^2 c_{\rm w}^2}{e^2}\left(\Delta\kappa_Z + \frac{s_{\rm w}^2}{c_{\rm w}^2}\Delta\kappa_\gamma - \Delta g_1^Z\right) \quad , \\
\ell_{11} &= \frac{\Lambda^2}{f_\pi^2}\frac{s_{\rm w}^2 c_{\rm w}^2}{e^2} g_5^Z \quad , \\
\ell_{12} &= -\frac{\Lambda^2}{f_\pi^2}\frac{s_{\rm w}^2 c_{\rm w}^2}{e^2} g_4^Z \quad , \\
\ell_{13} &= \frac{\Lambda^2}{f_\pi^2}\frac{s_{\rm w}^2 c_{\rm w}^2}{e^2}(\tilde{\kappa}_Z - \tilde{\kappa}_\gamma) \quad , \\
\ell_{14} &= -\frac{\Lambda^2}{f_\pi^2}\frac{s_{\rm w}^2 c_{\rm w}^2}{e^2}\left(\tilde{\kappa}_Z + \frac{s_{\rm w}^2}{c_{\rm w}^2}\tilde{\kappa}_\gamma\right) \quad .
\end{aligned} \tag{3.8}$$

Inputting the experimentally measured S, T, U and $g_{1,4,5}^{Z,\gamma}$, $\kappa_{Z,\gamma}$ and $\tilde{\kappa}_{Z,\gamma}$, we can derive constraints on all ℓ_n 's from (3.1) and (3.8). For example, a recent global fit at LEP [21] gives the following 1σ (i.e. 68.27% confidence level) bounds, for allowing only one TGC to be nonzero each time:

$$\begin{aligned}
-0.064 \;\le\; \Delta g_1^Z \;\le\; -0.002 \;\;,\quad -0.070 \;\le\; \lambda_\gamma \;\le\; -0.002 \;\;,\quad 0.004 \;\le\; \lambda_Z \;\le\; 0.094 \;\;, \\
-0.046 \;\le\; \Delta\kappa_Z \;\le\; 0.042 \;\;,\quad 0 \;\le\; \Delta\kappa_\gamma \;\le\; 0.112 \;\;.
\end{aligned} \tag{3.9}$$

From the above result we can estimate the constraints on $\ell_{2,3,9}$ as

$$\begin{aligned}
-12.1\left(\tfrac{\Lambda}{\Lambda_0}\right)^2 \;\le\; \ell_2 \;\le\; 32.3\left(\tfrac{\Lambda}{\Lambda_0}\right)^2 \quad , \\
-18.5\left(\tfrac{\Lambda}{\Lambda_0}\right)^2 \;\le\; \ell_3 \;\le\; 0.61\left(\tfrac{\Lambda}{\Lambda_0}\right)^2 \quad , \\
-13.3\left(\tfrac{\Lambda}{\Lambda_0}\right)^2 \;\le\; \ell_9 \;\le\; 18.5\left(\tfrac{\Lambda}{\Lambda_0}\right)^2 \quad ,
\end{aligned} \tag{3.10}$$

where $\Lambda \le \Lambda_0 \equiv 4\pi f_\pi \simeq 3.1$ TeV.

At the FermiLab Tevatron, the TGCs can be directly measured at the tree level instead of at the loop level. For instance, the CDF group gives, at the 95% confidence level (C.L.) [21],

$$\begin{aligned}
-1.1 \;<\; \Delta\kappa_V \;<\; 1.3 \;\;,\quad &(\text{ for } \lambda_V = \Delta g_1^V = 0\ ) \;, \\
-0.8 \;<\; \lambda_V \;<\; 0.8 \;\;,\quad &(\text{ for } \Delta\kappa_V = \Delta g_1^V = 0\ ) \;, \\
-1.2 \;<\; \Delta g_1^Z \;<\; 1.2 \;\;,\quad &(\text{ for } \lambda_V = \Delta\kappa_V = 0\ ) \;,
\end{aligned} \tag{3.11}$$

where $\Delta\kappa_\gamma = \Delta\kappa_Z$ and $\lambda_\gamma = \lambda_Z$ are assumed. Thus we can estimate the 95% C.L. constraints on $\ell_{3,9}$ as

$$-346\left(\frac{\Lambda}{\Lambda_0}\right)^2 < \ell_3 < 346\left(\frac{\Lambda}{\Lambda_0}\right)^2 \ , \qquad -412\left(\frac{\Lambda}{\Lambda_0}\right)^2 < \ell_9 < 488\left(\frac{\Lambda}{\Lambda_0}\right)^2 \ , \tag{3.12}$$

which gives, for $\Lambda = 2$ TeV ,

$$-145 < \ell_3 < 145 \ , \quad -173 < \ell_9 < 204 \ , \quad (\ \Lambda = 2 \text{ TeV}\ ) \ . \tag{3.12a}$$

As shown above, the indirect 1σ bounds from LEP/SLC allow $\ell_{2,3,9}$ to be around of $O(10)$, and the direct 95% C.L. bounds from Tevatron on $\ell_{3,9}$ are also too weak to be useful in discriminating different dynamical models whose effects to these coefficients ℓ_n 's are theoretically expected to be of $O(1)$ [14].

Since the operators $\mathcal{L}^{(4)}_{4,5,6,7,10}$ contain only quartic vertices, they cannot be constrained at tree level by any low energy data. The current experiments can only constrain these operators at one-loop level [i.e., of $O(1/\Lambda^4)$]. By calculating the one-loop logarithmic contributions (with all the constant terms ignored) to the low energy data from these operators, one can roughly estimate the indirect experimental bounds on their coefficients [24, 25]. Since the ignored constant terms are of the same order of magnitude as the logarithmic contributions, we should keep in mind that some uncertainties (like a factor of 2 to 3 or so) may naturally exist in these estimated bounds. It was found in Ref. [24] that, at the 90% C.L., the LEP data constraints (allowing only one non-zero coefficient at a time) are

$$-11 < \ell_4 < 11 \ , \quad -28 < \ell_5 < 26 \ , \tag{3.13}$$

for the cut-off scale $\Lambda = 2$ TeV. In another recent study [25], for $\Lambda = 2$ TeV and $m_t = 170$ GeV, the following LEP constraints are derived at the 90% C.L.:

$$\begin{array}{c} -3.97 \ \le \ \ell_4 \ \le \ 19.83 \ , \quad -9.91 \ \le \ \ell_5 \ \le \ 50.23 \ , \\ -0.66 \ \le \ \ell_6 \ \le \ 3.50 \ , \quad -5.09 \ \le \ \ell_7 \ \le \ 25.78 \ , \quad -0.67 \ \le \ \ell_{10} \ \le \ 3.44 \ . \end{array} \tag{3.14}$$

The above results show that the low energy bounds on the $SU(2)_C$-violating operators $\mathcal{L}_{6,10}$ are close to their theoretical expectation for $\ell_n \sim O(1)$, which are stronger than that for $\mathcal{L}_7$ and the $SU(2)_C$-conserving operators $\mathcal{L}_{4,5}$ (when turning off the $U(1)_Y$ gauge

coupling). Thus, $\mathcal{L}_{6,10}$ are more sensitive to the low energy data. But these numerical values should not be taken too seriously (except as a useful guideline) since all non-logarithmic contributions are ignored in the above estimates and the correlations among different operators are not considered for simplicity. We also note that the sensitivities of the $SU(2)_C$-violating operators to the low energy data do *not* have a naive power-like dependence on the number of $\mathcal{T}$-operators. (3.14) shows that the operators $\mathcal{L}_{6,10}$ (containing two and four $\mathcal{T}$-operators, respectively) have quite similar sensitivities to the low energy data and their bounds are much stronger than that for $\mathcal{L}_7$ (containing two $\mathcal{T}$'s). When further looking at the LEP 68.27% C.L. bounds (3.10) for the triple gauge boson couplings (TGCs) from the $SU(2)_C$-violating operators $\mathcal{L}_{2,9}$, we find that they are similar and are both much weaker than the 90% C.L. bounds for quartic couplings from $\mathcal{L}_{6,10}$ in (3.14) despite $\mathcal{L}_{2,9;6,10}$ containing one, two, two and four $\mathcal{T}$-operators, respectively. Intuitively, it would be natural to expect that the $SU(2)_C$-violating operators may get stronger bounds than the $SU(2)_C$-conserving ones [as implied in (3.14) for the quartic couplings of $\mathcal{L}_{6,10}$] when we consider the $SU(2)_C$ as a good approximate symmetry. But the real situation is more involved. From the LEP bounds (3.10) and the Tevatron bounds (3.12,12a), we see that, for TGCs, the $SU(2)_C$-violating operators $\mathcal{L}_{2,9}$ have weaker bounds than that of the $SU(2)_C$-conserving operator $\mathcal{L}_3$. Ref. [24] also estimated the 90% C.L. LEP bounds for $\mathcal{L}_{2,3}$ as $-47 < \ell_2 < 39$ and $-8 < \ell_3 < 11$ which impose stronger constraint on ℓ_3 . [The relations $L_{9R} = -2\ell_2$, $L_{9L} = -2\ell_3$, $L_5 = \ell_4$, $L_4 = \ell_5$ have been used to translate the eq. (39) of Ref. [24] into our notations.]

In summary, the results in (3.10), (3.12,12a), (3.13) and (3.14) indicate that the current bounds on $\ell_{2,3,9}$ and $\ell_{4,5,7}$ are still too weak. Concerning the $SU(2)_C$-violating operators, the bound on ℓ_0 (T) is most stringent while that on $\ell_{1,8,6,10}$ are all around $O(1)$ (or larger) as shown in (3.5) and (3.14). However, the updated constraints on other $SU(2)_C$-violating operators $\mathcal{L}_{2,9,7}$ can be of $O(10)$ or larger, implying that the current low energy tests do not well probe the $SU(2)_C$-violation effects from these operators. Although LEPII and the upgraded Tevatron are expected to improve the current bounds somewhat, to further improve the precision on ℓ_n 's and to fully probe the EWSB sector require finding the most sensitive high energy scattering processes to *independently test all* those coefficients in (2.2) at the LHC and the future linear colliders (LC).

4. The Precise Electroweak Power Counting Method

In this section, we develop the electroweak power counting method to precisely and separately count the power dependences on the energy E and all relevant mass scales. We have included both non-decoupling scenario (without Higgs boson) and the decoupling scenario (with Higgs boson). This method can correctly estimate any high energy scattering amplitude and is proven to be extremely convenient for our global analysis on classifying the complete set of NLO operators (instead of just a few of them). Its phenomenological applications will be given in Sec. 6 and 7.

4.1. Generalizing Weinberg's power counting rule to SSB gauge theories

Weinberg's power counting method was derived for only counting the energy dependence in the un-gauged nonlinear σ-model as a description of low energy QCD interaction [8]. But some of its essential features are very general: **(i).** The total dimension D_T of an S-matrix element T is determined by the number of external lines and the space-time dimension; **(ii).** Assume that all mass poles in the internal propagators of T are much smaller than the typical energy scale E of T, then the total dimension D_m of the E-independent coupling constants included in T can be directly counted according to the type of vertices contained. Hence, the total E-power D_E for T is given by $D_E = D_T - D_m$.

Here, we shall make a natural generalization of Weinberg's power counting method for the EWCL in which, except the light SM gauge bosons, fermions and would-be GB's, all possible heavy fields have been integrated out. It is clear that in this case the above conditions **(i)** and **(ii)** are satisfied. The total dimension of an L-loop S-matrix element T is

$$D_T = 4 - e \quad , \tag{4.1}$$

where $e = e_B + e_F$, and e_B (e_F) is the number of external bosonic (fermionic) lines. Here the dimensions of the external spinor wave functions are already included in D_T. For external fermionic lines, we only count the SM fermions with masses $m_f \leq m_t \sim O(M_W) \ll E$. So the spinor wave function of each external fermion will contribute an

energy factor $E^{1/2}$ for $E \gg m_f$, where the spinor wave functions are normalized as $\bar{u}(p,s)u(p,s') = 2m_f\delta_{ss'}$, etc.

Let us label the different types of vertices by an index n. If the vertex of type n contains b_n bosonic lines, f_n fermionic lines and d_n derivatives, then the dimension of the E-independent effective coupling constant in T is

$$D_m = \sum_n \mathcal{V}_n \left(4 - d_n - b_n - \frac{3}{2}f_n\right) \quad , \tag{4.2}$$

where $\mathcal{V}_n$ is the number of vertices of type n. Let i_B and i_F be the numbers of internal bosonic and fermionic lines, respectively. (i_B also includes possible internal ghost lines.) Define $i = i_B + i_F$, we have, in addition, the following general relations

$$\sum_n b_n\mathcal{V}_n = 2i_B + e_B \quad , \qquad \sum_n f_n\mathcal{V}_n = 2i_F + e_F \quad , \qquad L = 1 + i - \sum_n \mathcal{V}_n \quad . \tag{4.3}$$

These can further simplify the terms in (4.2).

Note that external vector-boson lines may cause extra contributions to the power of E in D_E due to the E-dependence of their polarization vectors since each longitudinal polarization vector ϵ_L^μ is of $O(E/M_W)$ for $E \gg M_W$. Thus, if we simply count all external V_L-lines directly, the relation between D_E, D_T and D_m will become $D_E = D_T - D_m + e_L - e_v$, where e_L and e_v denote the numbers of external V_L and v^a lines, respectively. [As shown in (5.17), each external v^a-line is a gauge-line V_μ^a suppressed by the factor $v^\mu = O(M_W/E)$.] However, when this relation is applied to the V_L-amplitudes with D_m given in (4.2), it does not lead to the correct results. To see this, let us take the $V_LV_L \to V_LV_L$ scattering amplitude as an example, in which $e_L = 4$ and $e_v = e_F = 0$. To lowest order of the EWCL, the leading powers of E in the amplitudes $T[V_L^{a_1}, \cdots, V_L^{a_4}]$, $T[\pi^{a_1}, \cdots, \pi^{a_4}]$ and the B-term [cf. (5.17)] are E^4, E^2 and E^0, respectively. This is not consistent with the prediction of the equivalence theorem (ET) [cf. eq.(5.17)]. The reason for this inconsistency is that this naive power counting for the V_L-amplitude only gives the leading E-power for individual Feynman diagrams. It does not reflect the fact that gauge invariance causes the cancellations of the E^4-terms between different diagrams, and leads to the final E^2-dependence of the whole V_L-amplitude. Thus directly counting the external V_L-lines in the V_L-amplitudes for D_E does not give the correct answer. This

problem can be elegantly solved by implementing the ET identity (5.17). We see that the power counting of the GB-amplitude plus the B-term does give the correct E-dependence because, unlike in the V_L-amplitude, there is generally no large E-power cancellations in the GB-amplitudes and the B-term. Therefore based upon the ET identity (5.17), the correct counting of the powers of E for the V_L-amplitude can be given by counting the corresponding GB-amplitude plus the B-term. Thus, in the following generalized power counting rule, we do not directly count the the external V_L-lines in a given diagram. Instead, they will be counted through counting the RHS of the ET identity (5.17). We shall therefore drop the e_L term in the above relation between D_E, D_T and D_m, and *make the convention that the number of external vector-boson lines e_V counts only the number of external V_T-lines and photon lines.* Then from (4.1), (4.2) and (4.3), the feasible formula for the leading energy power in T is

$$D_E \ = D_T - D_m - e_v \ = 2L + 2 + \sum_n \mathcal{V}_n \left(d_n + \frac{1}{2} f_n - 2 \right) - e_v \ . \tag{4.4}$$

This is just the Weinberg's counting rule [8] in its generalized form with the gauge boson, ghost and fermion fields and possible v_μ-factors included. (4.4) is clearly valid for any gauge theory satisfying the above conditions **(i)** and **(ii)**.

4.2. Constructing the precise electroweak power counting method

4.2.1. Non-decoupling scenario (without Higgs boson)

We want to *separately* count the power dependences of the amplitudes on the energy E, the cutoff scale Λ of the EWCL and the Fermi scale (vacuum expectation value) $f_\pi = 246\,\mathrm{GeV}$ ($\sim M_W, m_t$).[2] This is *crucial* for correctly estimating the order of magnitude of an amplitude at any given order of perturbative calculation. For instance, an amplitude of order $\frac{E^2}{f_\pi^2}$ differs by two orders of magnitude from an amplitude of order $\frac{E^2}{\Lambda^2}$ in spite that they have the same E-dependence. Also, the amplitudes $\frac{E^2}{f_\pi^2}$ and $\frac{E^2}{f_\pi^2}\frac{E^2}{\Lambda^2}$ have the

[2] This is essentially different from the previous counting result in the literature for the heavy Higgs SM [26] where only the *sum* of the powers of E and m_H has been counted.

same sum for the E and Λ powers, but are clearly of different orders in magnitude. E.g., in the typical case $E = 1$ TeV and $\Lambda \simeq 4\pi f_\pi \simeq 3.1$ TeV, they differ by a large factor ~ 10 . Since the weak-boson mass $M_W = g f_\pi/2$ and the fermion mass $m_f = y_f f_\pi/\sqrt{2}$, we can count them through powers of the coupling constants g and y_f and the vacuum expectation value f_π. The $SU(2)$ weak gauge coupling g and the top quark Yukawa coupling y_t are around of $O(1)$ and thus will not significantly affect the order of magnitude estimates. The electromagnetic $U(1)_{\rm em}$ coupling $e = g \sin\theta_W$ is smaller than g by about a factor of 2. The Yukawa couplings of all light SM fermions other than the top quark are negligibly small. In our following precise counting rule, the dependences on coupling constants g, g'(or e) and y_t are included, while all the light fermion Yukawa couplings [y_f $(\neq y_t) \ll 1$] are ignored.

To correctly estimate the magnitude of each given amplitude T, besides counting the power of E, it is crucial to also *separately* count the power dependences on the two typical mass scales of the EWCL: the vacuum expectation value f_π and the effective cutoff scale Λ. If the powers of f_π and Λ are not separately counted, $\Lambda/f_\pi \simeq 4\pi > 12$ will be mistakenly counted as 1. This can make the estimated results off by orders of magnitudes.

Consider the S-matrix element T at the L-loop order. Since we are dealing with a spontaneously broken gauge theory which has a nonvanishing vacuum expectation value f_π, T can always be written as $f_\pi^{D_T}$ times some dimensionless function of E, Λ, and f_π , etc. The E-power dependence has been given by our generalized Weinberg formula (4.4). We now count the power of Λ. The Λ-dependence in T can only come from two sources:

(i). From tree vertices: T contains $\mathcal{V} = \sum_n \mathcal{V}_n$ vertices, each of which contributes a factor $1/\Lambda^{a_n}$ so that the total factor from $\mathcal{V}$-vertices is $1/\left(\Lambda^{\sum_n a_n}\right)$;

(ii). From loop-level: Since each loop brings a factor $(1/4\pi)^2 = (f_\pi/\Lambda_0)^2$, the total Λ-dependence from loop contribution is $1/\Lambda_0^{2L}$, where $\Lambda_0 \equiv 4\pi f_\pi \geq \Lambda$.

Hence the total Λ-dependence given by the above two sources is $1/\left(\Lambda^{\sum_n a_n}\Lambda_0^{2L}\right)$, which reduces to $1/\left(\Lambda^{\sum_n a_n + 2L}\right)$ in the case $\Lambda \simeq \Lambda_0 = 4\pi f_\pi$. For generality,

we shall explicitly keep the loop factor $(1/4\pi)^{2L} = (f_\pi/\Lambda_0)^{2L}$ in eq. (4.5) because $\Lambda = \min(M_{SB}, \Lambda_0)$ can be somehow lower than $\Lambda_0 = 4\pi f_\pi \approx 3.1$ TeV for strongly coupled EWSB sector, as indicated by model buildings. From the above discussion, we conclude the following precise counting rule for T :

$$
\begin{aligned}
& T = c_T f_\pi^{D_T} \left(\frac{f_\pi}{\Lambda}\right)^{N_\mathcal{O}} \left(\frac{E}{f_\pi}\right)^{D_{E0}} \left(\frac{E}{\Lambda_0}\right)^{D_{EL}} \left(\frac{M_W}{E}\right)^{e_v} H(\ln E/\mu) \quad , \\
& N_\mathcal{O} = \sum_n a_n \ , \quad D_{E0} = 2 + \sum_n \mathcal{V}_n \left(d_n + \frac{1}{2} f_n - 2\right) \ , \quad D_{EL} = 2L \ , \quad \Lambda_0 = 4\pi f_\pi \ ,
\end{aligned}
\tag{4.5}
$$

where the dimensionless coefficient c_T contains possible powers of gauge couplings (g, g') and Yukawa couplings (y_f) from the vertices in T . H is a function of $\ln(E/\mu)$ which arises from loop integrations in the standard dimensional regularization [12, 27] and is insensitive to E. Here, μ denotes the relevant renormalization scale for loop corrections. In Ref. [27], it has been specially emphasized that the dimensional regularization supplemented by the minimal subtraction scheme is most convenient for loop calculations in the effective Lagrangian formalism.

It is useful to give the explicit and compact form of D_{E0} in (4.5) for the lowest order EWCL $\mathcal{L}_{\rm G} + \mathcal{L}^{(2)} + \mathcal{L}_{\rm F}$.[3] Expanding the interaction terms in $\mathcal{L}_{\rm G} + \mathcal{L}^{(2)} + \mathcal{L}_{\rm F}$, we find

$$
\begin{aligned}
& \textstyle\sum_n \mathcal{V}_n \equiv \mathcal{V} = \mathcal{V}_F + \mathcal{V}_d^{(V)} + \mathcal{V}_\pi + \mathcal{V}_4^{VVVV} + \mathcal{V}^{VV-\pi} + \mathcal{V}^{c\bar{c}-\pi} \quad , \\
& \textstyle\sum_n d_n \mathcal{V}_n = \mathcal{V}_d^{(V)} + 2\mathcal{V}_\pi \quad ,
\end{aligned}
\tag{4.6}
$$

with

$$
\begin{aligned}
& \mathcal{V}_F = \mathcal{V}_3^{F\bar{F}V} + \mathcal{V}^{F\bar{F}-\pi} \quad , \\
& \mathcal{V}_d^{(V)} \equiv \mathcal{V}_3^{\pi\pi V} + \textstyle\sum_{n=1}^\infty \mathcal{V}_{2n+2}^{V\pi^{2n+1}} + \mathcal{V}_3^{VVV} + \mathcal{V}^{c\bar{c}V} \quad , \\
& \mathcal{V}_\pi \equiv \textstyle\sum_{n=2}^\infty \mathcal{V}_{2n}^{\pi} \quad .
\end{aligned}
\tag{4.7}
$$

In the above equations, $\mathcal{V}_\pi$ denotes the number of vertices with pure GB self-interactions; $\mathcal{V}^{F\bar{F}-\pi}$ and $\mathcal{V}^{c\bar{c}-\pi}$ denote the numbers of fermion-GB vertices and ghost-GB vertices, respectively; $\mathcal{V}^{VV-\pi}$ denotes the V-V-π^n ($n \geq 1$) vertices; and $\mathcal{V}_3^{F\bar{F}V}$ denotes the

---

[3] It is straightforward to include the higher order operators in the EWCL for counting D_{E0} although the possible vertices in this case are more complicated.

three-point vertex F-$\bar{F}$-V, etc. (Note that $\mathcal{V}^{c\bar{c}-\pi}$ vanishes in the Landau gauge because of the decoupling of GB fields from ghost fields [12].) Hence, for $\mathcal{L}_{\rm G}+\mathcal{L}^{(2)}+\mathcal{L}_{\rm F}$, the D_{E0} factor in (4.5) is

$$D_{E0}=2-\left(\mathcal{V}_d^{(V)}+\mathcal{V}_F+2\mathcal{V}_4^{VVVV}+2\mathcal{V}^{VV-\pi}+2\mathcal{V}^{c\bar{c}-\pi}\right) \quad . \tag{4.8}$$

This clearly shows that the leading energy-power dependence at L-loop level ($L\geq 0$) is always given by those diagrams with pure GB self-interactions, i.e., $(D_E)_{max}=(D_{E0})_{max}+D_{EL}=2+2L$, because of the negative contribution from $-(\mathcal{V}_d^{(V)}+\mathcal{V}_F+2\mathcal{V}_4^{VVVV}+2\mathcal{V}^{c\bar{c}-\pi})$ in (4.8) which includes all types of vertices except the pure GB self-interactions. This conclusion can be directly generalized to all higher order chiral Lagrangian operators such as $\mathcal{L}_n$'s in (3.1.2), and is easy to understand since only pure GB self-interaction-vertices contain the highest powers of the momenta in each order of the momentum expansion. The same conclusion holds for pure V_L-scattering amplitudes since they can be decomposed into the corresponding GB-amplitudes plus the M_W/E-suppressed B-term [cf. (5.17)]. We finally conclude that *in the EWCL* $(D_E)_{\rm max}=2L+2$ *which is independent of the number of external lines of a Feynman diagram.* To lowest order of EWCL and at the tree level (i.e. $L=0$), $(D_E)_{\rm max}=2$, which is in accordance with the well-known low energy theorem [28]. For example, by (4.5) and (4.8), the model-independent tree level contributions to $\pi^{a_1}+\pi^{a_2}\to\pi^{a_3}+\cdots+\pi^{a_n}$ and $V_T^{a_1}+\pi^{a_2}\to\pi^{a_3}+\cdots+\pi^{a_n}$ ($n\geq 4$) are estimated as

$$\begin{aligned} &T_0[\pi^{a_1},\cdots,\pi^{a_n}]=O\left(\frac{E^2}{f_\pi^2}f_\pi^{n-4}\right) , && B_0^{(0)}=g^2f_\pi^{n-4} \ ; \\ &T_0[V_T^{a_1},\pi^{a_2},\cdots,\pi^{a_n}]=O\left(g\frac{E}{f_\pi}f_\pi^{n-4}\right) , && B_0^{(1)}=O\left(g^2\frac{M_W}{E}f_\pi^{n-4}\right) , \end{aligned} \tag{4.9}$$

where $B_0^{(0)}$ and $B_0^{(1)}$ are the leading order B-terms contained in the corresponding V_L-amplitudes for the above two processes.

4.2.2. Decoupling scenario (with Higgs Boson)

For completeness and for other possible applications, we also generalize Weinberg's power counting method to another popular effective Lagrangian formalism [29] for the

weakly coupled EWSB sector, which is usually called as the *decoupling scenario*. In this formalism, the lowest order Lagrangian is just the linear SM with a relatively light Higgs boson and all higher order new physics effective operators must have dimensions larger than 4 and are suppressed by the effective cutoff scale Λ . Even if a relatively light scalar is found in future colliders, it remains important to know whether such a scalar particle trivially serves as the SM Higgs boson or originates from a more complicated dynamics. For instance, the possible new physics effects parametrized in (4.10) should be probed in details for discriminating the SM Higgs boson from the non-SM Higgs boson at the LHC and the future linear colliders.

Following Ref. [29], we can generally write the $SU(2)_L \otimes U(1)_Y$ linear effective Lagrangian as follows

$$\mathcal{L}_{\rm eff}^{\rm linear} \;=\; \mathcal{L}_{\rm SM} + \sum_n \frac{\ell_n}{\Lambda^{d_n-4}} \mathcal{O}_n \tag{4.10}$$

where d_n (≥ 5) is the dimension of the effective operator $\mathcal{O}_n$. In (4.10), the lowest order Lagrangian $\mathcal{L}_{\rm SM}$ is just the SM Lagrangian with a relatively light Higgs boson. The interesting high energy region considered here is

$$M_W, m_H, m_t \;\ll\; E \;<\; \Lambda \tag{4.11}$$

in which $m_H = \sqrt{2\lambda} f_\pi$ denotes the Higgs boson mass.

Since the field content of $\mathcal{L}_{\rm eff}^{\rm linear}$ in (4.10) is the same as that of the SM and the masses of all the known fields are much lower than the typical high energy scale E under consideration [cf. eq. (4.11)], it is clear that all the essential features of Weinberg's counting method hold for this linear case. Following the same reasoning as done in Sec. 4.2.1-4.2.2 [cf. eqs. (4.1)-(4.4)], we find that, for a given S-matrix element T , the counting formula for the linear case is very similar to Eq. (4.5):

$$\begin{aligned} T &= c_T f_\pi^{D_T} \left(\frac{f_\pi}{\Lambda}\right)^{N_\mathcal{O}} \left(\frac{E}{f_\pi}\right)^{D_{E0}} \left(\frac{E}{\Lambda_0}\right)^{D_{EL}} \left(\frac{M_W}{E}\right)^{e_v} H(\ln E/\mu) \;\; , \\ N_\mathcal{O} &= \sum_n (d_n - 4) \;\; , \quad D_{E0} = 2 + \sum_n \mathcal{V}_n \left(d_n + \frac{1}{2} f_n - 2\right) \;\; , \quad D_{EL} = 2L \;\; , \quad \Lambda_0 = 4\pi f_\pi \;\; , \end{aligned} \tag{4.12}$$

where the only difference is that $N_\mathcal{O}$ is now determined by the canonical dimensional

counting in (4.1) instead of the naive dimensional analysis (NDA) [14] for the non-decoupling scenario discussed in Sec. 4.2.2.

For $\mathcal{L}_{\rm SM}$ (i.e., for $\ell_n = 0$ in (4.11)), the counting for D_E defined in (4.12) or (4.4) can be further simplified since we know that the total E-power dependence of the SM contributions will not increase as the loop number L increases because of the perturbative unitarity of the light Higgs SM. We shall show that, due to the renormalizable feature of $\mathcal{L}_{\rm SM}$, the D_{EL} term, $2L$, in (4.12) will be cancelled by a counter term from the vertex-contribution in the D_{E0} term.

In $\mathcal{L}_{\rm SM}$, there are only 3-point and 4-point vertices. Due to the renormalizability of the SM, all the 4-point vertices do not contain partial derivatives, while each 3-point vertex may contain at most one partial derivative. So, we have $d_n = 0$ or 1 . Thus,

$$\sum_n \mathcal{V}_n d_n = \mathcal{V}_d \quad , \quad \mathcal{V}_d \equiv \mathcal{V}_3^{VVV} + \mathcal{V}_3^{ssV} + \mathcal{V}_3^{c\bar{c}V} \quad , \tag{4.13}$$

where $\mathcal{V}_d$ is the number of all vertices containing one partial derivative and $\mathcal{V}_n^{\chi_1\cdots\chi_n}$ is the total number of n-point vertices of type χ_1-χ_2-$\cdots$-χ_n (χ denotes any possible field in the theory). The symbol s denotes scalar fields (Higgs or GB), c ($\bar{c}$) denotes (anti-)ghost field and F ($\bar{F}$) denotes (anti-)fermion field. Furthermore, in $\mathcal{L}_{\rm SM}$,

$$\begin{aligned}
&\mathcal{V} = \textstyle\sum_n \mathcal{V}_n = \mathcal{V}_3 + \mathcal{V}_4 \quad , \\
&\mathcal{V}_3 \equiv \mathcal{V}_d + \mathcal{V}_F + \bar{\mathcal{V}}_3 \quad , \quad \mathcal{V}_F \equiv \mathcal{V}_3^{sF\bar{F}} + \mathcal{V}_3^{VF\bar{F}} \quad , \quad \bar{\mathcal{V}}_3 \equiv \mathcal{V}_3^{sVV} + \mathcal{V}_3^{sc\bar{c}} + \mathcal{V}_3^{sss} \quad . \\
&\mathcal{V}_4 \equiv \mathcal{V}_4^{ssss} + \mathcal{V}_4^{ssVV} + \mathcal{V}_4^{VVVV} \quad ,
\end{aligned} \tag{4.14}$$

Substituting (4.13), (4.14) and the SM relation $\mathcal{V}_F = 2i_F + e_F$ into (4.12), we obtain

$$\begin{aligned}
D_E^{\rm SM} \;=\; D_{E0}^{\rm SM} + D_{EL}^{\rm SM} \;&=\; 2L + 2 - 2\mathcal{V} + \mathcal{V}_d + \mathcal{V}_F - e_v \\
&=\; 2L + 2 - (\mathcal{V}_d + \mathcal{V}_F + 2\bar{\mathcal{V}}_3 + 2\mathcal{V}_4) - e_v \quad ,
\end{aligned} \tag{4.15}$$

which, with the aid of another SM relation

$$\begin{aligned}
&3\mathcal{V}_3 + 4\mathcal{V}_4 = e + 2i \quad , \quad \text{or,} \\
&\mathcal{V}_d + \mathcal{V}_F = 4\mathcal{V} - \bar{\mathcal{V}}_3 - 2i - e = 2 - 2L + 2\mathcal{V} - \bar{\mathcal{V}}_3 - e \quad ,
\end{aligned} \tag{4.16}$$

can be further simplified as

$$D_E^{\rm SM} \;=\; 4 - e - e_v - \bar{\mathcal{V}}_3 \quad , \tag{4.17}$$

where $\bar{\mathcal{V}}_3 \equiv \mathcal{V}_3^{sVV} + \mathcal{V}_3^{sc\bar{c}} + \mathcal{V}_3^{sss}$. Note that the loop-dependence term $2L$ is indeed canceled by the counter term from the vertex-contribution [cf. (4.15) and (4.17)] as expected. This is the unique feature of the renormalizable SM and this feature is absent in the EWCL with the derivative expansion which has been fully studied in Sec. 3. In summary, for $\mathcal{L}_{\rm SM}$, a Feynman diagram with its external lines fixed can have the leading energy dependence if it does not contains the trilinear vertices s-V-V, s-c-$\bar{c}$ and s-s-s , and the v_μ-factor. Equivalently, (4.15) shows in another way that at a given L-loop level the leading energy behavior of a diagram corresponds to the minimal $(\mathcal{V}_d+\mathcal{V}_F+2\bar{\mathcal{V}}_3+2\mathcal{V}_4)$ and the vanishing e_v .

The NLO linear operators $\mathcal{O}_n$ in (4.10) have been fully compiled in Ref. [29]. Here are a few typical dimension-6 effective operators:

$$\begin{aligned}
\mathcal{O}_W &= -i4\mathrm{Tr}(\mathbf{W}_\mu{}^\nu \mathbf{W}_\nu{}^\rho \mathbf{W}_\rho{}^\mu) \ , & \mathcal{O}_{\partial\phi} &= \frac{1}{2}\partial_\mu(\phi^\dagger\phi)\partial^\mu(\phi^\dagger\phi) \ , \\
\mathcal{O}_{qq}^{(1,1)} &= \frac{1}{2}(\bar{q}\gamma_\mu q)(\bar{q}\gamma^\mu q) \ , & \mathcal{O}_{qq}^{(1,3)} &= \frac{1}{2}(\bar{q}\gamma_\mu \tau^a q)(\bar{q}\gamma^\mu \tau^a q) \ , \\
\mathcal{O}_{\phi W} &= (\phi^\dagger\phi)\mathrm{Tr}(\mathbf{W}_{\mu\nu}\mathbf{W}^{\mu\nu}) \ , & \mathcal{O}_{\phi B} &= (\phi^\dagger \mathbf{W}_{\mu\nu}\phi)B^{\mu\nu} \ , \\
\mathcal{O}_\phi^{(1)} &= \frac{1}{2}(\phi^\dagger\phi)(D_\mu\phi^\dagger D^\mu\phi) \ , & \mathcal{O}_\phi^{(3)} &= (\phi^\dagger D^\mu\phi)[(D_\mu\phi)^\dagger\phi] \ ,
\end{aligned} \tag{4.18}$$

where ϕ denotes the Higgs doublet which contains the linearly realized Higgs field (H) and three would-be Goldstone bosons ($\pi^\pm,\ \pi^0$).

It is straightforward to apply our power counting rule (4.12) [and (4.17)] for estimating various scattering amplitudes contributed by (4.10). Some typical examples are in order. First, we count the model-independent contributions from $\mathcal{L}_{\rm SM}$ to some $2\to 2$ scattering processes:

$$\begin{aligned}
T[V_T^{a_1}V_T^{a_2}\to V_T^{a_3}V_T^{a_4}] &= O(g^2) + O\left(\frac{g^4}{16\pi^2}\right) \ , \\
T[\pi^{a_1}\pi^{a_2}\to \pi^{a_3}\pi^{a_4}] &= O(g^2,\lambda) + O\left(\frac{g^4,\lambda^2}{16\pi^2}\right) \ , & B_0^{(0)} &= O\left((g^2,\lambda)\tfrac{M_W^2}{E^2}\right) \ , \\
T[V_T^{a_1}\pi^{a_2}\to \pi^{a_3}\pi^{a_4}] &= O\left((g^2,\lambda)\frac{M_W}{E}\right) + O\left(\frac{g^4}{16\pi^2}\right) \ , & B_0^{(1)} &= O\left(g^2\tfrac{M_W}{E}\right) \ .
\end{aligned} \tag{4.19}$$

Second, we count the NLO model-dependent contributions from (4.18) to some tree-level high energy processes at the $O(1/\Lambda^2)$:

$$\begin{aligned}
&T_1[V_T^{a_1}V_T^{a_2}\to V_T^{a_3}V_T^{a_4}](\mathcal{O}_W) \;=\; O\left(\ell_W\frac{gE^2}{\Lambda^2}\right)\quad,\\
&T_1[\pi^{a_1}\pi^{a_2}\to\pi^{a_3}\pi^{a_4}](\mathcal{O}_W) \;=\; 0\quad,\qquad B_1^{(0)} \;=\; O\left(\ell_W\frac{gM_W^2}{\Lambda^2}\right)\quad,\\
&T_1[\pi^{a_1}\pi^{a_2}\to HH](\mathcal{O}_{\partial\phi}) \;=\; O\left(\ell_{\partial\phi}\frac{E^2}{\Lambda^2}\right)\quad,\qquad B_1^{(0)} \;=\; O\left(\frac{M_W^2}{\Lambda^2}\right)\quad,\\
&T_1[q\bar{q}\to q\bar{q}](\mathcal{O}_{qq}^{(1,1)}) \;=\; O\left(\ell_{qq}^{(1,1)}\frac{E^2}{\Lambda^2}\right)\quad.
\end{aligned}\tag{4.20}$$

The above examples illustrate, in the linear effective Lagrangian formalism, how to conveniently apply our power counting rule (4.12) to determine the high energy behavior of any given amplitude and estimate its order of magnitude.

5. Longitudinal-Goldstone Boson Equivalence Theorem: *from mathematical formulation to its physical content for probing EWSB*

In this section, we analyze how the ET is deeply rooted in the underlying Higgs mechanism based upon rigorous Ward-Takahashi (WT) identities. Then, we review how the radiative-modification factors to the ET generally arise at the loop levels and how the radiative-modification-free formulation of the ET is constructed in our convenient renormalization schemes for general R_ξ-gauges including both the 't Hooft-Feynman and Landau gauges. After this, we focus on analyzing the additive modifications to the ET, where we discuss the issues of longitudinal-transverse ambiguity and the kinematic singularity concerning the validity of the ET. Finally, we formulate the ET as a necessary physical criterion for probing the EWSB sector.

5.1. ET and the Higgs mechanism

If there were no EWSB, the physical degrees of freedom of the weak gauge bosons V^a's (V^a stands for $W^\pm$ or Z^0) would only be their transverse components V_T^a's. In the theory

with EWSB, from the well-known Higgs mechanism [30], their longitudinal components (V_L^a's) are physical degrees of freedom as well due to absorbing the corresponding would-be Goldstone bosons (π^a's). Thus, the dynamics of V_L^a's reflects that of the π^a's which are generally described by the EWCL in (2.1)-(2.2). Intuitively, we expect that the amplitude of the V_L^a's is related to that of the π^a's, which will be quantitatively described by the so-called ET. This makes it possible to probe the EWSB mechanism via the experimentally measured processes involving V_L^a's. The tree-level form of the ET was first given in Ref. [31] which is

$$T[V_L^{a_1},\cdots,V_L^{a_n};\Phi_\alpha]=T[-i\pi^{a_1},\cdots,-i\pi^{a_n};\Phi_\alpha]+O(M_W/E)\,, \tag{5.1}$$

where Φ_α denotes other possible on-shell physical particles. This simple relation has been widely used. Since computing the π^a-amplitude is much easier than computing the V_L^a-amplitude, eq.(5.1) also provides a technical tool for simplifying the calculation of $T(V_L^{a_1},\cdots,V_L^{a_n};\Phi_\alpha)$. In Secs. 5.3-5.4, we further reveal and demonstrate the *profound physical content of the ET* which serves as a necessary criterion in classifying the sensitivities of probing the EWSB mechanism at high energy colliders.

Up to the quantum loop-level, the formulation of the ET becomes much more complicated and non-trivial. The study of the ET beyond tree-level was started in Ref. [32]. The existence of the (multiplicative) radiative-modification factors to the ET was revealed in Ref. [33]. The precise formulation of the ET to all orders in the SM and the EWCL theory was systematically studied in Refs. [34, 35] and [11] where both the multiplicative and additive modification-factors are precisely analyzed.[4] Generally speaking, it is unlikely that the simple relation (5.1) can always hold up to loop-level since the physical amplitude $T[V_L^{a_1},\cdots,V_L^{a_n};\Phi_\alpha]$ cannot be simply equal to the unphysical one $T[-i\pi^{a_1},\cdots,-i\pi^{a_n};\Phi_\alpha]$ even if we neglect the $O(M_W/E)$ terms. This is because the wavefunction renormalizations for the physical and unphysical fields are different and the latter has certain arbitrariness (allowed by the WT identities). So, we generally expect that *there should be certain multiplicative modification factors on the R.H.S. of (5.1) which ensure the*

[4] For some other discussions related to the ET, see Ref. [36, 37] for instance.

renormalization-scheme- and gauge-parameter- independence of the R.H.S. of (5.1). To see this, we consider a general gauge theory and start from deriving a useful Slavnov-Taylor (ST) identity. Let the subscript "0" denote unrenormalized quantities. We take the general R_ξ gauge

$$\begin{aligned} \mathcal{L}_{\rm GF} &= -\frac{1}{2}(F_0^a)^2 \quad , \\ F_0^a &\equiv (\xi_0^a)^{-\frac{1}{2}}\partial_\mu V_0^{a\mu} + (\xi_0^a)^{\frac{1}{2}}\kappa_0^a\pi_0^a \quad , \end{aligned} \tag{5.2}$$

in which we have put a free parameter κ_0^a instead of taking it to be the mass of $V_0^{a\mu}$ for generality. The invariance of the action under the Becchi-Rouet-Stora-Tyutin (BRST) transformation [38] leads to the following ST identity in the momentum representation [39, 40]

$$< 0|F_0^{a_1}(k_1)\cdots F_0^{a_n}(k_n)\Phi|0 >= 0 \ . \tag{5.3}$$

In (5.3) the external Φ legs have been amputated. Now we give a physical analysis of the ET and the Higgs mechanism, starting from (5.3).

First, we consider the case without spontaneous symmetry breaking (SSB). The two transverse components of $V_0^{a\mu}$ are physical, while the unphysical longitudinal and scalar components are constrained by the gauge fixing condition. Let us take the standard covariant gauge for the massless theory, i.e. the gauge fixing function (5.2) with $\kappa_0^a = 0$. The longitudinal and scalar polarization vectors of $V_0^{a\mu}$ can be written as

$$\epsilon_L^\mu(k) = (0, \vec{k}/k^0), \qquad \epsilon_S^\mu(k) = (1, \vec{0}) \ . \tag{5.4}$$

We then have

$$\epsilon_L^\mu(k) + \epsilon_S^\mu(k) = \frac{k^\mu}{k^0} \quad , \tag{5.5}$$

so that

$$F_0^a(k) = i(\xi_0^a)^{-\frac{1}{2}}k^0[V_{0L}^a(k) + V_{0S}^a(k)] \quad . \tag{5.6}$$

Substituting (5.6) into (5.3) and doing renormalization and F^a-leg amputation, we directly get the scattering amplitude

$$T[V_L^{a_1}(k_1) + V_S^{a_1}(k_1), \cdots, V_L^{a_n}(k_n) + V_S^{a_n}(k_n); \Phi_\alpha] = 0 \ , \tag{5.7}$$

which is just a quantitative formulation of the V_L^a-V_S^a constraint mechanism in the physical in/out states for a *massless* Abelian or non-Abelian gauge theory (without Higgs mechanism).

Next, we consider the case with the SSB. The gauge fields become massive and the longitudinal component V_L^a is "released" to be physical by the Higgs mechanism. We shall see that in the constraint (5.7) V_L^a will now be replaced by the unphysical would-be Goldstone boson field π^a. Now we can take the general R_ξ-gauge (5.2) with the arbitrary gauge-parameter κ_0^a (which can be *either zero or nonzero*).[5] The longitudinal and scalar polarization vectors for a massive vector field with a physical mass M_a can now be written as

$$\epsilon_L^\mu(k) = \frac{1}{M_a}(|\vec{k}|, k^0\vec{k}/|\vec{k}|) \ , \qquad \epsilon_S^\mu(k) = \frac{k^\mu}{M_a} \ . \tag{5.8}$$

Thus

$$F_0^a(k) = i(\xi_0^a)^{-\frac{1}{2}} M_a V_{0S}^a(k) + (\xi_0^a)^{\frac{1}{2}} \kappa_0^a \pi_0^a(k) \ . \tag{5.9}$$

Repeating the above procedures with care on the V_{0S}^a-π_0^a mixing and the renormalization, we get, corresponding to (5.7),

$$T[V_S^{a_1}(k_1) + iC^{a_1}(k_1^2)\pi^{a_1}(k_1), \cdots, V_S^{a_n}(k_n) + iC^{a_n}(k_n^2)\pi^{a_n}(k_n); \Phi_\alpha] = 0 \ , \tag{5.10}$$

where the exact expression for $C^a(k^2)$ will be derived in Sec. 5.2.

The rigorous identity (5.10) *generally holds for any gauge theory with SSB via the Higgs mechanism* and is very important. A few remarks are in order. First, (5.10) is a quantitative formulation of the V_S^a-π^a constraint in the physical in/out states, which deeply reflects the *essence of the underlying Higgs mechanism*: after the SSB, the would-be Goldstone-boson degree of freedom (π^a) becomes "confined" with the unphysical scalar component of the the massive gauge field V_μ^a so that the longitudinal component of V_μ^a can be "released" from the constraint (5.7) as the physical degree of freedom. Gauge-invariance forces the π^a's to be "confined" with V_S^a's via (5.10) (so that no any net effect of them can be observed from the physical S-matrix elements) and ensures the Higgs mechanism to exactly work as expected. As to be shown below, the identity (5.10) will directly result in the equivalence theorem (ET). Next, we comment on the new modification-factors [$C^a(k^2)$'s] in (5.10). Note that in (5.6) and (5.7) the V_L^a and V_S^a are two orthogonal projections

---

[5] The usual choice for the renormalized κ^a to be gauge-boson mass M_a is only for cancelling the tree-level V_μ^a-π^a mixing and making the propagators simpler.

of the *same* Lorentz vector field V_μ^a so that they will not mix and thus the amputation and renormalization of the F^a-leg are straightforward. However, in (5.9) and (5.10) the unphysical scalar component V_S^a and would-be GB π^a do mix with each other: if the gauge-parameter κ^a is chosen to cancel their tree-level mixing as usual, then they will mix again in all loop-orders. Furthermore, the component V_S^a (as the scalar projection of V_μ^a) and the GB (π^a) are two independent quantum fields and thus get renormalized in different ways. These are why the non-trivial modification factors [$C^a(k^2)$'s] generally arise in (5.10), in contrast with the case of massless theory (without SSB via Higgs mechanism). As a final remark, we note that, although the Higgs mechanism (and its basic consequence) was discovered a long time ago [30], to our knowledge, the mathematically quantitative formulation of it *at the level of S-matrix elements* [see (5.10)] in comparison with massless case (5.7) and its deep connection with the ET [see (5.16)-(5.17) below] were first revealed very recently [40] and are newly reviewed here in a comprehensive way.

Now, we continue our analysis on how the ET arises as a direct consequence of the Higgs mechanism (5.10). By noting that M_a is the characteristic of the SSB, we infer that (5.5) holds as $M_a \to 0$. Therefore, with $M_a \neq 0$, $\epsilon_L^\mu(k) + \epsilon_S^\mu(k)$ must be of the form

$$\epsilon_L^\mu(k) + \epsilon_S^\mu(k) = \frac{k^\mu}{A} + O\left(\frac{M_a}{E}\right) \ , \tag{5.11}$$

with " A " being certain normalization factor. Therefore , at high energy, $\epsilon_L^\mu(k)$ and $\epsilon_S^\mu(k)$ are related up to an $O(M_a/E)$ term. Indeed, if we take the $M_a \neq 0$ expressions (5.8), we see that $A = \frac{1}{2}M_a$, and thus

$$\epsilon_L^\mu(k) = \epsilon_S^\mu(k) + O(M_a/E) \ . \tag{5.12}$$

So we can define

$$V_L^a(k) \equiv V_S^a(k) + v^a(k) \ , \quad v^a = v^\mu V_\mu^a \ , \quad v^\mu = O(M_a/E) \ , \tag{5.13}$$

and

$$\begin{aligned} \bar{F}^a &\equiv V_S^a + iC^a\pi^a \equiv V_L^a - \bar{Q}^a \ , \\ \bar{Q}^a &\equiv -iC^a\pi^a + v^a = -iC^a\pi^a + O(M_a/E) \ . \end{aligned} \tag{5.14}$$

Then (5.10) becomes

$$0 = T(\bar{F}^{a_1}, \cdots, \bar{F}^{a_n}, \Phi) \ , \qquad (\ n \geq 1\ ) \ . \tag{5.15}$$

i.e.

$$
\begin{aligned}
0 = \; & T(V_L^{a_1} - \bar{Q}^{a_1}, \cdots, V_L^{a_n} - \bar{Q}^{a_n}, \Phi) \\
= \; & T(V_L^{a_1}, \cdots, V_L^{a_n}; \Phi_\alpha) + (-)^n T(\bar{Q}^{a_1}, \cdots, \bar{Q}^{a_n}; \Phi_\alpha) \\
& + \textstyle\sum_{1\le j\le n-1}^{P_j} T(V_L^{a_{l_1}}, \cdots, V_L^{a_{l_j}}, \bar{F}^{a_{l_{j+1}}} - V_L^{a_{l_{j+1}}}, \cdots, \bar{F}^{a_{l_n}} - V_L^{a_{l_n}}; \Phi_\alpha) \qquad [\; cf.\;\; (5.14) \;] \\
= \; & T(V_L^{a_1}, \cdots, V_L^{a_n}; \Phi_\alpha) + (-)^n T(\bar{Q}^{a_1}, \cdots, \bar{Q}^{a_n}; \Phi_\alpha) \\
& + \textstyle\sum_{1\le j\le n-1}^{P_j} T(V_L^{a_{l_1}}, \cdots, V_L^{a_{l_j}}, -V_L^{a_{l_{j+1}}}, \cdots, -V_L^{a_{l_n}}; \Phi_\alpha) \qquad [\; cf.\;\; (5.15) \;] \\
= \; & T(V_L^{a_1}, \cdots, V_L^{a_n}; \Phi_\alpha) + (-)^n T(\bar{Q}^{a_1}, \cdots, \bar{Q}^{a_n}; \Phi_\alpha) + \textstyle\sum_{j=1}^{n-1} C_n^j (-)^{n-j} T(V_L^{a_1}, \cdots, V_L^{a_n}; \Phi_\alpha) \;\; .
\end{aligned}
$$

Using the identity $\; 0 = (1-1)^n = 1 + (-)^n + \sum_{j=1}^{n-1} C_n^j (-)^{n-j} \;$, we have

$$
T[V_L^{a_1}, \cdots, V_L^{a_n}; \Phi_\alpha] = T[\bar{Q}^{a_1}, \cdots, \bar{Q}^{a_n}; \Phi_\alpha] \;\; . \tag{5.16}
$$

Substituting (5.14) into (5.16) we get the general formula

$$
T[V_L^{a_1}, \cdots, V_L^{a_n}; \Phi_\alpha] = C \cdot T[-i\pi^{a_1}, \cdots, -i\pi^{a_n}; \Phi_\alpha] + B \;\; , \tag{5.17}
$$

$$
\begin{aligned}
C \;\; & \equiv C_{\rm mod}^{a_1} \cdots C_{\rm mod}^{a_n} \;\; = \;\; 1 + O(\text{loop}) \;, \\
B \;\; & \equiv \textstyle\sum_{l=1}^{n} (\; C_{\rm mod}^{a_{l+1}} \cdots C_{\rm mod}^{a_n} T[v^{a_1}, \cdots, v^{a_l}, -i\pi^{a_{l+1}}, \cdots, -i\pi^{a_n}; \Phi_\alpha] + \text{ permutations }) \;\; , \\
v^a \;\; & \equiv v^\mu V_\mu^a \;\; , \qquad v^\mu \;\equiv \epsilon_L^\mu - k^\mu / M_V = O(M_V/E) \;\; , \quad (M_V = M_W, M_Z) \;\; ,
\end{aligned} \tag{5.17a,b,c}
$$

where $\; C_{mod}^a \equiv C^a(k^2)|_{k^2=M_a^2} \;$ and will be analyzed in Sec. 5.2. This is the general *ET identity* which leads to the precise formulation of the ET when the quantitative expression for C_{mod}^a and the condition for neglecting the B-term are derived (cf. the following subsections). To conclude, as rigorously shown above, *the ET directly results from the* V_S^a*-*ϕ^a *constraint in the SSB theory via the Higgs mechanism [cf. (5.10)] and the high energy relation (5.12)* . The above general analysis holds for the Higgs mechanisms either with or without elementary Higgs boson(s).

5.2. ET and its multiplicative modifications

In this subsection, we derive the quantitative expression for the modification factor $C_{\rm mod}^a$ and study the simplification of it. For simplicity, we shall first derive our results in

the $SU(2)_L$ Higgs theory by taking $g' = 0$ in the electroweak $SU(2)_L \otimes U(1)_Y$ standard model (SM). The generalizations to the full SM and to the effective Lagrangian formulations are straightforward (though there are some further complications) and will be given in the later part of this section. The field content for the $SU(2)_L$ Higgs theory consists of the physical fields, H, W^a_μ, and $f(\bar{f})$ representing the Higgs, the weak gauge bosons and the fermions, respectively, and the unphysical fields π^a, c^a, and $\bar{c}^a$ representing the would-be Goldstone bosons, the Faddeev-Popov ghosts, and the anti-ghosts respectively. We quantize the theory using the general R_ξ-gauge (5.2). For simplicity, we write (5.2) as

$$F^a_0 \;=\; (\xi^a_0)^{-\frac{1}{2}}\partial_\mu W^{a\mu}_0 + (\xi^a_0)^{\frac{1}{2}}\kappa^a_0\pi^a_0 \;=\; (\underline{\mathbf{K}}^a_0)^T\underline{\mathbf{W}}^a_0 \quad , \tag{5.18a}$$

$$\underline{\mathbf{K}}^a_0 \equiv \Big((\xi^a_0)^{-\frac{1}{2}}\partial_\mu, -(\xi^a_0)^{\frac{1}{2}}\kappa^a_0\Big)^T \quad , \quad \underline{\mathbf{W}}^a_0 \equiv (W^{a\mu}_0, -\pi^a_0)^T \quad , \tag{5.18b}$$

For the case of the $SU(2)_L$ theory, we can take $\xi^a_0 = \xi_0$, $\kappa^a_0 = \kappa_0$, for $a = 1, 2, 3$.

As we have seen in Sec. 5.1, the appearance of the modification factor $C^a_{\rm mod}$ to the ET is due to the amputation and the renormalization of external massive gauge bosons and their corresponding Goldstone-boson fields. For the amputation, we need a general ST identity for the propagators of the gauge boson, Goldstone boson and their mixing. The ST identity for the matrix propagator of $\underline{\mathbf{W}}^a_0$ is [34]

$$\underline{\mathbf{K}}^T_0\underline{\mathbf{D}}^{ab}_0(k) \;=\; -\Big[\underline{\mathbf{X}}^{ab}\Big]^T(k) \tag{5.19}$$

with

$$\underline{\mathbf{D}}^{ab}_0(k) \;=\; <0|T\underline{\mathbf{W}}^a_0(\underline{\mathbf{W}}^b_0)^T|0>(k) \quad , \quad \mathcal{S}_0(k)\delta^{ab} \;=\; <0|Tc^b_0\bar{c}^a_0|0>(k) \quad , \tag{5.20a}$$

$$\underline{\mathbf{X}}^{ab}(k) \;\equiv\; \underline{\hat{\mathbf{X}}}^{ab}(k)\mathcal{S}_0(k) \;\equiv\; \begin{pmatrix} \xi_0^{\frac{1}{2}} <0|T\hat{s}W^{b\mu}_0|0> \\ -\xi_0^{\frac{1}{2}} <0|T\hat{s}\pi^b_0|0> \end{pmatrix}_{(k)} \cdot\, \mathcal{S}_0(k) \quad . \tag{5.20b}$$

To explain how the modification factor $C^a_{\rm mod}$ to the ET arises, we start from (5.6) and set $n = 1$, i.e.,

$$0 = G[F^a_0(k);\Phi_\alpha] = \underline{\mathbf{K}}^T_0 G[\underline{\mathbf{W}}^a_0(k);\Phi_\alpha] = -[\underline{\mathbf{X}}^{ab}]^T T[\underline{\mathbf{W}}^a_0(k);\Phi_\alpha] \quad . \tag{5.21}$$

Here $G[\cdots]$ and $T[\cdots]$ denote the Green function and the S-matrix element, respectively. The identity (5.21) leads directly to

$$\frac{k_\mu}{M_{W0}} T[W^{a\,\mu}_0(k);\Phi_\alpha] = \widehat{C}^a_0(k^2)T[-i\pi^a_0;\Phi_\alpha] \tag{5.22}$$

with $\widehat{C}_0^a(k^2)$ defined as

$$\widehat{C}_0^a(k^2) \equiv \frac{1+\Delta_1^a(k^2)+\Delta_2^a(k^2)}{1+\Delta_3^a(k^2)} \quad , \tag{5.23}$$

in which the quantities Δ_i^a are the proper vertices of the composite operators

$$\begin{aligned}
\Delta_1^a(k^2)\delta^{ab} &= \frac{g_0}{2M_{W0}} < 0|T\left[\!\left[H_0 c_0^b\right]\!\right]|\bar{c}_0^a > (k) \quad , \\
\Delta_2^a(k^2)\delta^{ab} &= \frac{g_0}{2M_{W0}}\varepsilon^{bcd} < 0|T\left[\!\left[\pi_0^c c_0^d\right]\!\right]|\bar{c}_0^a > (k) \quad , \\
ik^\mu\Delta_3^a(k^2)\delta^{ab} &= -\frac{g_0}{2}\varepsilon^{bcd} < 0|T\left[\!\left[W_0^{\mu b} c_0^c\right]\!\right]|\bar{c}_0^a > (k) \quad ,
\end{aligned} \tag{5.24}$$

where expressions such as $\left[\!\left[W_0^{\mu b}c_0^c\right]\!\right](x)$ indicate the local composite operator fields formed from $W_0^{\mu b}(x)$ and $c_0^c(x)$. The formula (5.23)-(5.24) (valid for the $SU(2)$ Higgs theory) were derived in Ref. [33], and the complete expressions for the realistic $SU(2)_L \otimes U(1)_Y$ SM and EWCL were first given in Ref. [34, 35] which are shown to be much more complicated. However, we must emphasize that, contrary to all other previous studies, the essential advantage of our following approach [34, 35] is that we need *not* explicitly calculate any of these complicated loop level quantities (Δ_i's) and our simplifications of these multiplicative modification factors [cf. (5.33-38) below] are based on general WT identities and automatically determined by each renormalization scheme itself.

After renormalization, (5.22) becomes

$$\frac{k_\mu}{M_W}T[W^{a\mu}(k);\Phi_\alpha] = \widehat{C}^a(k^2)T[-i\pi^a;\Phi_\alpha] \tag{5.25}$$

with the finite renormalized coefficient

$$\widehat{C}^a(k^2) = Z_{M_W}\left(\frac{Z_W}{Z_\pi}\right)^{\frac{1}{2}}\widehat{C}_0^a(k^2) \quad . \tag{5.26}$$

The renormalization constants are defined as $W_0^{a\mu} = Z_W^{\frac{1}{2}}W^{a\mu}$, $\pi_0^a = Z_\pi^{\frac{1}{2}}\pi^a$, and $M_{W0} = Z_{M_W}M_W$. The modification factor to the ET is precisely the value of this finite renormalized coefficient $\widehat{C}^a(k^2)$ on the gauge boson mass-shell:

$$C^a_{\rm mod} = \frac{M_W}{M_W^{phys}}\,\widehat{C}^a(k^2)\Big|_{k^2=(M_W^{phys})^2} \quad , \tag{5.27}$$

where M_W^{phys} is the physical mass of M_W which is equal to M_W if the usual on-shell subtraction for M_W is adopted.

We see that the appearance of the factor $C \equiv C_{\rm mod}^{a_1} \cdots C_{\rm mod}^{a_n}$ on the R.H.S. of (5.17) is due to the amputation and renormalization of external $W^{a\mu}$ and π^a lines by using the ST identity (5.19). Thus it is natural that the factor $C_{\rm mod}^a$ contains $W^{a\mu}$-ghost, π^a-ghost and Higgs-ghost interactions expressed in terms of these Δ_i^a-quantities. In general, the loop-level Δ_i^a-quantities are non-vanishing and make $\widehat{C}_0(k^2) \neq 1$ and $C_{\rm mod}^a \neq 1$ order by order. In the Landau gauge, these Δ_i^a-quantities can be partially simplified, especially at the one-loop order, because the tree-level Higgs-ghost and π^a-ghost vertices vanish. This makes $\Delta_{1,2}^a = 0$ at one loop.[6] In general [35],

$$\Delta_1^a = \Delta_2^a = 0 + O(2 \text{ loop}) \ , \quad \Delta_3^a = O(1 \text{ loop}) \ , \qquad (\text{ in Landau gauge }) \ . \tag{5.28}$$

Beyond the one-loop order, $\Delta_{1,2}^a \neq 0$ since the Higgs and Goldstone-boson fields can still indirectly couple to the ghosts via loop diagrams containing internal gauge fields.

The explicit expressions for the Δ_i^a's will be further greatly complicated in the full $SU(2)_L \otimes U(1)_Y$ theory due to various mixing effects [34], as mentioned above. Since the calculation of these Δ_i^a's is very cumbersome, the use of the general loop-level form of the ET [cf. (5.40)] from the general identity (5.17) is much more inconvenient than that of the tree-level form (5.1). However, as we have already mentioned, both the modification factor $C \equiv C_{\rm mod}^{a_1} \cdots C_{\rm mod}^{a_n}$ and the GB-amplitude $T[-i\pi^{a_1}, \cdots, -i\pi^{a_n}; \Phi_\alpha]$ are unphysical quantities which are renormalization-scheme and gauge-parameter dependent [the unphysical parts of these two quantities cancel each other to make their product physical and be equal to the physical amplitude $T[V_L^{a_1}, \cdots, V_L^{a_n}; \Phi_\alpha]$ on the L.H.S. of (5.17)]. So that it is possible to choose certain renormalization schemes to simplify the expression of $C_{\rm mod}^a$. Especially, if we can find certain schemes to exactly make $C_{\rm mod}^a = 1$, (5.17) will be as convenient as (5.1) in these schemes. In the following, we shall deal with this simplification which concerns only the WT identities for the propagators and has

---

[6] We note that, in the non-Abelian case, the statement that $\Delta_{1,2}^a = 0$ for Landau gauge in Refs. [33, 34] is valid at the one-loop order.

nothing to do with the explicit calculation of the Δ_i^a's, so it really makes the use of (5.17) as simple as the tree-level case.

For this purpose, we consider the WT identities for the $W^{a\mu}$, π^a and the ghost-field propagators which, in the momentum representation, take the form [34]

$$\begin{aligned} i\mathcal{D}^{-1}_{\mu\nu,ab}(k) &= \left(g_{\mu\nu} - \frac{k_\mu k_\nu}{k^2}\right)[-k^2 + M_W^2 - \Pi_{WW}(k^2)] + \frac{k_\mu k_\nu}{k^2}[-\xi^{-1}k^2 + M_W^2 - \tilde{\Pi}_{WW}(k^2)]\delta_{ab} \ , \\ i\mathcal{D}^{-1}_{\pi\mu,ab}(k) &= ik_\mu[M_W - \kappa - \tilde{\Pi}_{W\pi}(k^2)]\delta_{ab} \ , \\ i\mathcal{D}^{-1}_{\pi\pi,ab}(k) &= k^2 - \xi\kappa^2 - \tilde{\Pi}_{\pi\pi}(k^2)\delta_{ab} \ , \\ iS^{-1}_{ab}(k) &= k^2 - \xi\kappa M_W - \tilde{\Pi}_{c\bar{c}}(k^2)\delta_{ab} \ , \end{aligned} \tag{5.29}$$

where Π_{WW} is the proper self-energy of the physical part of the gauge boson, and $\tilde{\Pi}^a_{ij}$'s are unphysical self-energies. these identities enables us to express $\widehat{C}^a(k^2)$ in (5.26) in terms of the self-energies as [34]

$$\widehat{C}^a(k^2) = \frac{M_W^2 - \tilde{\Pi}_{WW} + (\Omega_\xi^{-1} - 1)\xi^{-1}k^2}{M_W^2 - M_W\tilde{\Pi}_{W\pi}(k^2) + M_W\kappa(\Omega_\xi^{-1}\Omega_\kappa - 1)} = \frac{k^2}{M_W}\frac{M_W - \tilde{\Pi}_{W\pi} + (\Omega_\xi^{-1}\Omega_\kappa - 1)\kappa}{k^2 - \tilde{\Pi}_{\pi\pi} + (\Omega_\xi^{-1}\Omega_\kappa^2 - 1)\xi\kappa^2} \ , \tag{5.30}$$

where Ω_ξ and Ω_κ are finite constants appearing in the relations between the renormalization constants constrained by the WT identities (5.29) which are [34]

$$Z_\xi = \Omega_\xi Z_W \ , \qquad Z_\kappa = \Omega_\kappa Z_W^{1/2} Z_\pi^{-1/2} Z_\xi^{-1} \ , \qquad \text{etc.} \ , \tag{5.31}$$

and finite quantities $\Omega_{\xi,\kappa}(= 1 + O(\text{loop}))$ are to be determined by the normalization conditions at the subtraction point. From (5.30) we see that the modification factor $C^a_{\text{mod}} = \widehat{C}^a(k^2)|_{k^2=(M_W^{phys})^2}$ can be simplified by taking certain on-shell renormalization schemes in which the proper self-energies vanish at the subtraction point (mass-shell). For the physical sector, we take the standard on-shell scheme. For the unphysical sector, the prescription of the on-shell renormalization is arbitrary since changing the determination of the renormalization constants for the unphysical fields and parameters does not affect the physical observables. We can thus take this arbitrariness to construct certain on-shell renormalization schemes in the unphysical sector such that the on-shell conditions (for tree-mass-pole)

$$\tilde{\Pi}_{WW}(\xi\kappa M_W) = \tilde{\Pi}_{W\pi}(\xi\kappa M_W) = \tilde{\Pi}_{\pi\pi}(\xi\kappa M_W) = \tilde{\Pi}_{c\bar{c}}(\xi\kappa M_W) = 0 \tag{5.32}$$

are satisfied and the $C^a_{\rm mod}$-factor is rigorously simplified according to our general identity (5.30). We have developed four kinds of renormalization schemes in which $C^a_{\rm mod}$ is essentially simplified and no extra explicit calculations of $C^a_{\rm mod}$'s are needed [34][11][35].

a. *Scheme-I* [34]

This is closest to the conventional on-shell scheme. Take $\kappa = M_W$ and $\xi = 1$. Determine Ω_ξ and Ω_κ by the requirement (5.32), and determine other renormalization constants by the usual normalization conditions requiring the residues of the propagators to be unity at $k^2 = \xi\kappa M_W = M_W^2$. In this scheme, the modification factor is simplified as a *single known quantity :*

$$C^a_{\rm mod} = \Omega_\kappa^{-1}\,. \tag{5.33}$$

Note that Ω_κ is already determined by (5.32) during the renormalization, so that this simplification has nothing to do with the explicit calculation of the Δ^a_i's in (5.24).

b. *Scheme-II* [34]

This scheme is valid for gauges with $\xi \neq 0$ and particularly convenient in the 't Hooft-Feynman gauge ($\xi = 1$). We take $\kappa = \xi^{-1} M_W$ with arbitrary nonzero ξ. Set $\Omega_\kappa = 1$, and determine Ω_ξ and Z_π by the requirement (5.32). Other renormalization constants are determined by the usual normalization conditions. In this scheme, the modification factor is completely removed:

$$C^a_{\rm mod} = 1. \tag{5.34}$$

Note that the determination of Z_π in this scheme is different from the usual way. Instead of requiring the residue of $\mathcal{D}_{\pi\pi}$ to be unity, we require directly $\tilde{\Pi}_{\pi\pi} = 0$ at $k^2 = \xi\kappa M_W = M_W^2$. This renormalization procedure is as convenient as the usual one for practical applications.

c. *Scheme-III* [11]

This scheme is specially prescribed for studying the pure V^a_L-scatterings to the precision of neglecting the whole B-term in (5.17) which corresponds to keeping only terms independent of the gauge and Yukawa coupling constants g, e, and y_f. In this case, $C^a_{\rm mod}$ can be completely simplified to unity [as (5.34)] by choosing the renormalization constant Z^a_π

to be

$$Z_\pi^a = \left[\left(\frac{M_a}{M_a^{phys}} \right)^2 Z_{V^a} Z_{M_a}^2 \right]_{g,e,y_f=0} \quad . \tag{5.35}$$

d. *Scheme-IV* [35]

This scheme is prescribed for the R_ξ gauge with arbitrary finite ξ (including $\xi = 0$) and is specially convenient for the Landau gauge ($\xi = 0$). We take $\kappa = M_W$, and $\Omega_\xi = \Omega_\kappa = 1$. Other renormalization constants other than Z_π are determined in the usual normalization conditions at the subtraction point. Only Z_π is specially chosen as

$$Z_\pi = Z_W \frac{Z_{M_W}^2 M_W^2 - \tilde{\Pi}_{WW,0}(M_W^2)}{M_W^2 - \tilde{\Pi}_{\pi\pi,0}(M_W^2)} \tag{5.36}$$

for simplifying $C_{\rm mod}^a$ to be exactly unity [as (5.34)]. The choice of $\Omega_\xi = \Omega_\kappa = 1$ implies that

$$F_0^a = F^a \,, \tag{5.37}$$

i.e. the gauge fixing function is unchanged after the renormalization in this scheme. We finally remark that all the above *Scheme I-IV* are also valid for the $1/\mathcal{N}$-expansion [41] since our formulation is based upon the general WT identities (for self-energies) which take the *same* form in any perturbative expansion.

The generalization of these four renormalization schemes to the full $SU(2) \otimes U(1)$ SM is straightforward but complicated. But our final results are extremely simple and useful, which can be summarized as [34, 11, 35]

$$C_{\rm mod}^W = 1/\Omega_\kappa^{WW} \;, \qquad C_{\rm mod}^Z = 1/\Omega_\kappa^{ZZ} \;, \qquad ({\rm in}\ Scheme\ I)\,, \tag{5.38a}$$

and

$$C_{\rm mod}^W = 1 \;, \qquad C_{\rm mod}^Z = 1, \qquad ({\rm in}\ Scheme\ II - IV)\,. \tag{5.38b}$$

So far, we have completed the analysis of the multiplicative modification factor $C \equiv C_{\rm mod}^{a_1} \cdots C_{\rm mod}^{a_n}$ in (5.17). The remaining task for obtaining the precise formulation of the ET is to make clear the condition for neglecting the additive B-term in (5.17), which will be given in Sec. 5.3.

5.3. ET and its additive modifications

5.3.1. The longitudinal-transverse ambiguity and the precise formulation of the ET

Here we consider the condition for neglecting the B-term in (5.17). We see from (5.17) that the Lorentz invariant (LI) amplitude $T[V_L^{a_1}\cdots V_L^{a_n};\Phi_\alpha]$ can be decomposed into two parts: the 1st part is $C\cdot T[-i\pi^{a_1}\cdots -i\pi^{a_n};\Phi_\alpha]$ which is LI; the 2nd part is the v_μ-suppressed B-term which is Lorentz non-invariant (LNI) because it contains the external spin-1 V_μ-field(s). (Without losing generality [11], here we have assumed that Φ_α contains possible physical scalars, photons and light fermions.). Since the size of the LNI B-term is Lorentz frame dependent, we cannot talk about the condition for neglecting the B-term relative to the LI part $C\cdot T[-i\pi^{a_1}\cdots -i\pi^{a_n};\Phi_\alpha]$ in general Lorentz frames. It makes sense only in a group of Lorentz frames within which Lorentz transformations do not significantly change B (i.e. the V_L-V_T mixing effect is negligible). We call such frames *safe frames*. By examining the Lorentz transformation of B, we can generally estimate B as [11]

$$B=O\left(\frac{M_W^2}{E_j^2}\right)T[-i\pi^{a_1},\cdots,-i\pi^{a_n};\Phi_\alpha]+O\left(\frac{M_W}{E_j}\right)T[V_{T_j}^{a_{r_1}},-i\pi^{a_{r_2}},\cdots,-i\pi^{a_{r_n}};\Phi_\alpha]\ , \tag{5.39}$$

where E_j is the energy of the j-th external V_L^a-line. From (5.39) we see that the condition for a frame to be *safe* is $E_j\sim k_j\gg M_W$ $(j=1,\ 2,\cdots,\ n)$. For a given process, E_j can be easily obtained from the kinematics, so that this condition is easy to implement in practice. Note that the B-term is only $O(M_W/E_j)$-suppressed *relative* to the leading contributions in the GB-amplitude and is therefore *not necessarily* of the $O(M_W/E_j)$ in magnitude. (5.39) explicitly shows that the magnitude of the B-term depends on the size of the amplitudes $T[-i\pi^{a_1},\cdots]$ and $T[V_{T_j}^{a_{r_1}},-i\pi^{a_{r_2}},\cdots]$ so that it can be *either larger or smaller than* $O(M_W/E_j)$ [cf. Eq. (5.46) below].

With this consideration, we can *precisely formulate the ET* as

$$T[V_L^{a_1},\cdots,V_L^{a_n};\Phi_\alpha]=C\cdot T[-i\pi^{a_1},\cdots,-i\pi^{a_n};\Phi_\alpha]+O(M_W/E_j)\text{−suppressed}\ , \tag{5.40}$$

$$E_j\sim k_j\gg M_W,\qquad (\ j=1,2,\cdots,n\ )\ , \tag{5.40a}$$

$$C\cdot T[-i\pi^{a_1},\cdots,-i\pi^{a_n};\Phi_\alpha]\gg B\ , \tag{5.40b}$$

which is in general different from the naive tree-level form (5.1). In the renormalization *Scheme II-IV* the modification factor C in (5.40) is exactly simplified to $C = 1$. Eqs. (5.40a,b) are the precise conditions for the validity of the *longitudinal-Goldstone boson equivalence* in (5.40), i.e. the validity of the ET. Note that (5.40a) is stronger than the usual requirement $E \gg M_W$ (E stands for the center-of- mass energy) for the validity of the ET. The difference between (5.40a) and $E \gg M_W$ has physical significance which has been explicitly shown in Ref. [11].

We emphasize that, in principle, the complete set of diagrams (including those with internal gauge boson lines) has to be considered when calculating $T[-i\pi^{a_1}, \cdots, -i\pi^{a_n}; \Phi_\alpha]$, as already implied in (5.40). If not, this equivalence might not manifest for scattering processes involving t- or u- channel diagram in either forward or backward direction. A detailed discussion on this point is given in Sec. 5.3.2. Furthermore, the ET (5.40) and its high energy condition (5.40a) indicate the absence of infrared (IR) power divergences (like $\left(\frac{E_j}{M_W}\right)^r$, $r > 0$) in the $M_W \to 0$ limit for fixed energy $E_j \sim k_j$ [37]. This can be understood by noting that the limit $M_W \to 0$ implies $g \to 0$ after fixing the physical vacuum expectation value (VEV) at $f_\pi = 246$ GeV. Taking $g \to 0$ limit leads to the well-defined un-gauged linear or non- linear sigma-model which suggests turning off the gauge coupling to be a smooth procedure. The smoothness of the $g \to 0$ limit indicates the absence of IR power divergences for $M_W \to 0$. In our present formalism, we shall fix the gauge boson mass $M_W(M_Z)$ at its experimental value.

Finally, we remark that the condition (5.40b) for ignoring the additive B-term can be technically relaxed by a new prescription, called " Divided Equivalence Theorem " (DET) [35], based upon our (multiplicative) modification-free formulations in Sec. 5.2 (cf. *Scheme II-IV*). The basic observation is that, within *Scheme II-IV*, we have $C^a_{\rm mod} = 1$ so that the *equivalence* in (5.40) can be conveniently divided order by order in a given perturbative expansion: $T = \sum_{\ell=0}^N T_\ell$ and $B = \sum_{\ell=0}^N B_\ell$. I.e., the ET (5.40) can be expanded as

$$T_\ell[V_L^{a_1}, \cdots, V_L^{a_n}; \Phi_\alpha] = T_\ell[-i\pi^{a_1}, \cdots, -i\pi^{a_n}; \Phi_\alpha] + B_\ell \quad , \tag{5.41}$$

and the conditions (5.40a,b) become, at the ℓ-th order,

$$E_j \sim k_j \gg M_W, \qquad (\ j = 1, 2, \cdots, n\ ) \ , \tag{5.41a}$$

$$T_\ell[-i\pi^{a_1},\cdots,-i\pi^{a_n};\Phi_\alpha] \gg B_\ell \quad , \qquad (\ \ell = 0,1,2,\cdots\ ) \ . \tag{5.41b}$$

The ℓ-th order B-term is deduced from (5.39):

$$B_\ell = O\left(\frac{M_W^2}{E_j^2}\right) T_\ell[-i\pi^{a_1},\cdots,-i\pi^{a_n};\Phi_\alpha] + O\left(\frac{M_W}{E_j}\right) T_\ell[V_{T_j}^{a_{r_1}},-i\pi^{a_{r_2}},\cdots,-i\pi^{a_{r_n}};\Phi_\alpha] \ . \tag{5.42}$$

When the NLO ($\ell = 1$) contributions (containing possible new physics effects) are included, the main limitation on the predication of the ET for the V_L-amplitude via computing the GB-amplitude is due to ignoring the *leading order B_0-term.* This leading order B_0-term is of $O(g^2)$ [11] in the heavy Higgs SM and the EWCL and cannot always be neglected in comparison with the NLO GB-amplitude T_1 though we usually have $T_0 \gg B_0$ and $T_1 \gg B_1$ respectively (cf. Ref. [11, 9] and Sec. 6 below) because of (5.42). Based upon the above new equations (5.41)-(5.42), we can precisely formulate the ET at *each given order-ℓ* where only B_ℓ , *but not the whole B-term*, will be ignored to build the longitudinal-Goldstone boson equivalence. Hence, *the equivalence is divided order by order* in the perturbative expansion. The condition for this divided equivalence is $T_\ell \gg B_\ell$ (at the ℓ-th order) which is much weaker than $T_\ell \gg B_0$ [deduced from (5.40b)] by a factor of B_ℓ/B_0 (< 1) for $\ell \geq 1$. Therefore, to improve the numerical prediction of V_L-amplitude for most of the NLO contributions (in T_1) by using the ET, we propose the following simple new prescription (called the DET):

(i). Perform a direct and precise unitary gauge calculation for the tree-level V_L-amplitude $T_0[V_L]$ which is quite simple.

(ii). Make use of the DET (5.41) and deduce $T_1[V_L]$ from the Goldstone boson amplitude $T_1[GB]$, by ignoring B_1 only.

The direct tree-level unitary gauge calculation of V_L-amplitude avoids any approximation at this order and is shown [35] to be much simpler than computing the corresponding GB-amplitude plus the very complicated B_0-term in the R_ξ-gauge (as adopted in Ref. [42] before). In Ref. [35], we further demonstrated that, up to NLO of the EWCL, the precision of the DET (5.40-42) is typically increased by a factor of $B_0/B_1 \simeq \Lambda^2/E^2$ (~ 10 at the TeV scale) relative to the usual prescription of the ET [cf. (5.40a,b)] as ignoring the B-term is concerned. But, we need to clarify that, though the DET technically improves the

precision of predicating the V_L-amplitude, it does *not* increase the "equivalence" between the *whole* V_L and GB amplitudes [which is still limited by the condition *(5.40b)* besides (5.40a)]. The Lorentz non-invariant leading B_0-term is always there to modify the overall "equivalence" in (5.40) and sets up a necessary *physical criterion* for the sensitivity on probing the Goldstone dynamics from measuring the V_L-amplitude, in spite that we can numerically include B_0 via the DET. This important physical content of the ET will be further analyzed in Sec. 5.4.

5.3.2. On the kinematic singularity

Here we examine the validity of the ET in some special kinematic regions and its physical implication in probing the EWSB, which often cause confusion in the literature. It is known that there are kinematic regions in which the Mandelstam variables t or u is small or even vanishing despite the fact that $\sqrt{s} \gg M_W$ for high energy scatterings. Therefore, the amplitude that contains a t- or u-channel diagram with massless photon field can generate a kinematic singularity when the scattering angle θ approaches to 0° or 180°. In the following, we study in such special kinematic regions whether the B-term [cf. (5.17)] can be safely ignored to validate the ET and its physical consequence to probing the EWSB sector.

For illustration, let us consider the tree level $W_L^+W_L^- \to W_L^+W_L^-$ scattering in the chiral Lagrangian formalism. Generalization to loop orders is obvious since the kinematic problem analyzed here only concerns the one-particle-reducible (1PR) internal W, Z or photon line in the t-channel (or u-channel) diagram. Both the tree level $W_L^+W_L^- \to W_L^+W_L^-$ and $\pi^+\pi^- \to \pi^+\pi^-$ amplitudes in the chiral Lagrangian formalism contain contact diagrams, s-channel Z-exchange and photon-exchange diagrams, and t-channel Z-exchange and photon-exchange diagrams. In the C.M. frame, the precise tree-level

amplitudes $T[W_L]$ and $T[\mathrm{GB}]$ are:

$$T[W_L] = ig^2 \left[-(1+\kappa)^2 \sin^2\theta + 2\kappa(1+\kappa)(3\cos\theta - 1) - \mathrm{c}_\mathrm{w}^2 \frac{4\kappa(2\kappa+3)^2\cos\theta}{4\kappa + 3 - \mathrm{s}_\mathrm{w}^2 \mathrm{c}_\mathrm{w}^{-2}} \right.$$
$$\left. + \mathrm{c}_\mathrm{w}^2 \frac{8\kappa(1+\kappa)(1-\cos\theta)(1+3\cos\theta) + 2[(3+\cos\theta)\kappa + 2][(1-\cos\theta)\kappa - \cos\theta]^2}{2\kappa(1-\cos\theta) + \mathrm{c}_\mathrm{w}^{-2}} \right]$$
$$+ ie^2 \left[-\frac{\kappa(2\kappa+3)^2\cos\theta}{\kappa+1} + 4(1+\kappa)(1+3\cos\theta) + \frac{[(3+\cos\theta)\kappa+2][(1-\cos\theta)\kappa - \cos\theta]^2}{\kappa(1-\cos\theta)} \right] \quad , \tag{5.43a}$$

$$T[\mathrm{GB}] = ig^2 \left[\frac{(1+\cos\theta)}{2}\kappa + \frac{1}{3} + \frac{(\mathrm{c}_\mathrm{w}^2 - \mathrm{s}_\mathrm{w}^2)^2}{2\mathrm{c}_\mathrm{w}^2} \left(-\frac{2\kappa\cos\theta}{4\kappa + 3 - \mathrm{s}_\mathrm{w}^2\mathrm{c}_\mathrm{w}^{-2}} + \frac{(3+\cos\theta)\kappa + 2}{2(1-\cos\theta)\kappa + \mathrm{c}_\mathrm{w}^{-2}} \right) \right]$$
$$+ ie^2 \left[-\frac{4\kappa\cos\theta}{4\kappa+1} + \frac{(3+\cos\theta)\kappa + 2}{(1-\cos\theta)\kappa} \right] \quad , \tag{5.43b}$$

where $\kappa \equiv p^2/M_W^2$ with p equal to the C.M. momentum; $\mathrm{s_w} \equiv \sin\theta_\mathrm{W}$, $\mathrm{c_w} \equiv \cos\theta_\mathrm{W}$ with θ_W equal to the weak mixing angle; and θ is the scattering angle. In (5.43a) and (5.43b) the terms without a momentum factor in the denominator come from contact diagrams, terms with denominator independent of scattering angle come from s-channel diagrams and terms with denominator containing a factor $1-\cos\theta$ are contributed by t-channel diagrams. Let us consider two special kinematic regions defined below.

(i). In the limit of $\theta \to 0°$:

As $\theta \to 0°$, the t-channel photon propagator has a kinematic pole, but both W_L and GB amplitudes have the *same* pole structure, i.e.

$$\begin{aligned} (T[W_L] - T[\mathrm{GB}])_{\text{pole term}} &= -ie^2 \left[\frac{[(3+\cos\theta)\kappa + 2]\cos^2\theta}{(1-\cos\theta)\kappa} - \frac{(3+\cos\theta)\kappa + 2}{(1-\cos\theta)\kappa} \right] \\ &= -ie^2(1+\cos\theta)(3+\cos\theta+2\kappa^{-1}) = O(g^2) \quad , \end{aligned} \tag{5.44}$$

which is finite.[7] Hence, *the B-term, which is defined as the difference* $T[W_L] - T[\mathrm{GB}]$, *is finite at* $\theta = 0°$, *and is of* $O(g^2)$. This means that when θ is close to the t-channel

[7] This conclusion can be directly generalized to other t or u channel processes.

photon pole, the B-term is negligibly small relative to the GB-amplitude so that (5.40b) is satisfied and the ET works. More explicitly, in the limit of $\theta = 0^\circ$ (i.e. $t = 0$), and from (5.43a,b), the W_L and GB amplitudes are

$$\begin{aligned} T[W_L] &= i\left[4(3-8\mathrm{c}_\mathrm{w}^2+8\mathrm{c}_\mathrm{w}^4)\frac{p^2}{f_\pi^2}+2e^2\left(2+\frac{M_W^2}{p^2}\right)\frac{1}{1-c_0}\right]+O(g^2) \quad , \\ T[\mathrm{GB}] &= i\left[4(3-8\mathrm{c}_\mathrm{w}^2+8\mathrm{c}_\mathrm{w}^4)\frac{p^2}{f_\pi^2}+2e^2\left(2+\frac{M_W^2}{p^2}\right)\frac{1}{1-c_0}\right]+O(g^2) \quad , \\ T[W_L] &= T[\mathrm{GB}]+O(g^2) \quad , \end{aligned} \tag{5.45}$$

where $c_0 \equiv \lim_{\theta\to 0}\cos\theta$. Notice that in this case one cannot make the M_W^2/t expansion[8] because t vanishes identically. Since both W_L and GB amplitudes have exactly the same kinematic singularity and the B-term is much smaller than $T[\mathrm{GB}]$, *the ET still holds* in this special kinematic region. We also emphasize that *in the kinematic regions where t or u is not much larger than M_W^2, the t-channel or u-channel internal gauge boson lines must be included according to the precise formulation of the ET* [cf. (5.40) and (5.40a,b)]. This does not imply, in any sense, a violation of the ET since the ET, cf. (5.40) and (5.40a,b), does not require either $t \gg M_W$ or $u \gg M_W$.

(ii). In the limit of $\theta \to 180^\circ$:

In the kinematic region with $s,\ t \gg M_W^2$, (5.41a) and (5.41b) yield

$$\begin{aligned} T[W_L] &= i\left[2(1+\cos\theta)\frac{p^2}{f_\pi^2}+O(g^2)\right] \quad , \\ T[\mathrm{GB}] &= i\left[2(1+\cos\theta)\frac{p^2}{f_\pi^2}+O(g^2)\right] \quad , \\ T[W_L] &= T[\mathrm{GB}]+O(g^2) \quad , \end{aligned} \tag{5.46}$$

where the $O(g^2)$ term is the largest term we ignored which denotes the order of the B-term [cf. (5.48)]; all other terms we ignored in (5.44) are of $O(M_W^2/p^2)$ or $O(e^2)$ which are smaller than $O(g^2)$ and thus will not affect the order of magnitude estimate of the B-term. For $s,\ t \gg M_W^2$, the W_L and GB amplitudes are dominated by the p^2-term

---

[8] This expansion is *unnecessary* for the validity of the ET, cf. (5.40) and (5.40a,b).

in (5.46), which is actually proportional to u for this process. When the scattering angle θ is close to 180°, u becomes small and thus this leading p^2 term is largely suppressed so that both the W_L and GB amplitudes can be as small as the B-term, i.e. of $O(g^2)$. In this case our condition (5.40a) is satisfied while (5.40b) is not, which means that the EWSB sector cannot be sensitively probed for this kinematic region. Since the total cross section of this process is not dominated by this special kinematic region and is mainly determined by the un-suppressed leading large p^2-term, so *the kinematic dependence of the amplitude will not affect the order of magnitude of the total cross section.* Hence, *our application of the power counting analysis in Sec. 7 for computing the total event rates remains valid even though we have ignored the angular dependence in estimating the magnitude of the scattering amplitudes.* Neglecting the angular dependence in the amplitude may cause a small difference in the event rate as compared to that from a precise calculation. For the processes such as $W_L^\pm W_L^\pm \to W_L^\pm W_L^\pm$ and $W_L^+ W_L^- \to Z_L Z_L$, the leading p^2-term is proportional to s/f_π^2 with no angular dependence, so that the angular integration causes *no difference* between our power counting analysis and the exact calculation for the leading p^2-term contribution.[9] In the above example for $W_L^+ W_L^- \to W_L^+ W_L^-$ channel [cf. (5.46)], the leading amplitude is proportional to $-u/f_\pi^2$. When applying the power counting method, we ignore the θ-dependence and estimate it as s/f_π^2 . In computing the total rate, we integrate out the scattering angle. This generates a difference from the precise one:

$$\frac{\int_{-1}^{1} u^2 \, \mathrm{d}\cos\theta}{\int_{-1}^{1} s^2 \, \mathrm{d}\cos\theta} = \frac{1}{3} \quad ,$$

which, as expected, is only a factor of 3 and does not affect our order of magnitude estimates.

Finally, we make a precise numerical analysis on the equivalence between the W_L and the GB amplitudes to show how well the ET works in different kinematic regions and its implication to probing the EWSB sector. We use the full expressions (5.43a,b) for W_L and GB amplitudes as required by the ET, cf. (5.40) and (5.40a,b). In Fig. 1a, we plot the ratio

---

[9] The small difference (a factor of 1.4) in Fig. 4 mainly comes from neglecting the tree level sub-leading terms in our order of magnitude estimate for the amplitudes.

$|B/g^2|$ for scattering angle $\theta = 2°, 10°, 45°, 90°, 100°, 120°, 135°, 150°, 180°$. It shows that the LNI B-term is *always of* $O(g^2)$ *in the whole kinematic region,* and thus is irrelevant to the EWSB sector, in accordance with our general physical analysis in Sec. 5.4 below. Hence, to have a sensitive probe of the EWSB mechanism, condition (5.40b) [or (5.47)] must be satisfied. Fig. 1b shows that for $0° \leq \theta \leq 100°$, the ratio $|B/T[W_L]| \leq 10\%$ when $M_{WW} \geq 500\,\text{GeV}$. For $\theta \geq 120°$, this ratio becomes large and reaches $O(1)$ when θ is close to 180°. This is because the kinematic factor $(1 + \cos\theta)$, associated with the leading p^2 term [cf. (5.46)], becomes small. This, however, will not alter the conclusion that for $4W_L$-scattering the total cross section from T[GB] is much larger than that from the B-term as $M_{WW} \geq 500\,\text{GeV}$.[10] Note that in Fig. 1b, for $\theta \leq 10°$, i.e. close to the t-channel photon pole, the ratio $|B/T[W_L]|$ is below 1% and thus the ET holds very well. In Fig. 1c, we plot both the W_L and GB amplitudes for $\theta = 10°, 45°, 100°, 150°$. The solid lines denote the complete W_L amplitude and the dotted lines denote the GB amplitude. We find that when $\theta \leq 100°$, the GB amplitude is almost indistinguishable from the W_L amplitude. For $\theta = 150°$, the W_L amplitude is of the same order as the B-term, i.e. of $O(g^2)$, when $M_{WW} < 1\,\text{TeV}$. In this case the W_L or GB amplitude is too small and the strongly coupled EWSB sector cannot be sensitively probed. As the energy E increases, we see that the W_L and GB amplitudes rapidly dominate over the B-term and agree better and better even for large scattering angles. Finally, using the effective-W method [43], we compare the LHC production rates in Figs. 2a and 2b for the invariant mass (M_{WW}) and the polar angle ($\cos\theta$) distributions, respectively. To avoid the t-channel photon singularity (at $\theta = 0°$) in the phase space integration, we add an angular cut $-1.0 \leq \cos\theta \leq 0.8$ (i.e., $36.9° \leq \theta \leq 180°$). Fig. 2a shows that the total cross sections computed from the W_L and the GB amplitudes [cf. eq. (5.41)] indeed agree with each other very well. From Fig. 2b, we see that the difference clearly appears only for the region of large scattering angle (i.e., $\cos\theta < -0.6$ or $\theta > 127°$) where both the leading W_L and GB amplitudes are suppressed by the kinematic factor $1 + \cos\theta$ and

---

[10] In practice, this is even more true after applying the necessary kinematic cuts to require the final state W-bosons to be in the central rapidity region of the detector for detecting the signal event [4], so that the θ angle cannot be close to either 180° or 0°.

thus the event rates are too low to be sensitive to the EWSB sector. Hence, the difference from the large θ region has only *negligible* effects on the total cross sections, as clearly shown in Fig. 2a. This also agrees with our conclusion from Figs. 1a-c. We have also made the comparison with symmetric angular cuts (such as $|\cos\theta| \leq 0.8$) and found similar good agreement to that in Fig. 10d. This is clear since in the large θ region the event rates become much lower and are close to their difference, i.e., of $O(|R_B|)$.

The above conclusions hold for the tree level contributions from the lowest order operators in $\mathcal{L}_{\rm G} + \mathcal{L}^{(2)} + \mathcal{L}_{\rm F}$, cf. (5.2). However, independent of the kinematic region considered, not all the contributions from the NLO effective operators can dominate the B-term and satisfy the condition (5.40b) [or (5.47)]. This is why the condition (5.40b) [or (5.47)] can serve as the criterion for classifying the sensitivities of these NLO operators in probing the EWSB sector for a given scattering process.

We therefore conclude that for the process considered here *the B-term, as defined in (5.17), can be at most of* $O(g^2)$ *for all kinematic regions* (cf. Fig. 1a), and is insensitive to the EWSB mechanism, in accordance with our general analysis in Sec. 5.4. *When* t *or* u *is not large, the* t*- or* u*-channel internal lines must be included.* We find that in certain kinematic region *even* t *(or* u*) is close to zero, the ET still works well* [cf. Eq. (5.45) and Fig. 1b]. This is because the validity of the ET does not require either $t \gg M_W^2$ or $u \gg M_W^2$ [cf. (5.40) and (5.40a,b)]. For some scattering processes, there may be special kinematic regions in which the GB and the W_L amplitudes are largely suppressed[11] so that the EWSB sector cannot be sensitively probed in these special kinematic regions (cf. Figs. 1b,c and 2b). But, as shown in this work, measuring the total event rates from these processes can still be used to sensitively probe the EWSB sector (cf. Fig. 2a and Figs. 4-12).

5.4. Formulating the ET as a Criterion for Probing the EWSB

In Sec. 5.3.1, we decomposed the amplitude $T[V_L^{a_1}, \cdots, V_L^{a_n}; \Phi_\alpha]$ into the LI part and

[11] This large suppression can also arise from the polarization effects of the in/out states.

the LNI part. Such a decomposition shows the *essential difference* between the V_L- and the V_T-amplitudes: the former contains a LI GB-amplitude that can yield a large V_L-amplitude in the case of strongly coupled EWSB sector, but the latter does not. We note that only the LI part (the GB-amplitude) of the V_L-amplitude is *sensitive* to probing the EWSB sector, while its LNI part, containing a significant *Lorentz-frame-dependent* B-term (which is related to the V_L-V_T mixing effects under proper Lorentz transformations), is *insensitive* to the EWSB mechanism. Thus the B-term serves as an intrinsic background to the probe of the EWSB mechanism, and for a *sensitive and unambiguous* probe of the EWSB, the LI GB-amplitude should dominate the V_L-amplitude and the LNI B-term should be negligible. It is obvious that one can technically improve the prediction for the V_L-amplitude from the right-hand side (RHS) of (5.17) by including the complicated B-term (or part of B) [42] or even directly calculate its left-hand side (LHS) of (5.17) despite the complexity. However, this is *not* an improvement of the longitudinal-Goldstone boson *equivalence* and thus the sensitivity of probing the EWSB mechanism via V_L-scattering experiments. *The physical content of the ET is essentially independent of how to numerically compute the V_L-amplitude.*

Now we study the precise meaning of the condition (5.40b) for neglecting the B-term, i.e. the condition for sensitively probing the EWSB mechanism. The amplitude T, to a finite order, can be written as $T = \sum_{\ell=0}^{N} T_\ell$ in the perturbative calculation. Let $T_0 > T_1, \cdots, T_N \geq T_{\rm min}$, where $T_{\rm min} = \{T_0, \cdots, T_N\}_{\rm min}$, then condition (5.40b) and eq. (5.39) imply

$$T_{\rm min}[-i\pi^{a_1}, \cdots, -i\pi^{a_n}; \Phi_\alpha] \gg$$
$$O\left(\frac{M_W^2}{E_j^2}\right) T_0[-i\pi^{a_1}, \cdots, -i\pi^{a_n}; \Phi_\alpha] + O\left(\frac{M_W}{E_j}\right) T_0[V_{T_j}^{a_{r_1}}, -i\pi^{a_{r_2}}, \cdots, -i\pi^{a_{r_n}}; \Phi_\alpha] \quad . \tag{5.47}$$

Note that the above formulation of the ET discriminates processes which are insensitive to probing the EWSB sector when either (5.40a) or (5.40b) fails. Furthermore, *as a necessary criterion, condition (5.47) determines whether or not the corresponding V_L-scattering process in (5.40) is sensitive to probing the EWSB sector to the desired precision in perturbative calculations.*

From (5.39) or the RHS of (5.47) and the precise electroweak power counting rule (cf. Sec.3.2), we can directly estimate the *largest* model-independent B-term to be $B_{\rm max} =$

$O(g^2)f_\pi^{4-n}$ in the EWCL formalism, which comes from the n-particle pure V_L-amplitude. (This conclusion also holds for the heavy Higgs SM.) It is crucial to note that $B_{\rm max}$ is of the same order of magnitude as the leading V_T-amplitude:

$$B_{\rm max} \approx T_0[V_T^{a_1}, \cdots, V_T^{a_n}] = O(g^2)f_\pi^{4-n} \quad . \tag{5.48}$$

Since both the largest B-term and the leading V_T-amplitude are of $O(g^2)$, they are therefore irrelevant to the EWSB mechanism as pointed out in the above discussion. Thus, *(5.47) provides a useful criterion for discriminating physical processes which are sensitive, marginally sensitive, or insensitive to the EWSB sector.*

In conclusion, our formulation of the ET provides a necessary criterion for probing the EWSB sector as follows. If the ET is valid for a scattering process to the order of $T_{\rm min}$ [i.e. $T_{\rm min} \gg B_0$, cf. (5.47), where B_0 is the tree-level leading contribution to B.], this process is classified to be *sensitive* to probing $T_{\rm min}$. Otherwise, we classify this process to be either *marginally sensitive* (for $T_{\rm min} > B_0$ but $T_{\rm min} \not\gg B_0$) or *insensitive* (for $T_{\rm min} \leq B_0$) to testing $T_{\rm min}$. This classification is given at the level of the S-matrix elements. Up to the next-to-leading order, $T_{\rm min} = T_1$. For this case, by simply squaring both side of the condition (5.47) and integrating over the phase space, we can easily derive the corresponding condition (criterion) at the level of the constituent cross sections for $\hat{\sigma}_1 \simeq \int_{\rm phase} 2T_0T_1$ and $\hat{\sigma}_B \simeq \int_{\rm phase} 2T_0B_0$, where $\int_{\rm phase}$ denotes the phase space integration. The constituent cross sections ($\hat{\sigma}$) are functions of the invariant mass ($\sqrt{\hat{s}}$) of the final state weak bosons. Defining the differential parton luminosity (for either the incoming light fermion or the weak boson) as $\frac{{\rm d}\,\mathcal{L}_{\rm partons}}{{\rm d}\,\hat{s}}$, the total cross section is thus given by

$$\sigma \;=\; \int {\rm d}\,\hat{s}\,\frac{{\rm d}\,\mathcal{L}_{\rm partons}}{{\rm d}\,\hat{s}}\hat{\sigma}(\hat{s}) \quad . \tag{5.49}$$

Using (5.49) we can further derive the corresponding conditions for total event rates R_1 (calculated from $\hat{\sigma}_1$) and R_B (calculated from $\hat{\sigma}_B$), and then define the corresponding criterion for testing the sensitivities of various operators and processes at the level of event rates. They are: (i). Sensitive, if $R_1 \gg R_B$; (ii). Marginally sensitive, if $R_1 > R_B$, but $R_1 \not\gg R_B$; (iii). Insensitive, if $R_1 \leq R_B$. A specific application to the LHC physics is given in Sec. 7. We note that, at the event rate level, the above criterion is *necessary* but not sufficient since the leading B-term, of the same order as the LNI V_L-V_T

mixing effects [cf. (5.39)] and as an intrinsic background to any strong V_L-V_L scattering process, denotes a universal part of the full backgrounds [44]. The sufficiency will of course require detailed numerical analyses on the detection efficiency for suppressing the full backgrounds to observe the specific decay mode of the final state (cf. Ref. [4]). This is beyond our present first step theoretical global study. Some general discussions on the experimental detections will be presented in Sec. 8.

Before concluding this section, we note that in our power counting analysis (cf. Sec.4), *both the GB-amplitude and the B-term are explicitly estimated* (cf. Tables 1-4 in Sec.4). The issue of numerically including/ignoring B in an explicit calculation is *essentially irrelevant* here. If $T_1 \leq B$, this means that the sensitivity is poor so that the probe of T_1 is experimentally harder and requires a higher experimental precision of at least the order of B to test T_1.

6. Global Classifications for S-matrix Elements

Armed with the above counting rule (4.5), we can conveniently estimate contributions from all effective operators in the EWCL to any high energy scattering process. In the literature (cf. Ref. [4]), what usually done was to study only a small subset of all effective operators for simplicity. But, to discriminate different underlying theories for a complete test of the EWSB mechanism, it is necessary to measure all these operators via various high energy processes. As the first step global study, our electroweak power counting analysis makes it possible to quickly grasp the overall physical picture which provides a useful guideline for selecting relevant operators and scattering processes to perform further detailed numerical studies. In this and the next sections, we shall systematically classify all possible NLO effective operators for both the S-matrix elements and event rates at the LHC and the LC.

6.1. Power Counting Hierarchy

We concentrate on the high energy weak-boson fusion and quark-anti-quark annihilation processes. As shown in Refs. [4, 45], for the non-resonance case, the most

important fusion process for probing the EWSB sector is the same-charged channel: $W^\pm W^\pm \to W^\pm W^\pm$, which gets dominant contributions from the 4-GB vertices in the EWCL. In Tables Ia and 1b we estimate the contributions from the lowest order (model-independent) operators in $\mathcal{L}_{\rm MI} \equiv \mathcal{L}_{\rm G} + \mathcal{L}_{\rm F} + \mathcal{L}^{(2)}$ up to one-loop and from all the NLO (model-dependent) bosonic operators in (2.2) at the tree-level for $W^\pm W^\pm \to W^\pm W^\pm$. The contributions of different operators to a given amplitude are different due to their different structures. For instance, the commonly discussed operators $\mathcal{L}_{4,5}$ contribute the model-dependent leading term of $O\left(\frac{E^2}{f_\pi^2}\frac{E^2}{\Lambda^2}\right)$ to the $T[4W_L]$ amplitude, and the sub-leading term of $O\left(g\frac{E}{f_\pi}\frac{E^2}{\Lambda^2}\right)$ to the $T[3W_L, W_T]$ amplitude, while $\mathcal{L}_{3,9}$ give their largest contributions to $T[3W_L, W_T]$ rather than $T[4W_L]$ at high energies. The model-independent and model-dependent contributions to various B-terms are summarized in Tables IIa and IIb, in which $B_\ell^{(i)}$ $(i = 0, \cdots, 3;\ \ell = 0, 1, \cdots)$ denotes the B-term from V_L-amplitudes containing i external V_T-lines with $B_0^{(i)}$ obtained from the leading order and $B_1^{(i)}$ from the NLO calculations. We see that the largest B-term is $B_0^{(0)}$ from the $4W_L$ amplitudes, as given in (5.48). The term $B_0^{(0)}$ [of $O(g^2)$], is a model-independent constant containing only the SM gauge coupling constants. All the other B-terms are further suppressed by a factor of M_W/E or $(E/\Lambda)^2$, or their product.

For all the $q\bar{q}^{(\prime)} \to V^a V^b$ processes (with q or $q^{(\prime)}$ being light quarks except the top), which get dominant contributions from s-channel diagrams (containing the V_T-GB-GB vertices), the model-independent and the model-dependent contributions are estimated in Tables III and IV, respectively. Note that the tree-level $q\bar{q} \to ZZ$ annihilation process has no model-dependent NLO contribution, therefore to probe new physics in the EWSB sector, we have to study $q\bar{q}^{(\prime)} \to W^+W^-$, $W^\pm Z$ annihilations. As shown in Tables IVa and IVb, the operators $\mathcal{L}_{2,3,9}$ give the leading contributions, of $O\left(g^2\frac{E^2}{\Lambda^2}\right)$, to $q\bar{q} \to W^+W^-$ via $T_1[q\bar{q}; W_L^+W_L^-]$ channel;[12] and the operators $\mathcal{L}_{3,11,12}$ give the same leading contributions to $q\bar{q}' \to W^\pm Z$ via $T_1[q\bar{q}'; W_L^\pm Z_L]$ channel. But $\mathcal{L}^{(2)\prime}$ does not contribute any positive E-power term to any of the V^aV^b final states via tree-level

[12] We note that the contributions from $\mathcal{L}_2$ (and also $\mathcal{L}_{1,13}$) are always associated with a suppressing factor $\sin^2\theta_W \sim \frac{1}{4}$.

quark-anti-quark annihilations. Tables III and IV also show that the largest B-term is $B = B_0^{(1)} = O\left(g^2 \frac{M_W}{E}\right)$ which is model-independent and comes from $T_0[q\bar{q}^{(\prime)}; V_T, v]$, a part of the $T_0[q\bar{q}^{(\prime)}; V_T, V_L]$ amplitude (cf. Table IIIa). All model-dependent B-terms, as listed in Tables IVa and IVb, are either constant terms of $O\left((g^4, e^2g^2)\frac{f_\pi^2}{\Lambda^2}\right)$ or further suppressed by negative E-power(s) and are thus negligibly small.

From Tables I-II, we further classify in Table V the sensitivities to all the bosonic operators for probing the EWSB sector either directly (from pure GB interactions) or indirectly (from interactions suppressed by the SM gauge coupling constants). The same classification for all $q\bar{q}^{(\prime)} \to V^a V^b$ annihilation processes is separately given in Table VI. The classifications in Tables V and VI are based upon the following hierarchy in the power counting:

$$\frac{E^2}{f_\pi^2} \gg \left[\frac{E^2}{f_\pi^2}\frac{E^2}{\Lambda^2},\ g\frac{E}{f_\pi}\right] \gg \left[g\frac{E}{f_\pi}\frac{E^2}{\Lambda^2},\ g^2\right] \gg \left[g^2\frac{E^2}{\Lambda^2},\ g^3\frac{f_\pi}{E}\right] \gg \left[g^3\frac{Ef_\pi}{\Lambda^2},\ g^4\frac{f_\pi^2}{E^2}\right] \gg g^4\frac{f_\pi^2}{\Lambda^2} \quad . \tag{6.1}$$

In the typical TeV region, for $E \in (750\,\mathrm{GeV},\ 1.5\,\mathrm{TeV})$, this gives:

$$\begin{aligned}(9.3, 37) \gg [(0.55, 8.8), (2.0, 4.0)] \gg [(0.12, 0.93), (0.42, 0.42)] \gg \\ [(0.025, 0.099), (0.089, 0.045)] \gg [(5.3, 10.5), (19.0, 4.7)] \times 10^{-3} \gg (1.1, 1.1) \times 10^{-3}\ ,\end{aligned} \tag{6.2}$$

where E is taken to be the invariant mass of the VV pair. The numerical values in (6.2) convincingly show the existence of the power counting hierarchy in (6.1). This governs the order of magnitude of the results from detailed numerical calculations. This hierarchy makes it possible to conveniently and globally classify the sensitivities of various scattering processes to the complete set of the effective operators in the EWCL. The construction of this power counting hierarchy is based upon the property of the chiral perturbation expansion and can be understood as follows. The leading term $\frac{E^2}{f_\pi^2}$ in (6.1) comes from the model-independent lowest order $4V_L$ ($\neq 4Z_L$) scatterings. Starting from this leading term, (6.1) is built up by *increasing either the number of derivatives (i.e. the power of E/Λ) or the number of external transverse gauge bosons (i.e. the power of gauge coupling constants).* The NLO contributions from the derivative expansion are always suppressed by E^2/Λ^2 relative to the model-independent leading term. Also, for each given process, when an external V_L-line is replaced by a corresponding V_T-line, a factor

$\frac{E}{f_\pi}$ in the amplitude would be replaced by a gauge coupling g (or g').[13] This explains why the power counting hierarchy takes the form of (6.1).

6.2. Classifications for VV-fusions and $f\bar{f}'$-annihilations

Tables V and VI are organized in accordance with the power counting hierarchy given in (6.1) for all VV-fusion and $q\bar{q}^{(\prime)}$-annihilation amplitudes. It shows the *relevant* effective new physics operators and the corresponding physical processes for probing the EWSB sector when calculating the scattering amplitudes to the required precision. For instance, according to the classification of Table V, the model-independent operator $\mathcal{L}_{\rm MI}$ can be probed via studying the leading tree-level scattering amplitude $T_0[4V_L]$ $(\neq T_0[4Z_L])$ which is of $O\left(\frac{E^2}{f_\pi^2}\right)$. A sensitive probe of $\mathcal{L}_{\rm MI}$ via this amplitude requires $T_0 \gg B_0$, i.e., $O\left(\frac{E^2}{f_\pi^2}\right) \gg O(g^2)$ or $(2M_W/E)^2 \ll 1$ which can be well satisfied in the high energy region $E \geq 500$ GeV. We note that the test of the leading order operator $\mathcal{L}_{\rm MI}$ will first distinguish the strongly interacting EWSB sector from the weakly interacting one. To test the model-dependent operators $\mathcal{L}_{4,5,6,7,10}$ demands a higher precision than the leading tree level contribution by a factor of $\frac{E^2}{\Lambda^2}$. As an example, in order to sensitively test the $\mathcal{L}_{4,5}$ operators with coefficients of $O(1)$ via the $4V_L$-processes, the criterion (5.47) requires $O\left(\frac{E^2}{f_\pi^2}\frac{E^2}{\Lambda^2}\right) \gg O(g^2)$, or, $(0.7\text{TeV}/E)^4 \ll 1$. This indicates that sensitively probing $\mathcal{L}_{4,5}$ via the $4V_L^{\pm}$-scatterings requires $E \geq 1$ TeV. Thus, we find that, in the TeV region, the $4V_L$ scatterings can sensitively probe $\mathcal{L}_{4,5}$; while, similarily, $\mathcal{L}_{6,7}$ can be probed via $2W_L+2Z_L$ or $4Z_L$ scattering and $\mathcal{L}_{10}$ can only be tested via $4Z_L$ scattering. As shown in Table III, to probe the operators $\mathcal{L}_{2,3,9,11;12}$, one has to detect the $3V_L+V_T$ scatterings, which are further suppressed by a factor $\frac{M_W}{E}$ relative to the leading model-dependent contributions from the $\mathcal{L}_{4,5}$ and $\mathcal{L}_{6,7,10}$ via $4V_L$ processes. Since the model-independent leading order $2V_T+2V_L$ and $4V_T$ amplitudes (from $\mathcal{L}_{\rm MI}$) and the largest constant B-term

---

[13] The counting on the amplitudes $T_0[4W_T]$ and $T_0[q\bar{q}^{(\prime)}; V_TV_T]$ are exceptions of this rule since they have a contribution from the tree-level pure Yang-Mills gauge term $\mathcal{L}_{\rm G}$. These two similar exceptions can be found at the second line of Tables Ia and IIIa, respectively.

$\left(B_0^{(0)}\right)$ are all around of the same order, i.e. $O\left(g\frac{E}{f_\pi}\frac{E^2}{\Lambda^2}, g^2\right)$ [cf. (6.2)],[14] it requires a significantly higher precision to sensitively probe the operators $\mathcal{L}_{2,3,9,11;12}$ which can only contribute the g-suppressed indirect EWSB information and therefore are more difficult to be tested. Here the ratio $B_0/T_1 \sim g^2/\left[g\frac{E}{f_\pi}\frac{E^2}{\Lambda^2}\right]$ gives $(1.15\text{TeV}/E)^3 \simeq 0.45 \not\ll 1$ for $E = 1.5$ TeV, which shows the probe of these operators is at most marginally sensitive when their coefficients $\ell_n = O(1)$. Finally, the operators $\mathcal{L}_{1,8;13,14}$ can be probed via the amplitude $T_1[2V_L, 2V_T]$ $(\neq T_1[2Z_L, 2Z_T])$ which is of $O\left(g^2\frac{E^2}{\Lambda^2}, g^3\frac{f_\pi}{E}\right)$ and numerically much smaller [cf. (6.2)] in comparison with the leading B-term in (5.48). Therefore, $\mathcal{L}_{1,8;13,14}$ should be effectively probed via scattering processes other than the VV-fusions.

We then look at Table VI for $q\bar{q}^{(\prime)}$-annihilations. For the lowest order Lagrangian $\mathcal{L}_{\rm MI} = \mathcal{L}_{\rm G} + \mathcal{L}^{(2)} + \mathcal{L}_{\rm F}$, the model-independent operators $\mathcal{L}^{(2)}$ and $\mathcal{L}_{\rm G}$ can be probed via tree-level amplitudes [of $O(g^2)$] with V_LV_L and V_TV_T final states, respectively.[15] Thus, the contribution of $\mathcal{L}^{(2)}$ to V_LV_L final state is not enhanced by any E-power in the high energy region, in contrast to the case of VV-fusions (cf. Table Ia). So, the leading order $T_0[q\bar{q}^{(\prime)}; V_LV_L]$ amplitude, similar to the $T_0[q\bar{q}^{(\prime)}; V_TV_T]$ amplitude, is not sensitive to the strongly coupled EWSB sector. We then discuss the contributions of model-dependent NLO operators to the $q\bar{q}^{(\prime)}$-annihilations. We first note that the operators $\mathcal{L}_{4,5,6,7,10}$ cannot contribute to $q\bar{q}^{(\prime)}$-annihilations at $1/\Lambda^2$-order and thus should be best probed via VV-fusions (cf. Table V). Among all other NLO operators, the probe of $\mathcal{L}_{2,3,9}$ are most sensitive via $q\bar{q} \to W_L^+W_L^-$ amplitude and the probe of $\mathcal{L}_{3,11,12}$ are best via $q\bar{q}' \to W_L^\pm Z_L$ amplitude. For operators $\mathcal{L}_{1,8;13,14}$, the largest amplitudes are $T_1[q\bar{q}^{(\prime)}; W_L^+W_T^-/W_T^+W_L^-]$ and $T_1[q\bar{q}'; W_L^\pm Z_T/W_T^\pm Z_L]$, which are at most of $O\left(g^3\frac{Ef_\pi}{\Lambda^2}\right)$ and are suppressed by a factor $\frac{f_\pi}{E}$ relative to the model-dependent leading amplitudes of $O\left(g^2\frac{E^2}{\Lambda^2}\right)$.

---

[14] They can in principle be separated if the polarization of the external V-lines are identified. For the final state V's, one can study the angular distribution of the leptons from V-decay. For the incoming V's, one can use forward-jet tagging and central-jet vetoing to select longitudinal V's [46].

[15] $\mathcal{L}^{(2)}$ just gives the low energy theorem results and thus denotes the model-independent part of the EWSB sector, while $\mathcal{L}_{\rm G}$ is the standard tree-level Yang-Mills gauge term which is irrelevant to the EWSB mechanism.

In summary, applying the power counting technique allows us to conveniently estimate contributions of various operators to any scattering amplitude. For a given scattering process, this result tells us which operators can be sensitively probed. Similarly, the same result can also tell us which process would be most sensitive for probing new physics via a given effective operator. In the next section, we shall examine the important $W^\pm W^\pm \to W^\pm W^\pm$ fusion and $q\bar{q}' \to W^\pm Z$ annihilation processes at the LHC to illustrate how to use the electroweak power counting method to estimate the event rates and how to use the ET as a theoretical criterion to classify the sensitivities of these typical scattering processes to the NLO bosonic operators in the EWCL.

6.3. A comparative analysis for the LHC and LCs

The values of coefficients (ℓ_n's) of the 15 NLO operators in the EWCL (2.2) depend on the details of the underlying dynamics and reflect the possible new physics. Among the 15 NLO coefficients, ℓ_1, ℓ_0 and ℓ_8 correspond to S, T and U parameters [17]. They have been measured from the current low energy LEP/SLC data and will be further improved at LEPII and upgraded Tevatron. To distinguish different models of the EWSB, the rest of the ℓ_n's has to be measured by studying the scattering processes involving weak gauge bosons. What is usually done in the literature is to consider only a small subset of these operators at a time. For instance, in Ref. [4], a non-resonant model (called Delay-K model) was studied which includes $\mathcal{L}^{(2)}$ as well as the NLO operators $\mathcal{L}_4$ and $\mathcal{L}_5$. It was found that for the gold-plated mode (i.e. pure leptonic decay mode) of $W^\pm W^\pm$, a total number of about 10 signal events is expected at the LHC with a $100\,\mathrm{fb}^{-1}$ luminosity after imposing relevant kinematic cuts to suppress backgrounds. In the end of the analysis the ratio of signal to background is about 1. Another non-resonant model (called LET-CG model), which contains only the model-independent operator $\mathcal{L}^{(2)}$, was also studied in that paper. The difference between the predictions of these two models signals the effects from the NLO operators $\mathcal{L}_{4,5}$. With just a handful events, it requires higher integrated luminosities to probe these NLO operators and compare with the model-independent contributions from $\mathcal{L}^{(2)}$. Generally speaking, if one combines measurements from various VV-modes,

it is possible (although not easy) to distinguish models of EWSB which effectively include different subsets of the 15 NLO operators and the model-independent operator $\mathcal{L}^{(2)}$.

The important question to ask is: " How and to what extent can one measure *all* the NLO coefficients ℓ_n at future colliders to *fully* explore the EWSB sector? " To answer this question, as the first step, one should **(i)**. find out, for each given NLO operator, whether it can be measured via leading and/or sub-leading amplitudes of relevant processes at each collider; **(ii)**. determine whether a given NLO operator can be sensitively (or marginally sensitively) probed through its contributions to the leading (or sub-leading) amplitudes of the relevant scattering process at each given collider; **(iii)**. determine whether carrying out the above study for various high energy colliders can *complementarily* cover all the 15 NLO operators to probe the strongly interacting EWSB sector. For abbreviation, the above requirements **(i)**-**(iii)** will be referred hereafter as the " *Minimal Requirements* ".

The minimal requirements (i)-(ii) have been analyzed for V-V fusions and q-$\bar{q}^{(\prime)}$ annihilations in the last sub-section. This sub-section is mainly devoted to discuss our *Minimal Requirement*-**(iii)** for different high energy colliders besides including more channels. It is understood that the actual sensitivity of a collider to probe the NLO operators depends not only on the luminosities of the active partons (including weak-gauge bosons) inside hadrons or electrons, but also on the detection efficiency of the signal events after applying background-suppressing kinematic cuts to observe the specific decay mode of the final state weak-bosons (cf. Refs. [4, 5] and Sec. 8 below). However, all of these will only add fine structures to the sub-leading contributions listed in Table II but not affect our conclusions about the leading contributions as long as there are enough signal events produced. In this global analysis, we shall not perform a detailed numerical study like Refs. [4, 5], but only give a first-step qualitative global power counting analysis which serves as a useful guideline for further elaborating numerical calculations.

After examining all the relevant $2 \to 2$ and $2 \to 3$ hard scattering processes, we summarize in Table VII our global classification for the sensitivities of various future high energy colliders to probing the 15 model-dependent NLO bosonic operators. Here, the energy-E represents the typical energy scale of the hard scattering processes under consideration. The leading B-term for each high energy process is also listed and com-

pared with the corresponding V_L-amplitude. If the polarizations of the initial/final state gauge bosons are not distinguished but simply summed up, the largest B in each process (including all possible polarization states) should be considered for comparison. [If the leading B_0 (with just one v_μ-factor, cf. eq. (5.17b)) happens to be zero, then the largest next-to-leading term, either the part of B_0 term that contains 2 (or 3) v_μ-factors or the B_1 term, should be considered. Examples are the $ZZ \to ZZ$ and $f\bar{f} \to ZZZ$ processes.] By comparing T_1 with B in Table II and applying our criterion for classifying the sensitivities, we find that for the typical energy scale (E) of the relevant processes at each collider, the leading contributions (marked by $\surd$) can be sensitively probed, while the sub-leading contributions (marked by $\triangle$) can only be marginally sensitively probed.[16] (To save space, Table II does not list those processes to which the NLO operators *only* contribute sub-leading amplitudes. These processes are $WW \to W\gamma, Z\gamma$ + perm. and $f\bar{f}^{(\prime)} \to W\gamma, WW\gamma, WZ\gamma$, which all have one external transverse γ-line and are at most marginally sensitive.)

From Table VII, some of our conclusions can be drawn as follows.

(1). At LC(0.5), which is a LC with $\sqrt{S} = 0.5\,\text{TeV}$, $\ell_{2,3,9}$ can be sensitively probed via $e^-e^+ \to W_L^-W_L^+$.

(2). For pure $V_LV_L \to V_LV_L$ scattering amplitudes, the model-dependent operators $\mathcal{L}_{4,5}$ and $\mathcal{L}_{6,7}$ can be probed most sensitively. ℓ_{10} can only be sensitively probed via the scattering process $Z_LZ_L \to Z_LZ_L$ which is easier to detect at the LC(1.5) [a e^-e^+ or e^-e^- collider with $\sqrt{S} = 1.5\,\text{TeV}$] than at the LHC(14) [a pp collider with $\sqrt{S} = 14\,\text{TeV}$].

(3). The contributions from $\mathcal{L}^{(2)\prime}$ and $\mathcal{L}_{2,3,9}$ to the pure $4V_L$-scattering processes lose the E-power dependence by a factor of 2 (see, e.g., Table Ib). Hence, the pure $4V_L$-channel is less sensitive to these operators. [Note that $\mathcal{L}_{2,3,9}$ can be sensitively probed via $f\bar{f} \to W_L^-W_L^+$ process at LC(0.5) and LHC(14).] The pure $4V_L$-channel cannot probe $\mathcal{L}_{1,8,11\sim14}$ which can only be probed via processes with V_T('s). Among $\mathcal{L}_{1,8,11\sim14}$, the contributions from $\mathcal{L}_{11,12}$ to processes with V_T('s) are most important, although their

---

[16] The exceptions are $f\bar{f}^{(\prime)} \to W^+W^-/(LT), W^\pm Z/(LT)$ for which $T_1 \leq B_0$. Thus the probe of them is insensitive. (L/T denotes the longitudinal/transverse polarizations of $W^\pm$, Z^0 bosons.)

contributions are relatively suppressed by a factor gf_π/E as compared to the leading contributions from $\mathcal{L}_{4,5}$ to pure $4V_L$-scatterings. $\mathcal{L}_{1,8,13,14}$ are generally suppressed by higher powers of gf_π/E and are thus the least sensitive. The above conclusions hold for both LHC(14) and LC(1.5).

(4). At LHC(14), $\ell_{11,12}$ can be sensitively probed via $q\bar{q}' \to W^\pm Z$ whose final state is not electrically neutral. Thus, this final state is not accessible at LC. Hence, LC(0.5) will not be sensitive to these operators. To sensitively probe $\ell_{11,12}$ at LC(1.5), one has to measure $e^-e^+ \to W_L^- W_L^+ Z_L$.

(5). To sensitively probe $\ell_{13,14}$, a high energy $e^-\gamma$ linear collider is needed for studying the processes $e^-\gamma \to \nu_e W_L^- Z_L$, $e^- W_L^- W_L^+$, in which the backgrounds [47] are much less severe than processes like $\gamma\gamma \to W_L^+ W_L^-$ at a $\gamma\gamma$ collider [48, 6]. The amplitude of $\gamma\gamma \to W_L^+ W_L^-$ has the order of $e^2 \frac{E^2}{\Lambda^2}$, to which the $\mathcal{L}_{13,14}$ (and also $\mathcal{L}_{1,2,3,8,9}$) can contribute. Thus, this process would be useful for probing $\ell_{13,14}$ at a $\gamma\gamma$ collider if the backgrounds could be efficiently suppressed.

We also note that to measure the individual coefficient of the NLO operator, one has to be able to separate , for example, the $W^+W^- \to Z^0Z^0$ and the $Z^0Z^0 \to Z^0Z^0$ production processes. Although this task can be easily done at the LC by detecting a forward tagged lepton, it shall be a great challenge at the LHC because both the up- and down-type quarks from the initial state contribute to the scattering processes. From the above conclusion, we speculate[17] that if there is no new resonance below the TeV scale and the coefficients of the NLO operators are not much larger than that suggested by the naive dimensional analysis [50], the LHC alone may not be able to sensitively measure all these operators, and linear colliders are needed to *complementarily* cover the rest of the NLO operators. In fact, the different phases of 500 GeV and 1.5 TeV energies at the LC are necessary because they will be sensitive to different NLO operators. An electron-photon (or a photon-photon) collider is also useful for measuring some of the NLO operators that distinguish models of strongly coupled EWSB sector.

---

[17] To further reach a detailed quantitative conclusion, an elaborate and precise numerical study on all signal/background rates will be performed under this global guideline (cf. Ref. [49]).

7. Global Analysis at the Event Rate Level

In this section, we estimate the production rates for both weak boson fusions and quark-anti-quark annihilations at the LHC (a pp collider with $\sqrt{S} = 14\,\mathrm{TeV}$ and an integrated luminosity of $100\,\mathrm{fb}^{-1}$) and the LC (a e^-e^+ or e^-e^- collider with $\sqrt{S} = 1.5\,\mathrm{TeV}$ and an integrated luminosity of $200\,\mathrm{fb}^{-1}$). The gauge-boson fusion process $W^+W^+ \to W^+W^+$ and the quark-anti-quark annihilation process $q\bar{q}' \to W^+Z$ will be separately studied at the LHC.

To calculate the event rates for gauge-boson fusions, we multiply the luminosity of the incoming weak-boson pair VV (by the effective-W approximation (EWA) [43]) and the constituent cross section of the weak-boson scattering (from the amplitude estimated by the power counting analysis in the last section). Note that the validity of the EWA requires the VV invariant mass $M_{VV} \gg 2M_W$ [43], which coincides with the condition in (2.3a) for the validity of the ET. (Here, we reasonably take the typical energy scale E of the VV scattering to be M_{VV} for estimating the event rates.) Thus, the EWA and the ET have similar precisions in computing the event rate from V_LV_L fusion process in hadron collisions. As M_{VV} increases, they become more accurate. It is known that the EWA is less accurate for sub-processes involving initial transverse gauge boson(s) [51, 44]. Nevertheless, the EWA has been widely used in the literature for computing event rates from gauge-boson (either transversely or longitudinally polarized) fusion processes because it is easy to implement and can be used to reasonably estimate event rates before any exact calculation is available. As to be shown shortly, our power counting results agree well to the existing detailed calculations within about a factor of 2. Hence, it is appropriate to apply the power counting analysis together with the EWA for estimating the event rates from weak-boson fusions at the LHC. The coincidence for the case of the $q\bar{q}^{(\prime)}$-annihilation is even better, where the EWA is not needed.

7.1. Effective-W Approximation

The weak gauge boson ($V^a = W^\pm, Z^0$) radiated from the incoming fermions (quarks

or leptons)[18] can involve into a hard scattering (like VV-fusion) which can be enhanced at high energies. Consider the most interesting VV-fusion mechanism. The cross section of the whole scattering process $f_1 + f_2 \to f_1' + f_2' + X$ at the c.m. energy $\sqrt{s}$ can be factorized into the product of two parts: (i). the probability function $f_{f/V_{\lambda_j}}(x)$ for finding a vector boson V_{λ_j} (with helicity λ_j $(j = 1, 2)$) inside the incoming fermion f_j ; (ii). the hard vector boson scattering cross section $\hat{\sigma}(V^a_{\lambda_1} + V^b_{\lambda_2} \to X|\hat{s})$ at the reduced c.m. energy $\hat{s} \equiv x \cdot s$. So, we have

$$d\sigma(f_1 + f_2 \to f_1' + f_2' + X|s) = \int_{x_{\min}}^1 dx \sum_{\lambda_j} \mathcal{P}_{f_1 f_2/V^a_{\lambda_1} V^b_{\lambda_2}}(x) d\hat{\sigma}(V^a_{\lambda_1} + V^b_{\lambda_2} \to X|\hat{s}) \,, \quad (7.1)$$

where $\mathcal{P}_{f_1 f_2/V^a_{\lambda_1} V^b_{\lambda_2}}(x)$ is the luminosity of VV-pair from the two fermion system, which is usually factorized/approximated as the convolution of two single gauge-boson-distributions:[19]

$$\mathcal{P}_{f_1 f_2/V^a_{\lambda_1} V^b_{\lambda_2}}(x) = \int_x^1 \frac{dz}{z} f_{f_1/V^a_{\lambda_1}}(z) f_{f_1/V^b_{\lambda_2}}(x/z) \quad (7.2)$$

The above is usually called the *Effective-W Approximation* (EWA) [43]. Comparing (5.49) and (7.1), we establish the following relation for the two differential VV-luminosities:

$$\mathcal{P}_{f_1 f_2/V^a_{\lambda_1} V^b_{\lambda_2}}(x) \;=\; s \frac{d\mathcal{L}}{dM^2_{VV}} \quad , \quad (7.3)$$

where we ignored the subscript "partons" in (5.49) for simplicity and used the notation $M^2_{VV} (\equiv \hat{s})$.

The basic assumptions of the EWA method are:

(a). The initial *off-shell* gauge bosons $V^a_{\lambda_1}$ and $V^b_{\lambda_2}$ in the sub-process $V^a_{\lambda_1} + V^b_{\lambda_2} \to X$ are approximated as the *on-shell* ones.

(b). One approximates the moving direction of the radiated gauge boson $V^a_{\lambda_j}$ in the initial state to be along the direction of the corresponding incoming fermion. It is known as the *small angle approximation*.

---

[18] The similar consideration can be applied to high energy incoming photons [52].

[19] This factorization is very convenient, but is not essentially necessary. In principle, it can be avoided though this largely complicates the formalism and the practical applications.

(c). One approximates the two-gauge-boson-luminosity function as the convolution of the two single-gauge-boson-luminosity functions as given in the above equation. In the currently most popular/simple formulation, the single-gauge-boson-luminosity functions are further simplified by the *Leading Logarithm Approximation* (LLA).

(d). One assumes that, under proper kinematic cuts, the dominant contributions for producing the final state $f_1' + f_2' + X$ come from the VV-fusion sub-process process.

In this work, we shall use the simplest form of the EWA method, i.e. the LLA EWA, to estimate the production rates of signal and background from the VV fusion processes. In this case, the probability function to be used in the above equation is[20]

$$\begin{aligned} f_{f/V_L^a} &= \frac{(g_L^a)^2 + (g_R^a)^2}{8\pi^2} \frac{1-x}{x} \\ f_{f/V_T^a} &= \frac{(g_L^a)^2 + (g_R^a)^2}{16\pi^2} \frac{x^2 + 2(1-x)}{x} \ln \frac{\hat{s}}{M_V^2} \end{aligned} \qquad (7.4a,b)$$

Here, we have averaged over the left/right-handed V_T^a polarizations. We note that the longitudinal luminosity function f_{f/V_L^a} does not have any logarithmic dependence in the leading-Log limit, while the transverse luminosity has. Hence, the transverse luminosity function f_{f/V_T^a} is much less accurate than the longitudinal one because the scale choice inside the logarithmic argument is very uncertain. For instance, adding a non-leading term like

$$-\frac{x^2 + 2(1-x)}{x} \ln \frac{1}{x} \qquad (7.5)$$

to (7.4b), we find the log-factor $\ln \frac{\hat{s}}{M_V^2}$ changing into a larger one $\ln \frac{s}{M_V^2}$. In the literature, different choices for the logarithmic argument were suggested.[21] Also one may use different definitions for the scaling variable x . If one defines x as the ratio of the vector-boson energy (E_V) over that of the corresponding incoming fermion (E_f),[22] then

---

[20] For example, $g_L^a = g/\sqrt{2}$ and $g_R^a = 0$ for $V^a = W^\pm$.

[21] See: J. Lindfors, in Ref. [43].

[22] See: S. Dawson (1985), and G.L. Kane et al (1984), in Ref. [43].

the relation $s = \hat{s}/x$ between the f-f system and the sub-system V-V exactly holds only when the gauge boson is collinearly radiated (i.e., when the small angle approximation holds).

Substituting (7.4a,b) into (7.2)-(7.3), we get

$$\begin{aligned}
\frac{d\mathcal{L}_{LL}}{dM_{VV}^2} &= \frac{[(g_{L1}^a)^2+(g_{R1}^a)^2]\,[(g_{L2}^a)^2+(g_{R2}^a)^2]}{(8\pi^2)^2(s\cdot x)}\left[(1+x)\ln\frac{1}{x}-2(1-x)\right] \ , \\
\frac{d\mathcal{L}_{LT}}{dM_{VV}^2} &= \frac{[(g_{L1}^a)^2+(g_{R1}^a)^2]\,[(g_{L2}^a)^2+(g_{R2}^a)^2]}{(8\pi^2)^2(s\cdot x)}\left[(1+x)\ln\frac{1}{x}-\frac{1}{4}(1-x)(7+x)\right]\left[\ln\frac{s}{M_V^2}\right] \ , \\
\frac{d\mathcal{L}_{TT}}{dM_{VV}^2} &= \frac{[(g_{L1}^a)^2+(g_{R1}^a)^2]\,[(g_{L2}^a)^2+(g_{R2}^a)^2]}{(8\pi^2)^2(s\cdot x)}\left[\left(1+\frac{x}{2}\right)^2\ln\frac{1}{x}-\frac{1}{2}(1-x)(3+x)\right]\left[\ln\frac{s}{M_V^2}\right]^2 \ .
\end{aligned} \tag{7.6}$$

From (7.6), we plot in Fig. 3(a)-(f) the luminosity distribution ($d\mathcal{L}/dM_{VV}^2$) of the polarized VV-pair from the two fermion system, as a function of the invariant mass M_{VV} for the LHC and the LC.

7.2. At the LHC

7.2.1. Preliminaries

For the purpose of systematically analyzing the sensitivity to each bosonic operator in (2.2), in what follows, we separately compare the rates contributed by each individual operator with that by the B-term. The actual experiments contain the contributions from *all* possible operators and are thus more complicated. For simplicity and clearness, we follow the well-known naturalness assumption (i.e., contributions from different operators do not accidently cancel each other) and estimate the contributions from each operator separately.

Let us denote the production rate for the scattering process $W_\alpha^+ W_\beta^+ \to W_\gamma^+ W_\delta^+$ as $R_{\alpha\beta\gamma\delta(\ell)}$, where $\alpha,\beta,\gamma,\delta = L,T$ label the polarizations of the W-bosons and $\ell = 0,1$ indicates contributions from leading order and next-to-leading order, respectively. Up to

the one-loop level, we define

$$\begin{aligned} R_{\alpha\beta\gamma\delta} &= R_{\alpha\beta\gamma\delta(0)} + R_{\alpha\beta\gamma\delta(1)} \ , \\ R_{\alpha\beta\gamma\delta(\pm)} &= R_{\alpha\beta\gamma\delta(0)} \pm |R_{\alpha\beta\gamma\delta(1)}| \ . \end{aligned} \qquad (7.7a,b)$$

Also, R_B denotes the rate contributed by the largest B-term. For convenience, we use the subscript "$_S$" to stand for summing up the polarizations of the corresponding gauge boson. For the $q\bar{q}^{(\prime)} \to V_\alpha V_\beta$ processes, the rates are denoted by $R_{\alpha\beta(\ell)}$, and correspondingly we define $R_{\alpha\beta} = R_{\alpha\beta(0)} + R_{\alpha\beta(1)}$ and $R_{\alpha\beta(\pm)} = R_{\alpha\beta(0)} \pm |R_{\alpha\beta(1)}|$. We also note that when applying the power counting analysis, we have ignored the angular dependence in the scattering amplitudes (cf. Tables I∼II) because it does not affect the order of magnitude estimates for the total cross sections (or the event rates).

To check the reliability of our power counting method, we have compared our numerical results for the $W^+W^+ \to W_L^+W_L^+$ fusion and the $q\bar{q} \to W_L^+W_L^-$ annihilation with those in Fig. 8 and Fig. 5 of Ref. [53] in which the above constituent amplitudes were explicitly calculated and the polarizations of the initial weak-bosons were summed over for the fusion process. As shown in Figs. 4a and 4b, both results coincide well within about a factor of 2 or better. These are two typical examples showing that the correct physical picture can be consistently and quickly grasped by our power counting analysis.

We conclude this subsection by briefly commenting on a recent paper [by A. Dobado et al, *Z. Phys.* C17 (1996) 965]. The sole purpose of that paper was to avoid using the ET, but still within the EWA, to increase the calculation precision and to extend the results to lower energy regions. This approach is, however, inconsistent because the validity of the EWA also requires the *same high energy condition* $E \gg M_W$ as that of the ET. To study the operators $\mathcal{L}_{4,5}$ (dominated by pure V_L-modes), the approach in that paper cannot really get higher precision than previous studies [53, 4] (using the ET combined with the EWA) except making unnecessary complications and confusions in their calculation. To study other operators like $\mathcal{L}_{1,2,3,8,9,11}$, the V_T-modes must be included, for which the EWA is much worse [51, 44]. Hence, to get the *consistent and precise results* for these operators, one must go beyond the EWA for full calculations. This was not contained in the paper of A. Dobado et al. On the contrary, our present global power counting analysis provides the first complete and consistent estimate for all NLO operators in the EWCL (2.2).

7.2.2. Analyzing the Model-Independent Contributions to the Event Rates

In Fig. 5a we give the power counting estimates for the production rates of the $W_L^+W_L^+$ pairs at the LHC from the initial state W-bosons with different polarizations. In this figure, setting the renormalized coefficients $\ell_{0\sim14}$ to be zero, we include only the model-independent contributions up to one-loop.[23] As clearly shown in Fig. 5a, the rate from $4W_L$ scattering dominates over the rate from W_T+3W_L scattering. The latter is lower by about an order of magnitude for large M_{WW} in spite of the fact that the W_TW_L luminosity is larger than the W_LW_L luminosity in the initial state. Also separately shown in the same figure is the event rate $|R_B|$ contributed by the largest B-term [cf. (5.17) and (5.45)] which is even significantly lower than that from the W_T+3W_L scattering by a factor of $2\sim7$ for $M_{WW}>500\,\text{GeV}$. However, the rate from W_TW_T initial state is lower than that from the B-term in the $4W_L$ amplitude as $E\geq600\,\text{GeV}$. This implies that if the contribution from W_TW_T initial state is to be included in calculating the total production rate of the W_LW_L pair, the contribution from the B-term in the $4W_L$ amplitude should also be included because they are of the same order in magnitude. If, however, only the pure Goldstone boson amplitude $T[\pi^+\pi^+\to\pi^+\pi^+]$ is used to calculate the $4W_L$-amplitude (with the B-term ignored) the contribution from $T[W_T^+W_T^+\to W_L^+W_L^+]$ should also be consistently ignored for computing the total rate of $W_L^+W_L^+$ pair production via the weak-boson fusion mechanism.

As shown in Ref. [4], it is possible to statistically, though not on the event-by-event basis, choose event with longitudinally polarized W-bosons in the initial state by applying the techniques of forward-jet tagging and central-jet vetoing. In this work we do not intend to study the details of the event kinematics, and we shall sum over all the initial state polarizations for the rest of discussions. Let us first compare the rates for different polarizations in the final state. Fig. 5b shows that the rate of W_LW_L final state dominates, while the rate of B-term and the rates of W_LW_T and W_TW_T final states are of the same order, and all of them are about an $O(10)$ to $O(10^2)$ lower than the rate of W_LW_L final

---

[23] It is understood that the divergent pieces from one-loop calculations have been absorbed by the coefficients of the corresponding NLO effective operators [12, 14].

state in the energy region $E = M_{WW} > 500\,\mathrm{GeV}$. Therefore, if one wants to increase the precision in calculating the total event rates by including the small contribution from the B-term in pure $4W_L^+$ scattering, then the contributions from $W_S^+W_S^+ \to W_T^+W_T^+$ and $W_S^+W_S^+ \to W_L^+W_T^+$ scatterings should also be consistently included. Otherwise, they must be neglected all together. From Figs. 5a and 5b, we conclude that the scattering process $W_L^+W_L^+ \to W_L^+W_L^+$ dominates the W^+W^+-pair productions when the model-dependent coefficients $\ell_{0\sim 14}$ in (2.2) are set to be zero.

Similarly, we apply the power counting analysis to estimate the model-independent contribution to the rates of polarized W^+Z^0 pair produced from $q\bar{q}'$ fusion up to one-loop order. The results are plotted in Fig. 6. It shows that the $W_T^+Z_T^0$ and $W_L^+Z_L^0$ rates (i.e., R_{TT} and R_{LL}) are of the same order. They are much larger than the rate R_{LT} (from the $W_L^+Z_T^0$ and $W_T^+Z_L^0$ final states) and the rate $|R_B|$ (from the largest B-term contained in the $q\bar{q}' \to W_L^+Z_T^0, W_T^+Z_L^0$ amplitudes). The rate R_{LT} is only slightly above the $|R_B|$ because the leading GB-amplitude $T_0[q\bar{q}';\pi^+Z_T/\pi^0W_T^+]$ is of the same order as the term $B_0^{(1)}$ (cf. Table IIIa). Here we see that for the lowest order total signal rate, both R_{TT} and R_{LL} have to be included since they are of the same order and larger than the NLO model-dependent contributions. If one wants to further include R_{LT} , then R_B should also be included.

7.2.3. Estimating Sensitivities for Probing the Model-Dependent Operators

In this section, we classify the sensitivities to all the NLO bosonic operators at the LHC. Without knowing the values of the *model-dependent coefficients* (ℓ_n 's), we shall take them to vary from $O(1)$ to $O(10)$ except that ℓ_0, ℓ_1 and ℓ_8 are bounded to be of $O(1)$ by the low energy data [cf. (3.5)].

We first consider the scattering process $W^+W^+ \to W^+W^+$. Our theoretical criterion for discriminating different sensitivity levels (*sensitive, marginally sensitive*, or *insensitive*) to probe a particular operator via the production of W^+W^+ pairs is to compare its contribution to the event rate ($|R_{\alpha\beta\gamma\delta(1)}|$) with that from the largest model-independent contribution of the LNI B-term ($|R_B|$), according to the Sec.5. In Figs. 7-10, we show the results for varying $|\ell_n|$ from $O(1)$ to $O(10)$ (except ℓ_0, ℓ_1 and ℓ_8). Here, the

polarizations of the initial and the final states have been summed over. In Figs. 7a and 7b, we consider the coefficients (ℓ_n's) to be naturally of $O(1)$ according to the naive dimensional analysis [14]. Fig. 7a shows that the event rates/(100 fb^{-1}GeV) from operators $\mathcal{L}_{4,5}$ are larger than that from the B-term when $E = M_{WW} > 600$ GeV, while the rates from operators $\mathcal{L}_{3,9,11;12}$ can exceed $|R_B|$ only if $E = M_{WW} > 860$ GeV. As M_{WW} increases, the rates contributed by $\mathcal{L}_{4,5}$ remain flat, while the rates by $\mathcal{L}_{3,9,11;12}$ and the B-term decrease. The ratio of the event rates from $\mathcal{L}_{4,5}$ to $|R_B|$ is 5.0 at $E = M_{WW} = 1$ TeV, and rapidly increases to 19.6 at $E = M_{WW} = 1.5$ TeV. In contrast, the ratio between the rates from $\mathcal{L}_{3,9,11;12}$ and the B-term only varies from 1.4 to 3.0 for $E = M_{WW} = 1 \sim 1.5$ TeV. Fig. 7b shows that for the coefficients of $O(1)$, the event rates contributed by operators $\mathcal{L}^{(2)\prime}$ and $\mathcal{L}_{1,2,8;13,14}$ are all below $|R_B|$ for a wide region of energy up to about 2 TeV, so that they cannot be sensitively probed in this case. Especially, the contributions from $\mathcal{L}_{1,13}$ are about two orders of magnitude lower than that from the B-term. This suggests that $\mathcal{L}_{1,13}$ must be tested via other processes [10]. In Figs. 8a and 8b, different event rates are compared for the coefficients (except ℓ_0, ℓ_1, ℓ_8) to be of $O(10)$. Fig. 8a shows that the rates from $\mathcal{L}_{3,9,11;12}$ could significantly dominate over $|R_B|$ by an order of magnitude for $E = M_{WW} \sim 1$ TeV if their coefficients are increased by a factor of 10 relative to the natural size of $O(1)$. Fig. 8b shows that the rates from $\mathcal{L}_{13}$ is still lower than $|R_B|$ by about an order of magnitude, while the rate from $\mathcal{L}_2$ agrees with $|R_B|$ within a factor of 2. The contribution from $\mathcal{L}_{14}$ exceeds $|R_B|$ by about a factor $2 \sim 3$ at $E = M_{WW} = 1$ TeV and a factor of $3 \sim 5$ at $E = M_{WW} = 1.5$ TeV when its coefficients is of $O(10)$.

As discussed above, the cutoff scale Λ can be lower than $\Lambda_0 = 4\pi f_\pi \simeq 3.1$ TeV if there is any new heavy resonance below Λ_0. In that case, the signal rates $|R_1|$ will be higher than that reported in Figs. 7 and 8 by about a factor of $\left(\frac{\Lambda_0}{\Lambda}\right)^2$. For comparison, we repeat the above calculations for $\Lambda = 2$ TeV in Figs. 9 and 10. As indicated in Fig. 9a and 10b, the sensitivities to probing $\ell_{3,9,11,12} \sim O(1)$ and $\ell_{14,2} \sim O(10)$ via $W^+W^+ \to W^+W^+$ process increase for a lower Λ value.

From the above analyses, we conclude that studying the $W^+W^+ \to W^+W^+$ process can sensitively probe the operators $\mathcal{L}_{4,5}$, but is only marginally sensitive for probing

$\mathcal{L}_{3,9,11;12}$ and insensitive for $\mathcal{L}^{(2)\prime}$ and $\mathcal{L}_{1,2,8;13,14}$, if their coefficients are naturally of $O(1)$. In the case where these coefficients are of $O(10)$, the probe of $\mathcal{L}_{14}$ (for lower Λ) and $\mathcal{L}_{3,9,11;12}$ could become sensitive and that of $\mathcal{L}_2$ (for lower Λ) could become marginally sensitive, while $\mathcal{L}_{13}$ still cannot be sensitively or marginally sensitively measured.

Moreover, we note that the operators $\mathcal{L}_{6,7,10}$, which violate the custodial $SU(2)_C$ symmetry, do not contribute to the W^+W^+ pair productions up to $O(1/\Lambda^2)$. They can however contribute to the other scattering channels such as $WZ \to WZ$, $WW \to ZZ$, $ZZ \to WW$ and $ZZ \to ZZ$, cf. Table III. (Here, $\mathcal{L}_{10}$ only contributes to $ZZ \to ZZ$ channel.) By our order of magnitude estimates, we conclude that they will give the similar kind of contributions to the WZ or ZZ channel as $\mathcal{L}_{4,5}$ give to the W^+W^+ channel. This is because all these operators contain four covariant derivatives [cf. (3.1.2)] and thus become dominant in the high energy VV-fusion processes.

Let us consider the $W^-W^- \to W^-W^-$ production process. At the LHC, in the TeV region, the luminosity of W^-W^- is typically smaller than that of W^+W^+ by a factor of $3 \sim 5$. This is because in the TeV region, where the fraction of momentum (x) of proton carried by the quark (which emitting the initial state W-boson) is large (for $x = \frac{E}{\sqrt{S}} \sim 0.1$), the parton luminosity is dominated by the valence quark contributions. Since in the large-x region, the probability of finding a down-type valence quark in the proton is smaller than finding an up-type valence quark, the luminosity of W^-W^- is smaller than that of W^+W^+. However, as long as there are enough W^-W^- pairs detected, which requires a large integrated luminosity of the machine and a high detection efficiency of the detector, conclusion similar to probing the effective operators for the W^+W^+ channel can also be drawn for this channel. For $M_{WW} > 1.5$ TeV, the W^-W^- production rate becomes about an order of magnitude smaller than the W^+W^+ rate for any given operator. Thus, this process will not be sensitive to probing the NLO operators when $M_{WW} > 1.5$ TeV.

Next, we examine the W^+Z^0 production rates in the $q\bar{q}' \to W^+Z^0$ channel. As shown in Figs. 11, for $\Lambda = 3.1$ TeV, when the coefficients are of $O(1)$, the probe of $\mathcal{L}_{3,11,12}$ is sensitive when $E > 750$ GeV, while that of $\mathcal{L}_{8,9,14}$ is marginally sensitive if $E > 950$ GeV. The probe of $\mathcal{L}^{(2)\prime}$ becomes marginally sensitive if $E > 1.4$ TeV, and that of $\mathcal{L}_{1,2,13}$ is insensitive for $E < 1.9$ TeV. When the coefficients other than ℓ_0, ℓ_1, ℓ_8

are of $O(10)$, $\mathcal{L}_{3,11,12,9,14}$ could all be sensitively probed when $E > 500$ GeV, and the probe of $\mathcal{L}_{2,13}$ could be sensitive when $E > 1.2$ TeV. For $\Lambda = 2$ TeV, the sensitivities are increased overall by a factor $\left(\frac{\Lambda_0}{\Lambda}\right)^2 \simeq 2.4$, as shown in Fig. 12. The event rate for $q\bar{q}' \to W^- Z^0$ is slightly lower than that of $q\bar{q}' \to W^+ Z^0$ by only about a factor of 1.5 due to the lower luminosity for producing W^- bosons in pp collisions. Hence, the above conclusion also holds for the $q\bar{q}' \to W^- Z^0$ process.

We note that the $q\bar{q}' \to W^\pm Z^0$ annihilation provides *complementary* information on probing the EWSB sector, in comparison with the $W^\pm W^\pm \to W^\pm W^\pm$ fusion. In the former, $\mathcal{L}_{3,11,12}$ can be unambiguously probed, while in the latter, $\mathcal{L}_{4,5}$ can be sensitively probed. Furthermore, as shown in Table V and VI, the operators $\mathcal{L}_{6,7}$ can be probed from either $T_1[2W_L, 2Z_L]$ or $T_1[4Z_L]$, and $\mathcal{L}_{10}$ can only be probed from $T_1[4Z_L]$, while $\mathcal{L}_{2,9}$ can be tested from $T_1[q\bar{q}; W_L^+ W_L^-]$. It is therefore necessary and useful to measure all the the gauge boson fusion and quark-anti-quark annihilation processes for completely exploring the EWSB sector.

7.3. At the LCs

At the LCs, by our global power counting analysis, we only need to take into account the corresponding collider energy and its integrated luminosity. All analytic power counting formula for the scattering amplitudes of the V-V fusion and the f-$\bar{f}^{(\prime)}$ annihilation processes (given in Sec. 6) are still the same. For the 14 TeV LHC and the 1.5 TeV $e^- e^+$ LC, the c.m. energy of the V-V fusion and the f-$\bar{f}^{(\prime)}$ annihilation processes is typically of $O(1)$ TeV. Hence, the different sensitivities of the LHC and the LCs to probing the complete set of the NLO operators can be easily obtained by comparing their VV-pair luminosities at the TeV scale, which have been shown in Fig. 3.

Needless to say, the background processes to the VV fusion signal event at the LHC and the LCs can be very different. Hence, it may require different techniques to suppress the backgrounds and enhance the ratio of signal to background to detect the strongly coupled EWSB sector and measure all these model-dependent NLO operators. Although we do not intend to perform such a detailed Monte Carlo study in this work to illustrate

how to extract out the signal rate, we shall briefly discuss various techniques useful for studying the $VV \to VV$ processes. This is the subject of the next section. (For more elaborate numerical analyses for LCs, see Refs. [54, 49].)

8. How to Study TeV $W_LW_L \to W_LW_L$ Interactions Experimentally

In this section, we discuss how to experimentally study the EWSB sector by observing $W_LW_L \to W_LW_L$ interactions in the TeV region. (Here, W symbolizes either $W^\pm$ or Z^0 boson unless specified otherwise.) We analyze some general features of the event structure in the signals and backgrounds. Various techniques to enhance the signal-to-background ratio are also presented.

For completeness, we shall also discuss in this section the experimental techniques for detecting heavy resonance(s) (with mass of the order of TeV) predicted in some models of strongly coupled EWSB sector, although in the rest part of this article we have discarded such models. Since for models with light resonance(s) in the symmetry breaking sector, the interactions among the Goldstone bosons in the TeV region cannot become strong,[24] we shall not consider that class of models here.

8.1. Signal

The event signature of the signal is mainly a longitudinal W-pair produced in the final state. Assuming no light resonance(s) [55], the electroweak symmetry breaking sector in the TeV region may either contain a scalar- or vector-resonance, *etc.*, or no resonance at all. For a model with a TeV scalar (spin-0,isospin-0) resonance, the most useful detection modes are the W^+W^- and Z^0Z^0 modes which contain large isospin-0 channel contributions. For a model with a TeV vector (spin-1,isospin-1) resonance, the most useful mode is the $W^\pm Z^0$ mode because it contains a large isospin-1 channel

[24] The potentially bad high energy behavior of the scattering matrix element (if without any light resonance) is cut off by the tail of the light resonance.

contribution. If there is no resonance present in the symmetry breaking sector, all the WW modes are equally important, so the $W^{\pm}W^{\pm}$ mode is also useful. Actually, because of the small SM backgrounds for the $W^{\pm}W^{\pm}$ mode, this can become the most important detection mode if no TeV resonance is present in the EWSB sector.

Before we discuss the backgrounds, we have to specify the decay mode of the W-bosons in the final state. Let's first concentrate on the cleanest final state, i.e. the pure leptonic decay mode. The branching ratios of $W^+ \to \ell^+\nu$ and $Z^0 \to \ell^+\ell^-$ are 2/9 and 0.06, respectively, for $\ell^+ = e^+$ or μ^+. If the Z^0Z^0 pair signal is large enough, the $Z^0(\to \ell^+\ell^-)Z^0(\to \ell^+\ell^-)$ and $Z^0(\to \ell^+\ell^-)Z^0(\to \nu\bar{\nu})$ modes would be most useful at hadron colliders [56]. Otherwise, it is also necessary to include the $W^{\pm}W^{\mp}$, $W^{\pm}Z^0$ and $W^{\pm}W^{\pm}$ modes [57]. Although the pure leptonic mode gives the cleanest signal signature, its event rate is small because of the relatively small branching ratio. To improve the signal event rate for discriminating models of EWSB, one should also study the other decay modes, such as the lepton plus jet modes at the LHC and the LC, or the pure jet mode at the LC [54]. (Because of the large QCD background rate, the pure jet mode will be extremely difficult to utilize at hadron colliders.)

8.2. Backgrounds

For each decay mode of the WW pair, the relevant backgrounds vary. But, in general, one of the dominant background processes is the *intrinsic* electroweak background, which contains the same final state as the signal event. This background rate in the TeV region can be generated by calculating the Standard Model production rate of $f\bar{f} \to f\bar{f}WW$ with a light (e.g., 100 GeV) SM Higgs boson [57]. For example, the W_LW_L signal rate in the TeV region from a 1 TeV Higgs boson is equal to the difference between the event rates calculated using a 1 TeV Higgs boson and a 100 GeV Higgs boson [57].

The other important backgrounds are: the electroweak-QCD process W + jets (which contains a "fake W" mimicked by two QCD jets), and the $t\bar{t}$ pair (which subsequently decays to a WW pair), *etc.* We now discuss these backgrounds in various WW decay modes. Without the loss of generality, in the rest of this article we shall only consider the

major background processes at the hadron collider LHC. The backgrounds at the Linear Collider (LC) are usually easier to deal with because the initial state does not involve strong QCD interactions.

8.2.1. $Z^0(\to \ell^+\ell^-)Z^0(\to \ell^+\ell^-)$ *and* $Z^0(\to \ell^+\ell^-)Z^0(\to \nu\bar{\nu})$ *modes*

The signature for the signal in this mode is either an event with four isolated leptons with high transverse momenta, or two isolated leptons associated with large missing transverse momentum in the event. The dominant background processes for this mode are $q\bar{q} \to Z^0Z^0X$, $gg \to Z^0Z^0X$ [57], where X can be additional QCD jet(s). The final state Z^0 pairs produced from the above processes tend to be transversely polarized. Similarly, the Z^0 pairs produced from the *intrinsic* electroweak background process are also mostly transversely polarized. This is because the coupling of a transverse W boson to a light fermion (either quarks or leptons) is stronger than that of a longitudinal W in the high energy region. Hence, to discriminate the above backgrounds from the signals, we have to study the polarization of the final state W boson. For the same reason, the gauge boson emitted from the initial state fermions are likely to be transversely polarized. To improve the ratio of signal to background rates, some kinematic cuts (to be discussed in the next section) can be used to enhance the event sample in which the W bosons emitted from the incoming fermions are mostly longitudinally polarized, and therefore can enhance the $W_LW_L \to W_LW_L$ signal event.

Since it is easy to detect $Z^0 \to \ell^+\ell^-$ with a good accuracy, we do not expect backgrounds other than those discussed above to be large. Similarly, because of the large missing transverse momentum of the signal event, the $Z^0 \to \nu\bar{\nu}$ signature is difficult to mimic by the other SM background processes.

8.2.2. $W^+(\to \ell^+\nu)W^-(\to \ell^-\bar{\nu})$ *mode*

For this mode, in addition to the background processes $q\bar{q} \to q\bar{q}W^+W^-$, $q\bar{q} \to W^+W^-X$ and $gg \to W^+W^-X$, the $t\bar{t}$ + jet process can also mimic the signal event because the final state top quark pair can decay into a W^+W^- pair for the heavy top quark [57].

8.2.3. $W^{\pm}(\rightarrow \ell^{\pm}\nu)Z^0(\rightarrow \ell^+\ell^-)$ *and* $W^{\pm}(\rightarrow \ell^{\pm}\nu)W^{\pm}(\rightarrow \ell^{\pm}\nu)$ *modes*

Besides the background processes similar to those discussed above, the $Z^0t\bar{t}$ event can also mimic the $W^{\pm}Z^0$ signal.

For the purely leptonic decay mode of $W^{\pm}W^{\pm}$ [58], the signature is two like-sign isolated leptons with high P_T and large $\not\!\!E_T$. There are no low-order backgrounds from quark-antiquark or gluon-gluon fusion processes. However, other backgrounds can be important, such as the production of the transversely polarized W-pairs from the *intrinsic* electroweak background process [59] or from the QCD-gluon exchange process [60], and the $W^{\pm}t\bar{t}$ production from the electroweak-QCD process [57].

8.2.4. $W^+(\rightarrow \ell^+\nu)W^-(\rightarrow q_1\bar{q}_2)$ *mode*

The dominant background processes for this mode are $q\bar{q} \rightarrow q\bar{q}W^+W^-$, $q\bar{q} \rightarrow W^+W^-X$, and $gg \rightarrow W^+W^-X$ [61, 62, 63, 64]. The signature for the signal in this mode is an isolated lepton with high transverse momentum P_T, a large missing transverse energy $\not\!\!E_T$, and two jets whose invariant mass is about the mass of the W-boson. The electroweak-QCD process $W^+ +$ jets can mimic the signal when the invariant mass of the two QCD jets is around M_W [65, 66]. Other potential background processes for this mode are the QCD processes $q\bar{q}$, $gg \rightarrow t\bar{t}X$, $Wt\bar{b}$ and $t\bar{t}+$ jet(s) [67, 68, 69, 70, 71], in which a W boson can come from the decay of t or $\bar{t}$.

8.2.5. $W^+(\rightarrow \ell^+\nu)Z^0(\rightarrow q\bar{q})$ *mode*

The signature of the signal in this mode is an isolated lepton with high P_T, a large missing transverse energy $\not\!\!E_T$, and a two jet invariant mass around M_Z. The dominant background processes for this mode are similar to those for the $W^+(\rightarrow \ell^+\nu)W^-(\rightarrow q_1\bar{q}_2)$ mode discussed above. They are $q_1\bar{q}_2 \rightarrow W^+Z^0$, $W^+Z^0 +$ jet(s), $W^+ +$ jets and $Zt\bar{t}$ production processes [64, 65, 66, 72, 73].

To separate this signal from $W^+(\rightarrow \ell^+\nu)W^-(\rightarrow q_1\bar{q}_2)$ a good jet energy resolution is needed to distinguish the invariant mass of the two jets between M_Z and M_W, which differ by about 10 GeV. Another technique to distinguish these two kinds of events is to

measure the average electric charge of the jets, which has been applied successfully at LEP experiments [74].

As noted above, because of the large branching ratio, the pure jet mode from the W boson decay can also be useful at the future lepton colliders [54], where the dominant background for the detection of the $W_LW_L \to W_LW_L$ signal event is again the *intrinsic* electroweak process.

In general, without imposing any kinematic cuts, the raw event rate of the signal is significantly smaller than that of the backgrounds. However, the signature of the signal can actually be distinguished from that of the backgrounds so that some kinematic cuts can be applied to suppress the backgrounds and enhance the signal-to-background ratio. We shall examine the characteristic differences between the event structures of the signal and the backgrounds in the next section.

8.3. How to Distinguish Signal from Background

The signature of the signal event can be distinguished from that of the background events in many ways. We first discuss differences in the global features of the signal and the background events, then point out some distinct kinematics of the signal events. To simplify our discussion, we shall only concentrate on the $W^+(\to \ell^+\nu)W^-(\to q_1\bar{q}_2)$ mode in this section.

8.3.1. Global Features

The signal of interest is the WW pair produced from the W-fusion process. The spectator quark jet that emitted the W-boson in the W-fusion process tends to go into the high rapidity region. This jet typically has a high energy, about 1 TeV, for $M_{WW} \sim 1$ TeV (M_{WW} is the invariant mass of the WW pair.) Therefore, one can tag this forward jet to suppress backgrounds [75, 76, 57]. As noted in the previous section, the W boson pairs produced from the *intrinsic* electroweak process $q\bar{q} \to q\bar{q}W^+W^-$ tend to be transversely polarized, and the initial state gauge bosons are likely to be transversely polarized as well. To see how the forward jet can be used to discriminate the signal from the background

events, we consider the W^+W^- fusion process as an example. Since the coupling of the $W^\pm$ boson and the incoming quark is purely left-handed, the out-going quark tends to go along with the incoming quark direction when emitting a longitudinal W boson, and opposite direction when emitting a transverse (left-handed) W. This can be easily understood from the helicity conservation. Hence, in the *intrinsic* background event, the out-going quark jet is less forward (and less energetic) than that in the signal event.

Furthermore, because the production mechanism of the signal event is purely electroweak, the charged particle multiplicity of the signal event is smaller than that of a typical electroweak-QCD process such as $q\bar{q} \to gW^+W^-(\to q_1\bar{q}_2)$ or $qg \to qW^+q_1\bar{q}_2$. Because of the small hadronic activity in the signal event, in the central rapidity region there will be fewer hard QCD jets produced. At the parton level, they are the two quark jets produced from the W-boson decay plus soft gluon radiation. However, for the background process, such as $t\bar{t}$ production, there will be more than two hard jets in the central rapidity region both because of the additional jets from the decay of t and $\bar{t}$ and because of the stronger hadronic activity from the effect of QCD color structure of the event. Therefore, one can reject events with more than two hard jets produced in the central rapidity region to suppress the backgrounds. This was first suggested in Ref. [69] using a hadron level analysis to show how the $t\bar{t}$ background can be suppressed.

A similar trick of vetoing extra jets in the central rapidity region was also applied at the parton level [77, 57] for studying the pure leptonic decay mode of W's. An equivalent way of making use of the global difference in the hadronic activity of the events is to apply cuts on the number of charged particles. This was first pointed out in Refs. [78] and [79]. The same idea was later packaged in the context of selecting events with "rapidity gap" to enhance the signal-to-background ratio [80].

In the W-fusion process, the typical transverse momentum of the final state W-pair is about $M_W/2$ [75]. However, in the TeV region, the P_T of the W-pair produced from the background process, such as $q\bar{q} \to gWW$, can be of a few hundred GeV. Therefore, the two W's (either both real or one real and one fake) produced in the background event are less back-to-back in the transverse plane than those in the signal event.

8.3.2. Isolated Lepton in $W^+ \to \ell^+\nu$

Because the background event typically has more hadronic activity in the central rapidity region, the lepton produced from the W-boson decay is usually less isolated than that in the signal event. Therefore, requiring an isolated lepton with high P_T is a useful method to suppress the backgrounds. This requirement together with large missing transverse energy in the event insures the presence of a W-boson. Finally, it is also important to be able to measure the sign of the lepton charge to reduce the backgrounds for the detection of the $W^+(\to \ell^+\nu)W^+(\to \ell^+\nu)$ mode [57]

8.3.3. $W \to q_1\bar{q}_2$ decay mode

To identify the signal, we have to reconstruct the two highest P_T jets in the central rapidity region to obtain the invariant mass of the W-boson. It has been shown [79] that an efficient way of finding these two jets is to first find a big cone jet with invariant mass around M_W, then demand that there are two jets with smaller cone size inside this big cone jet. Because we must measure any new activity in $W_LW_L \to W_LW_L$, and because the W-boson in the background event is mainly transversely polarized [79], [25] one must measure the fraction of longitudinally polarized W-bosons in the WW pair data sample and compare with that predicted by various models of EWSB sector.

It was shown in Ref. [81] that a large fraction ($\sim 65\%$ for a 175 GeV top quark) of the W bosons from the top quark decays is longitudinally polarized.[26] This can in principle complicate the above method of using the fraction of longitudinally W bosons to detect the signal. Fortunately, after imposing the global cuts such as vetoing the central jet and tagging the forward jet, the $t\bar{t}$ backgrounds are small. (If necessary, it can be further suppressed by vetoing event with b jet, because for every background event with top

---

[25] The same conclusion also holds for the QCD background event with "fake W", which usually consists of one hard jet and one soft jet. Hence, after boosting these two jets back into the rest frame of the "fake W", its angular distribution resembles that from a transverse W boson.

[26] The ratio of the longitudinal versus the transverse W's from top quark decays is about $m_t^2/(2M_W^2)$.

quark there is always a b quark from the SM top decay.) To suppress the $W^+t\bar{b}$ and $W^-\bar{t}b$ backgrounds [70], which have smaller raw production rate than the $t\bar{t}$ event, the same tricks can be used. Furthermore, the top quark produced in the $W^+t\bar{b}$ event is mostly left-handed polarized because the coupling of t-b-W is purely left-handed in the SM. The kinematic cut of vetoing events with additional jets in the central rapidity region will reduce the fraction of the events in which the W boson from the top quark (with energy of the order 1 TeV) decay is longitudinally polarized. This is because in the rest frame of a left-handedly polarized top quark, which decays into a longitudinal W-boson, the decay b-quark prefers to move along the moving direction of the top quark in the center-of-mass frame of the W^+t pair. Hence, such a background event will produce an additional hard jet in the central rapidity region [81].

In the next section, we show how to observe the signals predicted by various models of the symmetry breaking sector. Some of them were studied at the hadron level, some at the parton level. We shall not reproduce those analyses but only sketch the ideas of various techniques used in detecting $W_LW_L \to W_LW_L$ interactions. The procedures discussed here are not necessarily the ones used in the analyses previously performed in the literature. If the signal event rates are large enough to observe the purely leptonic mode, then studying the symmetry breaking sector at the LHC shall be possible. However, a parton level study in Ref. [57] shows that the event rates are generally small after imposing the necessary kinematic cuts to suppress the backgrounds. To clearly identify the EWSB mechanism from the $W_LW_L \to W_LW_L$ interactions, the $\ell^\pm$ + jet mode of the WW pair should also be studied because of its larger branching ratio than the pure leptonic mode.[27] That is the decay mode we shall concentrate on in the following section for discussing the detection of various models of EWSB sector.

8.4. Various Models

[27] At the LC, because its initial state is colorless, the pure jet decay mode (with the largest branching ratio) of the W boson can also be useful.

8.4.1. A TeV Scalar Resonance

Based on the triviality argument [82], the mass of the SM Higgs boson cannot be much larger than $\sim$ 650 GeV, otherwise the theory would be inconsistent. (If the SM is an effective theory valid up to the energy scale much higher than 1 TeV, then this number is even lower.) However, one may consider an effective theory, such as an electroweak chiral lagrangian, in which a TeV scalar (spin-0,isospin-0) resonance couples to the would-be Goldstone bosons in the same way as the Higgs boson in the Standard Model [83, 84, 57]. (The mass and the width of the scalar resonance are the two free parameters in this model.) Then one can ask how to detect such a TeV scalar resonance. This study was already done at the hadron level in Ref. [79].

The tricks of enhancing the ratio of signal to background are as follows. First of all, we trigger on a high P_T lepton. The lepton is said to be isolated if there is no more than a certain amount of hadronic energy inside a cone of size ΔR surrounding the lepton. ($\Delta R = \sqrt{(\Delta\phi)^2 + (\Delta\eta)^2}$, ϕ is the azimuthal angle and η is the pseudo-rapidity.) A TeV resonance produces a W-boson with typical P_T at the order of $\sim 1/2$ TeV, therefore, the P_T of the lepton from the W-decay is at the order of a few hundred GeV. The kinematic cut on the P_T of an isolated lepton alone can suppress a large fraction of $t\bar{t}$ background events because the lepton produced from the decay of the W-boson typically has $P_T \sim m_t/3$, where m_t is the mass of the top quark. Furthermore, the lepton is also less isolated in the $t\bar{t}$ event than that in the signal event. After selecting the events with an isolated lepton with high P_T, we can make use of the fact that the background event contains more hadronic activity than the signal event to further suppress the background. One can make a cut on the charged particle multiplicity of the event to enhance the signal-to-background ratio. The alternative way of making use of this fact is to demand that there is only one big cone jet in the central rapidity region of the detector [79]. The background process typically produces more hard jets than the signal, hence vetoing the events with more than one big cone jet in the central rapidity region is also a useful technique. The W^+ + jets and $t\bar{t}$ background processes can further be suppressed by demanding that the large cone jet has invariant mass $\sim M_W$ and high P_T. Inside this big cone jet, one requires two small cone jets corresponding to the two decay quark jets of the W-boson.

As discussed above, measuring the polarization of the W bosons in the final state can be a very useful tool for detecting and discriminating mechanisms of EWSB. Therefore, the best strategy for analyzing the the experimental data is not to bias the information on the polarization of the W boson. Some of the methods that can preserve the information on the polarization of the W boson were presented in Ref. [79]. It was shown that it is possible to measure the fraction of longitudinal W's in the candidate W samples to distinguish various models of EWSB sector. One of the techniques which would not bias the polarization of the W-boson is to count the charged particle multiplicity inside the big cone jet. A real W-boson decays into a color singlet state of $q\bar{q}$ with the same multiplicity regardless of its energy, hence the charged particle multiplicity of these two jets is less than that of a pair of non-singlet QCD jets (which form the "fake W"), either quark or gluon jets. Furthermore, the QCD background events usually have more complicated color structure at the parton level, so that the hadron multiplicity of the background event is generally larger than that of the signal event in which the WW system is a color singlet state. Since the above methods only rely on the global features of the events, they will not bias the information on the W boson polarization.

Up to this point, we have only discussed the event structure in the central rapidity region. As discussed in the previous section, in the large rapidity region the signal event tends to have an energetic forward jet. It has been shown that tagging one such forward jet can further suppress the background at very little cost to the signal event rate [57].

Furthermore, with rapidity coverage down to 5, one can have a good measurement on the missing energy ($\not\!\!E_T$). Because the typical $\not\!\!E_T$ due to the neutrino from the W-boson, with energy $\sim 1\,\mathrm{TeV}$, decay is of the order of a few hundred GeV, the mis-measurement of neutrino transverse momentum due to the underlying hadronic activity is negligible. Knowing $\not\!\!E_T$ and the momentum of the lepton, one can determine the longitudinal momentum of the neutrino up to a two-fold solution by constraining the invariant mass of the lepton and neutrino to be M_W [79]. From the invariant mass of ℓ, ν, q_1, and $\bar{q}_2$, one can reconstruct M_{WW} to discriminate background from signal events.

If the width of the heavy resonance is small,[28] then one can detect a "bump" in the M_{WW} distributions. However, if its width is too large, then the best way to detect this new physics effect is to measure the fraction (f_L) of longitudinal W's in the event sample.

8.4.2. A TeV Vector Resonance

An example of this type of resonance is a techni-rho in the techni-color model [85]. What we have in mind here is a vector (spin-1,isospin-1) resonance in the electroweak chiral lagrangian. The mass and the width of the vector resonance are the two free parameters in this model. Because this resonance gives a large contribution in the isospin-1 channel, the most useful mode to look for such a resonance is the $W^{\pm}Z^0$ mode. If the signal event rate is large enough, the resonance can be observed by the pure leptonic decay mode $W^+(\to \ell^+\nu)Z^0(\to \ell^+\ell^-)$ in which all the leptons have $P_T \sim$ few hundred GeV and are well isolated. If the $W^+(\to \ell^+\nu)Z^0(\to q\bar{q})$ mode is necessary for the signal to be observed, the strategies discussed in the previous subsection for the $W^+(\to \ell^+\nu)W^-(\to q_1\bar{q}_2)$ mode can be applied in this case as well. Needless to say, in this case, the invariant mass of the two jets peaks around M_Z not M_W. It could be very valuable to improve the techniques that separate $W(\to jj)$ from $Z(\to jj)$ by identifying the average electric charge of each of the two decay jets.[29] Obviously, the two jets from the Z^0 boson decay should have the same electric charges.

8.4.3. No Resonance

If there is no resonance at all, the interactions among the longitudinal W's become strong in the TeV region. Although the non-resonance scenario is among the most difficult cases to be probed, this does *not* imply that it is less likely than the others to describe

---

[28] For a SM Higgs boson with mass m_H in unit of TeV, its decay width would be about equal to $m_H^3/2$ (in TeV), which is not small.

[29] For the techniques used in identifying the average electric charge of a QCD jet, see, for example, Ref. [74].

the underlying dynamics of the electroweak symmetry breaking. For example, it was argued in Ref. [86] that the non-resonance scenario may likely be realized. Within this non-resonance scenario, the electroweak chiral lagrangian (EWCL) provides the most economic way to parameterize models of strongly coupled EWSB sector. The model with only the lowest order term (containing two derivatives) in the EWCL is known as the low energy theorem model. The signal of this model can be detected from studying the $W^+(\to \ell^+\nu)W^-(\to q_1\bar{q}_2)$ mode in the TeV region Ref. [79]. The techniques of observing this signal are identical to those discussed above.

In Ref. [57], it was shown that it is possible to study the pure leptonic mode $W^+(\to \ell^+\nu)W^+(\to \ell^+\nu)$ in the multi-TeV region to test the low energy theorem model as long as the integrated luminosity (or, the event rate) is large enough. The dominant backgrounds for this mode are the *intrinsic* background, $W^+t\bar{t}$, and QCD-gluon exchange processes. The signal event can be triggered by two like-sign charged leptons with high P_T ($\sim$ few hundred GeV). One can further require these leptons to be isolated and veto events with additional high P_T jets in the central rapidity region. There are two missing neutrinos in the event so that it is difficult to reconstruct the W-boson and measure its polarization. Hence, in the absence of a "bump" structure in any distribution, one has to know the background event rate well to study the EWSB sector, unless the signal rate is very large. Similarly, measuring the charged or total particle multiplicity of the event and tagging a forward jet can further improve the signal-to-background ratio.

Particularly for the case of no resonance, when the signal rate is not large, it is important to avoid imposing kinematic cuts which greatly reduce the signal or bias the polarization information of the W bosons in the data sample. The specific technique for measuring f_L, as proposed in Ref. [79], will probably have to be used to study the non-resonance case, and to probe the EWSB sector. This technique takes advantage of the fact that the SM is well tested, and will be much better tested in the TeV region by the time the study of W_LW_L interactions is under way. Every event of a real or fake W_LW_L interaction will be clearly identified as originating either from SM or new physics. The real SM events (from $q\bar{q}$, $gg \to WW$, Wjj, $t\bar{t}$, *etc.*) can all be calculated and independently measured. Thus, one can first make global cuts such as requiring a high

energy spectator jet and low total particle multiplicity, and then examine all remaining candidate events to see if they are consistent with SM processes or if they suggest new physics, in particular new sources of longitudinal W's. In principle, only one new quantity needs to be measured: the fraction of W_LW_L events compared to the total number of all WW events including real and fake W's. This can be done by the usual approach of a maximum likelihood analysis, or probably even better by the emerging neural network techniques [87], for which this analysis appears to be ideally suited.

Ultimately, recognizing that *in the TeV region* every event must originate from either the well understood Standard Model physics or beyond will be the most powerful approach to discovering any deviations from the perturbative Standard Model predictions. Most of the proposals discussed here have been examined at the parton level but not in detector simulations [88]. They have been demonstrated to be promising techniques, but we cannot be sure they will work until the detector simulations are carried out by experimentalists. Fortunately, there will be plenty of time to do those studies before the data is available.

9. Conclusions

In the absence of light resonance in the EWSB sector, the longitudinal-W boson scatterings must become strong in the TeV region. In this review, after introducing the EWCL formalism to economically describe the EWSB sector in Sec. 2, we first discuss the current low energy bounds on these NLO EWSB parameters in Sec. 3. Then, in Sec. 4, we systematically develop a precise electroweak power counting rule (4.5), from a natural generalization of Weinberg's counting method for the ungauged non-linear sigma model. For completeness and for other possible applications, we also generalize our power counting rule for a linearly realized effective Lagrangian [29] which is often studied in the literature and called the decoupling scenario. The renormalizable SM with a light Higgs boson is included in the linear effective Lagrangian formalism at the lowest order. The corresponding power counting analysis for this decoupling scenario is given in Sec. 4.2.2. Furthermore, based upon our recent study on the intrinsic connection between the longitudinal weak-boson scatterings and probing the EWSB sector, we formulate, in Sec. 5,

the physical content of the electroweak equivalence theorem (ET) as a criterion for discriminating processes which are sensitive/insensitive to probing the EWSB mechanism. Our recent works on the other aspects of the precise formulation and application of the ET, including its deep connection with the underlying Higgs mechanism (with or without elementary Higgs boson), are comprehensively reviewed in the rest parts of Sec. 5 for the first time.

Armed with the powerful precise counting method and using the ET as a necessary criterion for probing the EWSB sector, we then systematically classify the sensitivities of various scattering processes to the complete set of bosonic operators at the level of S-matrix elements (cf. Tables I-VII and Sec. 6). The power counting hierarchy in (6.1) governs the order of magnitude of all relevant scattering amplitudes.

Finally, based on the above power counting analysis combined with the EWA, we study the phenomenology for probing the EWSB sector at the LHC and the LC via the $V^aV^b \to V^cV^d$ fusion and the $f\bar{f}' \to V^aV^b$ annihilation processes. In this simple power counting analysis, our numerical results for the production rates agree, within about a factor of 2 (cf. Fig. 4.), with the explicit calculations performed in the literature in which only a small subset of the NLO operators were studied. This indicates that our power counting analysis conveniently and reasonably grasps the overall physical picture. With this powerful tool, we perform the first complete survey on estimating the sensitivities of all fifteen next-to-leading order CP-conserving and CP-violating effective operators at the LHC via $W^\pm W^\pm$-fusions and $q\bar{q}' \to W^\pm Z^0$ annihilations. The results are shown in Figs. 7-10 and Fig. 11-12, respectively. We find that, for W^+W^+-channel, when the coefficients ℓ_n's are naturally of $O(1)$, $\mathcal{L}_{4,5}$ are most sensitive, $\mathcal{L}_{3,9,11;12}$ are marginally sensitive, and $\mathcal{L}^{(2)\prime}$ and $\mathcal{L}_{1,2,8;13,14}$ are insensitive. For the case where the coefficients other than ℓ_0, ℓ_1, ℓ_8 are of $O(10)$, the probe of $\mathcal{L}_{14}$ (for lower Λ) and $\mathcal{L}_{3,9,11;12}$ could become sensitive and that of $\mathcal{L}_2$ (for lower Λ) could become marginally sensitive. However, $\mathcal{L}_{13}$ cannot be sensitively probed via this process so that it must be measured via other processes.[30] A similar conclusion holds for the W^-W^- channel

[30] We note that $\mathcal{L}_{13}$ (and $\mathcal{L}_{14}$) can be sensitively probed via $e^-\gamma \to \nu_e W_L^- Z_L^0$ or $e^- W_L^- W_L^+$ processes

except that the event rate is lower by about a factor of $3 \sim 5$ in the TeV region because the quark luminosity for producing a W^-W^- pair is smaller than that for a W^+W^+ pair in pp collisions. Up to the next-to-leading order, the $SU(2)_C$-violating operators $\mathcal{L}_{6,7,10}$ do not contribute to the $W^\pm W^\pm$ channel. They, however, can be probed via the $WZ \to WZ$, $WW \to ZZ$, $ZZ \to WW$, and $ZZ \to ZZ$ processes [10].

For the $q\bar{q}' \to W^\pm Z^0$ process, the conclusion is quite different. The operators $\mathcal{L}_{4,5,6,7,10}$ do not contribute at the tree level. Using this process, $\mathcal{L}_{3,11,12}$ can be sensitively probed in the high energy range ($E > 750$ GeV), and the probe of $\mathcal{L}_{8,9,14}$ can be marginally sensitive for $E > 950$ GeV if their coefficients are of $O(1)$ and that of $\mathcal{L}_{9,14}$ can be sensitive if their coefficients are of $O(10)$. The results are plotted in Figs. 11-12. We conclude that the VV-fusion and the $q\bar{q}^{(\prime)}$-annihilation processes are *complementary* to each other for probing the complete set of the NLO effective operators in the electroweak chiral Lagrangian (2.2). A comparative analysis for the LHC and LCs is further performed and reviewed in Secs. 6.3 and 7.3.

From the above global analysis, we speculate[31] that before having a large number of signal events at the LHC (i.e. with large integrated luminosity), the LHC alone will not be able to sensitively measure all these operators, the linear collider is needed to *complementarily* cover the rest of the NLO operators. In fact, the different phases of 500 GeV and 1.5 TeV energies at the LC are necessary because they will be sensitive to different NLO operators in the EWCL. An electron-photon (or a photon-photon) collider is also very useful for measuring all the NLO operators which distinguish different models of the EWSB in the strongly interacting scenario.

Finally, we have discussed, in section 8, how to experimentally test the strong $W_LW_L \to W_LW_L$ interactions in the TeV region, with emphasis on the general features of the event structure for the signals and backgrounds. Various techniques for enhancing

---

at the future TeV linear collider [10].

[31] To further reach a detailed quantitative conclusion, an elaborate and precise numerical study on all signal/background rates should be performed under the guideline of this global analysis (cf. Ref. [49]).

the ratio of signal to background have also been presented. We show that it is possible to probe the electroweak symmetry breaking (EWSB) sector in the TeV regime even when the $W_L W_L$ scattering is non-resonant, as maybe the most likely outcome of a strong EWSB dynamics [86].

Acknowledgements C.P.Y. would like to thank Professors Yu-Ping Kuang and Qing Wang, and all those involved in organizing this Workshop for their warm hospitality. We also thank many colleagues, especially Michael Chanowitz, John Donoghue, Tao Han and Peter Zerwas, for useful discussions on this subject. H.J.H. is supported by the AvH of Germany. Y.P.K. is supported by the NSF of China and the FRF of Tsinghua University; C.P.Y. is supported in part by the NSF grant No. PHY-9507683.

References

1. M. Veltman, *Acta. Phys. Pol.* **B8**, 475 (1977).
2. M. Carena and P.M. Zerwas (Conv.), *Higgs Physics At LEP2 ,* CERN-96-01, Report on Physics at LEP2, Vol. 1, Ed. G. Altarelli et al, CERN.
3. J. Gunion, et al, hep-ph/9703330, and Haber, et al, hep-ph/9703391, Summary Reports, June 25–July 12, 1996, Snowmass, CO.
4. J. Bagger, V. Barger, K. Cheung, J. Gunion, T. Han, G.A. Ladinsky, R. Rosenfeld, C.–P. Yuan, *Phys. Rev.* **D49**, 1246 (1994); **D52**, 3878 (1995).
5. V. Barger, J.F. Beacom, K. Cheung, T. Han, *Phys. Rev.* **D50**, 6704 (1993).
6. E.g., *Physics and Experiments with Linear e^+e^- Colliders*, Waikoloa, USA, 1993, Ed. F.A. Harris et al; and M.S. Chanowitz, *Physics at High Energy γ-γ Colliders, Nucl. Instr. & Meth.* **A355**, 42 (1995); H. Murayama and M.E. Peskin, *Ann. Rev. Nucl. Part. Sci.*, **46**, 533 (1996) and hep-ex/9606003; S. Kuhlman et al (NLC ZDR Design Group and NLC Physics Working Group), SLAC-R-0485 and hep-ex/9605011.
7. E.g., M. Peskin, Talk at the Snowmass Conference (June, 1996), and the working group summary report, hep-ph/9704217.
8. S. Weinberg, *Physica* **96A**, 327 (1979).
9. H.-J. He, Y.-P. Kuang, and C.-P. Yuan, *Phys. Rev.* **D55**, 3038 (1997) and hep-ph/9611316; *Mod. Phys. Lett.* **A11**, 3061 (1996) and hep-ph/9509278.
10. H.-J. He, Y.-P. Kuang and C.-P. Yuan, *Phys. Lett.* **B382**, 149 (1996) and hep-ph/9604309; and MSUHEP-51201, Published in Proc. of International Workshop on *Physics and Experiments with Linear Colliders,* pp. 510-519, September 8-12, 1995, Iwate, Japan, and in Proc. of Fermilab Linear Collider Workshop: *Physics with High Energy e^+e^- Colliders,* November 16-18, 1995, Batavia, USA.
11. H.-J. He, Y.-P. Kuang, and C.-P. Yuan, *Phys. Rev.* **D51**, 6463 (1995); and hep-ph/9503359, Published in Proc. International Symposium on *Beyond The Standard Model IV,* pp. 610, Eds. J.F. Gunion, T. Han, J. Ohnemus, December 13-18, 1994, Tahoe, California, USA.
12. T. Appelquist and C. Bernard, *Phys. Rev.* **D22**, 200 (1980); A.C. Longhitano,

Nucl. Phys. **B188**, 118 (1981); T. Appelquist and G.-H. Wu, *Phys. Rev.* **D48**, 3235 (1993); **D51**, 240 (1995); and references therein.

13. E. Malkawi and C.-P. Yuan, *Phys. Rev.* **D50**, 4462 (1994); F. Larios, E. Malkawi, and C.-P. Yuan, hep-ph/9609482; R.D. Peccei, S. Peris and X. Zhang, *Nucl. Phys.* **B349**, 305 (1991); and references therein.
14. H. Georgi, *Weak Interaction and Modern Particle Theory*, Benjamin Publishing Company, 1984; A. Manohar and H. Georgi, *Nucl. Phys.* **B234**, 189 (1984).
15. See: C. Arzt, *Phys. Lett.* **B342**, 189 (1995); and references therein.
16. For recent reviews, H. Georgi, *Ann. Rev. Nucl. & Part. Sci.,* **43**, 209 (1994); F. Feruglio, *Inter. J. Mod. Phys.* **A8**, 4937 (1993).
17. M. Peskin and T. Takeuchi, *Phys. Rev. Lett.* **65**, 964 (1990).
18. P. Langacker and J. Erler, hep-ph/9703428 (updated); and *Phys. Rev.* **D54**, 103 (1996).
19. A. Blondel, Plenary talk at 28th International Conference on High Energy Physics, Warsaw, July, 1996; W. de Boer, A. Dabelstein, W. Hollik, W. Mösle, U. Schwickerath, IEKP-KA/96-08 and hep-ph/9609209 (revised version).
20. A.C. Longhitano, in Ref. [12].
21. H. Aihara, et al, hep-ph/9503425, published in *Electroweak Symmetry Breaking and Beyond the Standard Model*, Eds. T.L. Barklow, et al; U. Baur, T. Han and J. Ohnemus, *Phys. Rev.* **D53**, 1098 (1996); and references therein.
22. T.L. Barklow, et al, DPF-Report, hep-ph/9505296; and G. Gounaris, J.L. Kneur, and D. Zeppenfeld, hep-ph/9601233; and references therein.
23. T. Appelquist and G.-H. Wu, in Ref. [12].
24. S. Dawson and G. Valencia, *Nucl. Phys.* **B439**, 3 (1995).
25. A. Brunstein, O.J.P. Eboli, M.C. Gonzalez-Garcia, *Phys. Lett.* **B375**, 233 (1996); O.J.P. Eboli, et al, *Phys. Lett.* **B339**, 119 (1995).
26. See, *e.g.*, H. Veltman, in Ref. [36] and C. Grosse-Knette, in Ref. [42].
27. H. Georgi, *Ann. Rev. Nucl. & Part. Sci.,* **43**, 209 (1994); C.P. Burgess and D. London, *Phys. Rev.* **D48**, 4337 (1993); *Phys. Rev. Lett.* **69**, 3428 (1992).
28. M.S. Chanowitz, H. Georgi and M. Golden, *Phys. Rev. Lett.* **57**, 616 (1987); *Phys. Rev.* **D36**, 1490 (1987).

29. W. Buchmüller and D. Wyler, *Nucl. Phys.* **B268**, 621 (1986).
30. P.W. Higgs, *Phy. Rev. Lett.* **13**, 508(1964); *Phys. Rev.* **145**, 1156(1966); G.S. Guralnik, C.R. Hagen, and T.W.B. Kibble, *Phys. Rev. Lett.* **13**, 585 (1984); T.W.B. Kibble, *Phys. Rev.* **155**, 1554 (1967).
31. J.M. Cornwall, D.N. Levin, and G. Tiktopoulos, *Phys. Rev.* **D10**, 1145 (1974); C.E. Vayonakis, *Lett. Nuovo. Cimento* **17**, 383 (1976); B.W. Lee, C. Quigg, and H. Thacker, *Phys. Rev.* **D16**, 1519 (1977).
32. M.S. Chanowitz and M.K. Gaillard, *Nucl. Phys.* **B261**, 379 (1985); G.J. Gounaris, R. Kögerler, and H. Neufeld, *Phys. Rev.* **D34**, 3257 (1986).
33. Y.-P. Yao and C.-P. Yuan, *Phys. Rev.* **D38**, 2237 (1988); J. Bagger and C. Schmidt, *Phys. Rev.* **D41**, 264 (1990).
34. H.-J. He, Y.-P. Kuang, and X. Li, *Phys. Rev. Lett.* **69**, 2619 (1992); *Phys. Rev.* **D49**, 4842 (1994); *Phys. Lett.* **B329**, 278 (1994).
35. H.-J. He and W.B. Kilgore, *Phys. Rev.* **D55**, 1515 (1997) and hep-ph/9609326.
36. E.g., S.D. Willenbrock, *Ann. Phys.* **186**, 15 (1988); H. Veltman, *Phys. Rev.* **D41**, 2294 (1990); W.B. Kilgore, *Phys. Lett.* **B294**, 257 (1992); A. Dobado, J.R. Pelaez, *ibid*, **B329**, 469 (1994) (Erratum, B335, 554); C. Grosse-Knetter, I. Kuss, *Z. Phys.* **C95**, 66 (1995); J.F. Donoghue, J. Tandean, *Phys. Lett.* **B361**, 69 (1995); J. Horejsi, PRA-HEP 95/9; A. Denner, S. Dittmaier, BI-TP-96/02 and hep-ph/9603341.
37. T. Torma, *Phys. Rev.* **D54**, 2168 (1996) and hep-ph/9510217.
38. C. Becchi, A. Rouet, B. Stora, *Comm. Math. Phys.* **42**, 127 (1975); *Ann. Phys.* **98**, 287 (1976).
39. G.J. Gounaris, R. Kögerler, and H. Neufeld, in Ref. [32].
40. H.-J. He, Y.-P. Kuang, and X. Li, *Phys. Rev.* **D49**, 4842 (1994).
41. E.g., M.B. Einhorn, *Nucl. Phys.* **B246**, 75 (1984); and references therein.
42. See, *e.g.*, C. Grosse-Knetter, BI-TP/25; D. Espriu et al, UE-CBM-PF-94/61.
43. R.N. Cahn and S. Dawson, *Phys. Lett.* **B136**, 196 (1984), **B138**, 464(E) (1984); M.S. Chanowitz and M.K. Gaillard, *Phys. Lett.* **B142**, 85 (1984); G.L. Kane, W.W. Repko and W.R. Rolnick, *Phys. Lett.* **B148**, 367 (1984); S. Dawson, *Nucl. Phys.* **B249**, 427 (1985);

J. Lindfors, *Z. Phys.* **C28**, 427 (1985);
W.B. Rolnick, *Nucl. Phys.* **B274**, 171 (1986);
P.W. Johnson, F.I. Olness and W.-K. Tung, *Phys. Rev.* **D36**, 291 (1987);
Z. Kunszt and D.E. Soper, *Nucl. Phys.* **B296**, 253 (1988);
A. Abbasabadi, W.W. Repko, D.A. Dicus and R. Vega, *Phys. Rev.* **D38**, 2770 (1988); S. Dawson, *Phys. Lett.* **B217**, 347 (1989);
S. Cortese and R. Petronzio, *Phys. Lett.* **B276**, 203 (1992);
I. Kuss and H. Spiesberger, *Phys. Rev.* **D53**, 6078 (1996).

44. M.S. Chanowitz, private communications, and *Phys. Lett.* **B373**, 141 (1996) and hep-ph/9512358.
45. M.S. Chanowitz and W.B. Kilgore, *Phys. Lett.* **B322**, 147 (1994).
46. C.-P. Yuan, published in *Perspectives on Higgs Physics,* edited by Gordon L. Kane, World Scientific, 1992; G.L. Kane and C.-P. Yuan, *Phys. Rev.* **D40**, 2231 (1989).
47. K. Cheung, S. Dawson, T. Han, G. Valencia, *Phys. Rev.* **D51**, 5 (1995).
48. E.g., M. Golden, T. Han, G. Valencia, hep-ph/9511206, October, 1995.
49. H.-J. He, DESY-97-037 and invited talk in the proceedings of " *The Higgs Puzzle—What can we learn from LEPII, LHC, NLC, and FMC?* ", Ringberg Castle, Munich, Dec. 8-13, 1996, Ed. Bernd Kniehl; E. Boos, H.-J. He, W. Kilian, A. Pukhov, C.-P. Yuan, and P.M. Zerwas, DESY-96-256.
50. H. Georgi, *Weak Interaction and Modern Particle Theory*, (Benjamin Publishing Company, 1984); A. Manohar and H. Georgi, *Nucl. Phys.* **B234**, 189 (1984);
H. Georgi, *Ann. Rev. Nucl. & Part. Sci.* **43**, 209 (1994).
51. J.F. Gunion, J. Kalinowksi, A. Tofighi-Niaki, *Phys. Rev. Lett.* **57**, 2351 (1986).
52. E.g., S.J. Brodsky and P.M. Zerwas, " *High Energy Photon-Photon Collisions* ", *Nucl. Instr. & Meth.* **A355**, 19 (1995). V.M. Budnev, et al, *Phys. Rep.* **C15**, 182 (1975).
53. J. Bagger, S. Dawson and G. Valencia, *Nucl. Phys.* **B399**, 364 (1993).
54. For studies on the purely hadronic mode of WW at lepton colliders, see
V. Barger, K. Cheung, T. Han, R.J.N. Phillips, *Phys. Rev.* **D52**, 3815 (1995);
V. Barger, M.S. Berger, J.F. Gunion, T. Han, *Phys. Rev.* **D55**, 142 (1997).
55. For a review, see: J.F. Gunion, H.E. Haber, G.L. Kane and S. Dawson, *The Higgs*

Hunter's Guide, (Addison-Wesley Pub. Company, 1990); and references therein.

56. R.N. Cahn and M.S. Chanowitz, *Phys. Rev. Lett.* **56**, 1327 (1986); U. Baur and E.W.N. Glover, *Phys. Rev.* **D44**, 99 (1991), and references therein.
57. For studies on the purely leptonic mode of WW at hadron colliders, see J. Bagger, V. Barger, K. Cheung, J. Gunion, T. Han, G. Ladinsky, R. Rosenfeld and C.–P. Yuan, *Phys. Rev.* **D49**, 1246 (1994); *Phys. Rev.* **D52**, 3878 (1995).
58. M.S. Chanowitz and M. Golden, *Phys. Rev. Lett.* **61** (1988) 1053; **63**, 466 (1989) (E); V. Barger, K. Cheung, T. Han and R.J.N. Phillips, *Phys. Rev.* **D42**, 3052 (1990), and references therein.
59. R. Vega and D.A. Dicus, *Nucl. Phys.* **B329**, 533 (1990).
60. D. Dicus and R. Vega, *Phys. Lett.* **217**, 194 (1989).
61. K.O. Mikaelian, M.A. Samuel, D. Brown, *Nuovo. Cim. Lett.* **27**, 211 (1980).
62. C. Kao and D.A. Dicus, *Phys. Rev.* **D43**, 1555 (1991).
63. D.A. Dicus and R. Vega, *Phys. Rev. Lett.* **57**, 1110 (1986); J.F. Gunion, J. Kalinowski and A. Tofighi-Niaki, *Phys. Rev. Lett.* **57**, 2351 (1986).
64. U. Baur, E.W.N. Glover and J.J. van der Bij, *Nucl. Phys.* **B318**, 106 (1989); V. Barger, T. Han, J. Ohnemus and D. Zeppenfeld, *Phys. Rev.* **D41**, 2782 (1990), and references therein.
65. S.D. Ellis, R. Kleiss and W.J. Stirling, *Phys. Lett.* **154B**, 435 (1985); J.F. Gunion, Z. Kunszt and M. Soldate, *Phys. Lett.* **163B**, 389 (1985); **168B**, 427 (1986) (E).
66. F.A. Berends, W.T. Giele, H. Kuijf, R. Kleiss and W.J. Stirling, *Phys. Lett.* **B224**, 237 (1989); V. Barger, T. Han, J. Ohnemus and D. Zeppenfeld, *Phys. Rev. Lett.* **62**, 1971 (1989); *Phys. Rev.* **D40**, 2888 (1989); **D41**, 1715 (1990) (E), and references therein.
67. B.C. Combridge, *Phys. Scr.* **20**, 5 (1979).
68. P. Nason, S. Dawson and R.K. Ellis, *Nucl. Phys.* **B303**, 607 (1988); **B327**, 49 (1989); W. Beenakker, H. Kuijf, W.L. van Neerven and J. Smith, *Phys. Rev.* **D40**, 54 (1989); R. Meng, G.A. Schuler, J. Smith and W.L. van Neerven, *Nucl. Phys.* **B339**, 325 (1990).
69. R. Kauffman and C.–P. Yuan, *Phys. Rev.* **D42**, 956 (1990).

70. G.A. Ladinsky and C.–P. Yuan, *Phys. Rev.* **D43**, 789 (1991).
71. V. Barger, K. Cheung, T. Han and R. Phillips, *Phys. Rev.* **D42**, 3052 (1990);
D. Dicus, J.F. Gunion, L.H. Orr and R. Vega, *Nucl. Phys.* **B377**, 31 (1992), and references therein.
72. R.W. Brown, D. Sahdev, K.O. Mikaelian, *Phys. Rev.* **D20**, 1164 (1979).
73. V. Barger, K. Cheung, T. Han, A. Stange and D. Zeppenfeld, *Phys. Rev.* **D46**, 2028 (1991), and references therein.
74. W. Ash et al, *Phys. Rev. Lett.* **58**, 1080 (1987);
OPAL Collaboration (R. Akers et al.), *Phys. Lett.* **B327**, 411 (1994);
ALEPH Collaboration (D. Buskulic et al.), *Z. Phys.* **C71**, 357 (1996).
75. R.N. Cahn, S.D. Ellis, R. Kleiss, W.J. Stirling, *Phys. Rev.* **D35**, 1626 (1987).
76. V. Barger, T. Han, and R.J. Phillips, *Phys. Rev.* **D37**, 2005 (1988);
R. Kleiss and W.J. Stirling, *Phys. Lett.* **B200**, 193 (1988);
U. Baur and E.W. Glover, *Nucl. Phys.* **B347**, 12 (1990);
D. Dicus, J. Gunion, L. Orr, and R. Vega, *Nucl. Phys.* **B377**, 31 (1992).
77. V. Barger, K. Cheung, T. Han, and R.J. Phillips, *Phys. Rev.* **D42**, 3052 (1990);
D. Dicus, J. Gunion, and R. Vega, *Phys. Lett.* **B258**, 475 (1991).
78. J. F. Gunion, G. L. Kane, H.F.-W. Sadrozinski, A. Seiden, A.J. Weinstein, and C.–P. Yuan, *Phys. Rev.* **D40**, 2223 (1989).
79. G.L. Kane and C.–P. Yuan, *Phys. Rev.* **D40**, 2231 (1989).
80. V. Barger, R.J.N. Phillips, D. Zeppenfeld, *Phys. Lett.* **346B**, 106 (1995), and references therein.
81. G.L. Kane, G.A. Ladinsky and C.–P. Yuan, *Phys. Rev.* **D45**, 124 (1992).
82. R. Dashen and H. Neuberger, *Phys. Rev. Lett.* **50**, 1897 (1983);
M. Lindner, *Z. Phys.* **C31**, 295 (1986), and references therein.
83. S. Weinberg, *Phys. Rev.* **166**, 1568 (1968);
S. Coleman, J. Wess and B. Zumino, *Phys. Rev.* **177**, 2239 (1969);
C. Callan, S. Coleman, J. Wess and B. Zumino, *Phys. Rev.* **177**, 2247 (1969).
84. J. Gasser and H. Leutwyler, *Ann. Phys.* **158**, 142 (1984); *Nucl. Phys.* **B250**, 465 (1985).
85. E. Farhi and L. Susskind, *Phys. Rep.* **74**, 277 (1981);

For a review of the current status of technicolor models, see
Kenneth Lane, *Technicolor*, talk given at International Conference on the History of Original Ideas and Basic Discoveries in Particle Physics, Erice, Italy, 1994, e-Print Archive: hep-ph/9501249.

86. H. Veltman and M. Veltman, *Acta. Phys. Polon.* **B22**, 669 (1991).
87. B. Denby, in La Londe-les-Maures 1992, Proceedings, New computing techniques in physics research II, pp. 287-325. and FERMILAB-Conf-92-121, 1992.
88. Some studies beyond the parton level were listed in Ref. [79]. For more references, see, for example,
Solenoidal Detector Collaboration, *Technical Design Report*, SDC-92-201, 1992;
GEM Collaboration, *Letter of Intent*, SSCL-SR-1184, 1991;
The CMS detector and physics at the LHC, by CMS Collaboration (D. Denegri for the collaboration), CERN-PPE-95-183, Nov 1995, published in Valencia Elementary Particle Physics 1995, pp. 160-182;
The ATLAS detector for the LHC, by M.A. Parker, CAMBRIDGE-HEP-92-10, 1992, published in Dallas HEP 1992, pp. 1837-1841.

Table Captions

Table I. Estimates of amplitudes for $W^\pm W^\pm \to W^\pm W^\pm$ scattering.

Table Ia. Model-independent contributions from $\mathcal{L}_G + \mathcal{L}_F + \mathcal{L}^{(2)}$.

Table Ib. Model-dependent contributions from the next-to-leading order operators.

Table II. Order estimates of B-terms for $W^\pm W^\pm \to W^\pm W^\pm$ scattering.

Table IIa. Model-independent contributions.

Table IIb. Relevant operators for model-dependent contributions.[a]

Table III. Estimates of amplitudes for $q\bar{q}^{(\prime)} \to V^a V^b$: Model-independent contributions.

Table IIIa. For $q\bar{q}^{(\prime)} \to W^+W^-$, $W^\pm Z$.

Table IIIb. For $q\bar{q} \to ZZ$.

Table IV. Estimates of amplitudes for $q\bar{q}^{(\prime)} \to V^a V^b$: Model-dependent contributions.[a]

Table IVa. For $q\bar{q} \to W^+W^-$.

Table IVb. For $q\bar{q}' \to W^\pm Z$.

Table V. Global classification of sensitivities to probing direct and indirect EWSB information from effective operators at the level of S-matrix elements (A).[a]

Notes:

[a] The contributions from $\mathcal{L}_{1,2,13}$ are *always* associated with a factor of $\sin^2\theta_W$, unless specified otherwise. Also, for contributions to the B-term in a given V_L-amplitude, we list them separately with the B-term specified.

[b] MI = model-independent, MD = model-dependent.

[c] There is no contribution when all the external lines are electrically neutral.

[d] $B_0^{(1)} \simeq T_0[2\pi, v, V_T]$ $(\not\simeq T_0[2\pi^0, v^0, Z_T])$, $B_0^{(3)} \simeq T_0[v, 3V_T]$ $(\not\simeq T_0[v^0, 3Z_T])$.

[e] $T_1[2V_L, 2V_T] = T_1[2Z_L, 2W_T]$, $T_1[2W_L, 2Z_T]$, or $T_1[Z_L, W_L, Z_T, W_T]$.

[f] $\mathcal{L}_2$ only contributes to $T_1[2\pi^\pm, \pi^0, v^0]$ and $T_1[2\pi^0, \pi^\pm, v^\pm]$ at this order; $\mathcal{L}_{6,7}$ do not contribute to $T_1[3\pi^\pm, v^\pm]$.

[g] $\mathcal{L}_{10}$ contributes only to $T_1[\cdots]$ with all the external lines being electrically neutral.

$^{(h)}$ $B_0^{(2)}$ is dominated by $T_0[2V_T, 2v]$ since $T_0[\pi, 2V_T, v]$ contains a suppressing factor $\sin^2\theta_W$ as can be deduced from $T_0[\pi, 3V_T]$ (cf. Table 1a) times the factor $v^\mu = O\left(\frac{M_W}{E}\right)$.

$^{(i)}$ Here, $T_1[2W_L, 2W_T]$ contains a coupling $e^4 = g^4 \sin^4\theta_W$.

$^{(j)}$ $\mathcal{L}_2$ only contributes to $T_1[3\pi^\pm, v^\pm]$.

$^{(k)}$ $\mathcal{L}_{1,13}$ do not contribute to $T_1[2\pi^\pm, 2v^\pm]$.

Table VI. Global classification of sensitivities to probing direct and indirect EWSB information from effective operators at the level of S-matrix elements (B). $^{(a)}$

Table VII. Probing the EWSB sector at high energy colliders: a global classification for the NLO bosonic operators.

Figure Captions

Fig. 1. Examination on the kinematic dependence and the validity of the ET for the $W_L^+W_L^- \to W_L^+W_L^-$ scattering process .

(1a). The ratio $|B/g^2|$ for $\theta = 2°,\ 10°,\ 45°,\ 90°,\ 100°,\ 120°,\ 135°,\ 150°,\ 180°$.

(1b). Same as (10a), but for the ratio $|B/T[W_L]|$.

(1c). Comparison of the W_L-amplitude (solid lines) and the corresponding GB-amplitude (dotted lines) for $\theta = 10°,\ 45°,\ 100°,\ 150°$. Here, $B\,[150°]$ denotes the B-term at $\theta = 150°$.

Fig. 2. Comparison of the LHC production rates contributed by the exact W_L-amplitude (solid line) and the GB-amplitude (dotted line) from eq. (5.43).

(2a). For the WW invariant mass distribution.

(2b). For the angular distribution.

Fig. 3. The differential luminosity distribution ($d\mathcal{L}/dM_{VV}^2$) of the polarized VV-pair from the two fermion system, as a function of the invariant mass M_{VV}, for the LHC (a 14 TeV pp collider) and the LC (a 1.5 TeV e^-e^+ or e^-e^- collider). In each plot, three curves are presented for different combinations, i.e. LL, LT and TT (from the bottom to top), of the polarizations of the VV pair at LHC (solid lines) and LC (dashed lines).

(3a). For the W^-W^- mode.

(3b). For the W^+W^+ mode (LHC only).

(3c). For the W^+W^- mode.

(3d). For the Z^0Z^0 mode.

(3e). For the W^+Z^0 mode.

(3f). For the W^-Z^0 mode.

Fig. 4. Comparison of the power counting predictions with the corresponding ones in Fig. 8 of Ref. [53] up to one-loop for a pp collider with $\sqrt{S} = 40$ TeV. The solid lines are given by our power counting analysis; the dashed lines are from Ref. [53]. [The meanings of the rates $R_{\alpha\beta\gamma\delta}$'s and $R_{\alpha\beta}$'s are defined in eq. (7.7a,b) and below.]

(4a). $W^+W^+ \to W_L^+W_L^+$.

(4b). $q\bar{q}' \to W_L^+ W_L^-$.

Fig. 5.
(5a). Comparison of the $W_L^+W_L^+$ production rates up to one-loop (for $\ell_{0-14} = 0$) with $W_L^+W_L^+$, $W_L^+W_T^+$ and $W_T^+W_T^+$ initial states, at the 14 TeV LHC.
(5b). Comparison of the production rates for different final-state polarizations up to one-loop (for $\ell_{0-14} = 0$) after summing over the polarizations of the initial states, at the 14 TeV LHC.

Fig. 6. Comparison of the production rates for different final-state polarizations up to one-loop (for $\ell_{0-14} = 0$) via $q\bar{q}' \to W^+Z^0$ at the 14 TeV LHC.

Fig. 7. Sensitivities of the operators $\mathcal{L}^{(2)\prime}$ and $\mathcal{L}_{1\sim14}$ at the 14 TeV LHC with $\Lambda = 3.1$ TeV. The coefficients ℓ_n's are taken to be of $O(1)$,

(7a). For operators $\mathcal{L}_{3,4,5,9,11,12}$.
(7b). For operators $\mathcal{L}^{(2)\prime}$ and $\mathcal{L}_{1,2,8,13,14}$.

Fig. 8. Same as Fig. 7, but the coefficients ℓ_n's are taken to be of $O(10)$ except $\ell_{0,1,8}$ which are already constrained by low energy data to be of $O(1)$.

(8a). For operators $\mathcal{L}_{3,4,5,9,11,12}$.
(8b). For operators $\mathcal{L}_{2,13,14}$.

Fig. 9 Same as Fig. 7, but with $\Lambda = 2.0$ TeV .

Fig. 10. Same as Fig. 8, but with $\Lambda = 2.0$ TeV .

Fig. 11. Sensitivities of the operators $\mathcal{L}^{(2)\prime}$ and $\mathcal{L}_{1-14}$ in $q\bar{q}' \to W^+Z^0$ at the 14 TeV LHC with $\Lambda = 3.1$ TeV .

(11a). The coefficients ℓ_n 's are taken to be of $O(1)$.
(11b). The coefficients ℓ_n 's are taken to be of $O(10)$ except $\ell_{0,1,8}$ which are already constrained by low energy data to be of $O(1)$.

Fig. 12. Same as Fig. 11, but with $\Lambda = 2.0$ TeV .

TABLES

Table I. Estimates of amplitudes for $W^{\pm}W^{\pm} \to W^{\pm}W^{\pm}$ scattering.

Table Ia. Model-independent contributions from $\mathcal{L}_G + \mathcal{L}_F + \mathcal{L}^{(2)}$.

$\mathcal{L}_G + \mathcal{L}_F + \mathcal{L}^{(2)}$	$T_\ell[4\pi]$	$T_\ell[3\pi, W_T]$	$T_\ell[2\pi, 2W_T]$	$T_\ell[\pi, 3W_T]$	$T_\ell[4W_T]$
Tree-Level ($\ell = 0$)	$\frac{E^2}{f_\pi^2}$	$g\frac{E}{f_\pi}$	g^2	$e^2 g \frac{f_\pi}{E}$	g^2
One-Loop ($\ell = 1$)	$\frac{E^2}{f_\pi^2}\frac{E^2}{\Lambda_0^2}$	$g\frac{E}{f_\pi}\frac{E^2}{\Lambda_0^2}$	$g^2\frac{E^2}{\Lambda_0^2}$	$g^3\frac{f_\pi E}{\Lambda_0^2}$	$g^4\frac{f_\pi^2}{\Lambda_0^2}$

Table Ib. Model-dependent contributions from the next-to-leading order operators.

Operators	$T_1[4\pi]$	$T_1[3\pi, W_T]$	$T_1[2\pi, 2W_T]$	$T_1[\pi, 3W_T]$	$T_1[4W_T]$
$\mathcal{L}^{(2)\prime}$	$\ell_0 \ \frac{E^2}{\Lambda^2}$	$\ell_0 \ g\frac{f_\pi E}{\Lambda^2}$	$\ell_0 \ g^2\frac{f_\pi^2}{\Lambda^2}$	$\ell_0 \ g^3\frac{f_\pi^3}{E\Lambda^2}$	/
$\mathcal{L}_{1,13}$	/	$\ell_{1,13} \ e^2 g\frac{f_\pi E}{\Lambda^2}$	$\ell_{1,13} \ e^4\frac{f_\pi^2}{\Lambda^2}$	$\ell_{1,13} \ e^2 g\frac{f_\pi E}{\Lambda^2}$	$\ell_{1,13} \ e^2 g^2\frac{f_\pi^2}{\Lambda^2}$
$\mathcal{L}_2$	$\ell_2 \ e^2\frac{E^2}{\Lambda^2}$	$\ell_2 \ e^2 g\frac{f_\pi E}{\Lambda^2}$	$\ell_2 \ e^2\frac{E^2}{\Lambda^2}$	$\ell_2 \ e^2 g\frac{f_\pi E}{\Lambda^2}$	$\ell_2 \ e^2 g^2\frac{f_\pi^2}{\Lambda^2}$
$\mathcal{L}_3$	$\ell_3 \ g^2\frac{E^2}{\Lambda^2}$	$\ell_3 \ g\frac{E}{f_\pi}\frac{E^2}{\Lambda^2}$	$\ell_3 \ g^2\frac{E^2}{\Lambda^2}$	$\ell_3 \ g^3\frac{f_\pi E}{\Lambda^2}$	$\ell_3 \ g^4\frac{f_\pi^2}{\Lambda^2}$
$\mathcal{L}_{4,5}$	$\ell_{4,5} \ \frac{E^2}{f_\pi^2}\frac{E^2}{\Lambda^2}$	$\ell_{4,5} \ g\frac{E}{f_\pi}\frac{E^2}{\Lambda^2}$	$\ell_{4,5} \ g^2\frac{E^2}{\Lambda^2}$	$\ell_{4,5} \ g^3\frac{f_\pi E}{\Lambda^2}$	$\ell_{4,5} \ g^4\frac{f_\pi^2}{\Lambda^2}$
$\mathcal{L}_{6,7,10}$	/	/	/	/	/
$\mathcal{L}_{8,14}$	/	$\ell_{8,14} \ g^3\frac{f_\pi E}{\Lambda^2}$	$\ell_{8,14} \ g^2\frac{E^2}{\Lambda^2}$	$\ell_{8,14} \ g^3\frac{f_\pi E}{\Lambda^2}$	$\ell_{8,14} \ g^4\frac{f_\pi^2}{\Lambda^2}$
$\mathcal{L}_9$	$\ell_9 \ g^2\frac{E^2}{\Lambda^2}$	$\ell_9 \ g\frac{E}{f_\pi}\frac{E^2}{\Lambda^2}$	$\ell_9 \ g^2\frac{E^2}{\Lambda^2}$	$\ell_9 \ g^3\frac{f_\pi E}{\Lambda^2}$	$\ell_9 \ g^4\frac{f_\pi^2}{\Lambda^2}$
$\mathcal{L}_{11,12}$	/	$\ell_{11,12} \ g\frac{E}{f_\pi}\frac{E^2}{\Lambda^2}$	$\ell_{11,12} \ g^2\frac{E^2}{\Lambda^2}$	$\ell_{11,12} \ g^3\frac{f_\pi E}{\Lambda^2}$	$\ell_{11,12} \ g^4\frac{f_\pi^2}{\Lambda^2}$

Table II. Order estimates of B-terms for $W^{\pm}W^{\pm} \to W^{\pm}W^{\pm}$ scattering.

Table IIa. Model-independent contributions.

$\mathcal{L}_G + \mathcal{L}_F + \mathcal{L}^{(2)}$	$B_\ell^{(0)}$	$B_\ell^{(1)}$	$B_\ell^{(2)}$	$B_\ell^{(3)}$
Tree-Level ($\ell = 0$)	g^2	$g^2 \frac{M_W}{E}$	$g^2 \frac{M_W^2}{E^2}$	$g^2 \frac{M_W}{E}$
One-Loop ($\ell = 1$)	$g^2 \frac{E^2}{\Lambda_0^2}$	$g^3 \frac{E f_\pi}{\Lambda_0^2}$	$g^4 \frac{f_\pi^2}{\Lambda_0^2}$	$g^4 \frac{f_\pi^2}{\Lambda_0^2} \frac{M_W}{E}$

Table IIb. Relevant operators for model-dependent contributions.[a]

$O(g^2 \frac{E^2}{\Lambda^2})$ (from $B_1^{(0)}$)	$O(g^3 \frac{E f_\pi}{\Lambda^2})$ (from $B_1^{(1)}$)	$O(g^2 \frac{f_\pi^2}{\Lambda^2})$ (from $B_1^{(0)}$)	$O(g^4 \frac{f_\pi^2}{\Lambda^2})$ (from $B_1^{(2)}$ or $B_1^{(0)}$)
$\mathcal{L}_{3,4,5,9,11,12}$	$\mathcal{L}_{2,3,4,5,8,9,11,12,14}$	$\mathcal{L}^{(2)\prime}$	$\mathcal{L}_{1\sim5,8,9,11\sim14}$ $(B_1^{(2)})$ $\mathcal{L}_{1,2,8,13,14}$ $(B_1^{(0)})$ $\mathcal{L}_{2\sim5,8,9,11,12,14}$ $(B_1^{(0)})$ [b]

[a] We list the relevant operators for each order of B-terms.

[b] Here $B_1^{(0)}$ is contributed by $T_1[2\pi^{\pm}, 2v^{\pm}]$.

Table III. Estimates of amplitudes for $q\bar{q}^{(\prime)} \to V^a V^b$: Model-independent contributions.

Table IIIa. For $q\bar{q}^{(\prime)} \to W^+W^-$, $W^\pm Z$.

$\mathcal{L}_G + \mathcal{L}_F + \mathcal{L}^{(2)}$	$T_\ell[q\bar{q}^{(\prime)} \to \pi\pi]$	$T_\ell[q\bar{q}^{(\prime)} \to \pi V_T]$	$T_\ell[q\bar{q}^{(\prime)} \to V_T V_T]$	$B_\ell^{(0)}$	$B_\ell^{(1)}$
Tree-Level ($\ell = 0$)	g^2	$e^2 g \frac{f_\pi}{E}$	g^2	$g^2 \frac{M_W^2}{E^2}$	$g^2 \frac{M_W}{E}$
One-Loop ($\ell = 1$)	$g^2 \frac{E^2}{\Lambda_0^2}$	$g^3 \frac{f_\pi E}{\Lambda_0^2}$	$g^4 \frac{f_\pi^2}{\Lambda_0^2}$	$g^3 \frac{f_\pi M_W}{\Lambda_0^2}$	$g^4 \frac{f_\pi^2}{\Lambda_0^2} \frac{M_W}{E}$

Table IIIb. For $q\bar{q} \to ZZ$.

$\mathcal{L}_G + \mathcal{L}_F + \mathcal{L}^{(2)}$	$T_\ell[q\bar{q} \to \pi\pi]$	$T_\ell[q\bar{q} \to \pi Z_T]$	$T_\ell[q\bar{q} \to Z_T Z_T]$	$B_\ell^{(0)}$	$B_\ell^{(1)}$
Tree-Level ($\ell = 0$)	/	/	g^2	$g^2 \frac{M_W^2}{E^2}$	$g^2 \frac{M_W}{E}$
One-Loop ($\ell = 1$)	$g^2 \frac{E^2}{\Lambda_0^2}$	$g^3 \frac{f_\pi E}{\Lambda_0^2}$	$g^4 \frac{f_\pi^2}{\Lambda_0^2}$	$g^3 \frac{f_\pi M_W}{\Lambda_0^2}$	$g^4 \frac{f_\pi^2}{\Lambda_0^2} \frac{M_W}{E}$

Table IV. Estimates of amplitudes for $q\bar{q}^{(\prime)} \to V^a V^b$: Model-dependent contributions.[(a)]

Table IVa. For $q\bar{q} \to W^+W^-$.

Operators	$T_1[q\bar{q} \to \pi\pi]$	$T_1[q\bar{q} \to \pi V_T]$	$T_1[q\bar{q} \to V_T V_T]$	$B_1^{(0)}$	$B_1^{(1)}$
$\mathcal{L}^{(2)\prime}$	$\ell_0\ g^2\frac{f_\pi^2}{\Lambda^2}$	$\ell_0\ g^3\frac{f_\pi^3}{E\Lambda^2}$	/	$g^2\frac{f_\pi^2}{\Lambda^2}\frac{M_W^2}{E^2}$	/
$\mathcal{L}_{1,13}$	/	$\ell_{1,13}\ e^2 g\frac{f_\pi E}{\Lambda^2}$	$\ell_{1,13}\ e^2 g^2\frac{f_\pi^2}{\Lambda^2}$	$e^2 g^2\frac{f_\pi^2}{\Lambda^2}$	$e^2 g^2\frac{f_\pi^2}{\Lambda^2}\frac{M_W}{E}$
$\mathcal{L}_2$	$\ell_2\ e^2\frac{E^2}{\Lambda^2}$	$\ell_2\ e^2 g\frac{f_\pi E}{\Lambda^2}$	$\ell_2\ e^2 g^2\frac{f_\pi^2}{\Lambda^2}$	$e^2 g^2\frac{f_\pi^2}{\Lambda^2}$	$e^2 g^2\frac{f_\pi^2}{\Lambda^2}\frac{M_W}{E}$
$\mathcal{L}_3$	$\ell_3\ g^2\frac{E^2}{\Lambda^2}$	$\ell_3\ g^3\frac{f_\pi E}{\Lambda^2}$	$\ell_3\ g^4\frac{f_\pi^2}{\Lambda^2}$	$g^4\frac{f_\pi^2}{\Lambda^2}$	$g^4\frac{f_\pi^2}{\Lambda^2}\frac{M_W}{E}$
$\mathcal{L}_{8,14}$	/	$\ell_{8,14}\ g^3\frac{f_\pi E}{\Lambda^2}$	$\ell_{8,14}\ g^4\frac{f_\pi^2}{\Lambda^2}$	$g^4\frac{f_\pi^2}{\Lambda^2}$	$g^4\frac{f_\pi^2}{\Lambda^2}\frac{M_W}{E}$
$\mathcal{L}_9$	$\ell_9\ g^2\frac{E^2}{\Lambda^2}$	$\ell_9\ g^3\frac{f_\pi E}{\Lambda^2}$	$\ell_9\ g^4\frac{f_\pi^2}{\Lambda^2}$	$g^4\frac{f_\pi^2}{\Lambda^2}$	$g^4\frac{f_\pi^2}{\Lambda^2}\frac{M_W}{E}$
$\mathcal{L}_{11,12}$	/	$\ell_{11,12}\ g^3\frac{f_\pi E}{\Lambda^2}$	$\ell_{11,12}\ g^4\frac{f_\pi^2}{\Lambda^2}$	$g^4\frac{f_\pi^2}{\Lambda^2}$	$g^4\frac{f_\pi^2}{\Lambda^2}\frac{M_W}{E}$

[(a)] Here we only consider the light quarks ($q \neq t$) whose Yukawa coupling $y_q \approx 0$. At tree level, $q\bar{q} \to ZZ$ contains no model-dependent contribution and the operators $\mathcal{L}_{4,5,6,7,10}$ do not contribute to $q\bar{q}^{(\prime)} \to W^+W^-,\ W^\pm Z$.

Table IVb. For $q\bar{q}' \to W^{\pm}Z$.

Operators	$T_1[q\bar{q}' \to \pi^{\pm}\pi^0]$	$T_1[q\bar{q}' \to \pi V_T]$	$T_1[q\bar{q}' \to W_T^{\pm}Z_T]$	$B_1^{(0)}$	$B_1^{(1)}$
$\mathcal{L}^{(2)\prime}$	$\ell_0\ g^2\frac{f_\pi^2}{\Lambda^2}$	$\ell_0\ g^3\frac{f_\pi^3}{E\Lambda^2}$	/	$g^2\frac{f_\pi^2}{\Lambda^2}\frac{M_W^2}{E^2}$	/
$\mathcal{L}_{1,13}$	/	$\ell_{1,13}\ e^2g\frac{f_\pi E}{\Lambda^2}$	$\ell_{1,13}\ e^2g^2\frac{f_\pi^2}{\Lambda^2}$	$e^2g^2\frac{f_\pi^2}{\Lambda^2}$	$e^2g^2\frac{f_\pi^2}{\Lambda^2}\frac{M_W}{E}$
$\mathcal{L}_2$	/	$\ell_2\ e^2g\frac{f_\pi E}{\Lambda^2}$	$\ell_2\ e^2g^2\frac{f_\pi^2}{\Lambda^2}$	$e^2g^2\frac{f_\pi^2}{\Lambda^2}$	$e^2g^2\frac{f_\pi^2}{\Lambda^2}\frac{M_W}{E}$
$\mathcal{L}_3$	$\ell_3\ g^2\frac{E^2}{\Lambda^2}$	$\ell_3\ g^3\frac{f_\pi E}{\Lambda^2}$	$\ell_3\ g^4\frac{f_\pi^2}{\Lambda^2}$	$g^4\frac{f_\pi^2}{\Lambda^2}$	$g^4\frac{f_\pi^2}{\Lambda^2}\frac{M_W}{E}$
$\mathcal{L}_{8,14}$	/	$\ell_{8,14}\ g^3\frac{f_\pi E}{\Lambda^2}$	$\ell_{8,14}\ g^4\frac{f_\pi^2}{\Lambda^2}$	$g^4\frac{f_\pi^2}{\Lambda^2}$	$g^4\frac{f_\pi^2}{\Lambda^2}\frac{M_W}{E}$
$\mathcal{L}_9$	/	$\ell_9\ g^3\frac{f_\pi E}{\Lambda^2}$	$\ell_9\ g^4\frac{f_\pi^2}{\Lambda^2}$	$g^4\frac{f_\pi^2}{\Lambda^2}$	$g^4\frac{f_\pi^2}{\Lambda^2}\frac{M_W}{E}$
$\mathcal{L}_{11,12}$	$\ell_{11,12}\ g^2\frac{E^2}{\Lambda^2}$	$\ell_{11,12}\ g^3\frac{f_\pi E}{\Lambda^2}$	$\ell_{11,12}\ g^4\frac{f_\pi^2}{\Lambda^2}$	$g^4\frac{f_\pi^2}{\Lambda^2}$	$g^4\frac{f_\pi^2}{\Lambda^2}\frac{M_W}{E}$

Table V. Global classification of sensitivities to probing direct and indirect EWSB information from effective operators at the level of S-matrix elements (A).[a]

Required Precision	Relevant Operators	Relevant Amplitudes	MI or MD [b] ?
$O\left(\frac{E^2}{f_\pi^2}\right)$	$\mathcal{L}_{\rm MI}$ $(\equiv \mathcal{L}_{\rm G}+\mathcal{L}_{\rm F}+\mathcal{L}^{(2)})$	$T_0[4V_L] (\neq T_0[4Z_L])$	MI
$O\left(\frac{E^2}{f_\pi^2}\frac{E^2}{\Lambda^2},\ g\frac{E}{f_\pi}\right)$	$\mathcal{L}_{4,5}$	$T_1[4V_L]$	MD
	$\mathcal{L}_{6,7}$	$T_1[2Z_L,2W_L],\ T_1[4Z_L]$	MD
	$\mathcal{L}_{10}$	$T_1[4Z_L]$	MD
	$\mathcal{L}_{\rm MI}$	$T_0[3V_L,V_T]$ $(\neq T_0[3Z_L,Z_T])$	MI
	$\mathcal{L}_{\rm MI}$	$T_1[4V_L]$	MI
$O\left(g\frac{E}{f_\pi}\frac{E^2}{\Lambda^2},\ g^2\right)$	$\mathcal{L}_{3,4,5,9,11,12}$	$T_1[3W_L,W_T]$	MD
	$\mathcal{L}_{2,3,4,5,6,7,9,11,12}$	$T_1[2W_L,Z_L,Z_T],\ T_1[2Z_L,W_L,W_T]$	MD
	$\mathcal{L}_{3,4,5,6,7,10}$	$T_1[3Z_L,Z_T]$	MD
	$\mathcal{L}_{\rm MI}$	$T_0[2V_L,2V_T],\ T_0[4V_T]$ [c]	MI
	$\mathcal{L}_{\rm MI}$	$T_1[3V_L,V_T]$	MI
	$\mathcal{L}_{\rm MI}$	$B_0^{(0)}\simeq T_0[3\pi,v]$ $(\neq T_0[3\pi^0,v^0])$	MI
$O\left(\frac{E^2}{\Lambda^2}\right)$	$\mathcal{L}^{(2)\prime}$	$T_1[4W_L],\ T_1[2W_L,2Z_L]$	MD
$O\left(g^2\frac{E^2}{\Lambda^2},\ g^3\frac{f_\pi}{E}\right)$	$\mathcal{L}_{\rm MI}$	$T_0[V_L,3V_T], T_1[2V_L,2V_T], B_0^{(1,3)}$ [c,d]	MI
	$\mathcal{L}_{2,3,9}$	$T_1[4W_L]$	MD
	$\mathcal{L}_{3,11,12}$	$T_1[2Z_L,2W_L]$	MD
	$\mathcal{L}_{2,3,4,5,8,9,11,12,14}$	$T_1[2W_L,2W_T]$	MD
	$\mathcal{L}_{1\sim9,11\sim14}$	$T_1[2V_L,2V_T]$ [e]	MD
	$\mathcal{L}_{4,5,6,7,10}$	$T_1[2Z_L,2Z_T]$	MD
	$\mathcal{L}_{\rm MI,2,3,4,5,6,7,9\sim12}$	$B_1^{(0)}\simeq T_1[3\pi,v]$ [f,g]	MI + MD
$O\left(g^3\frac{Ef_\pi}{\Lambda^2},\ g^4\frac{f_\pi^2}{E^2}\right)$	$\mathcal{L}_{\rm MI,1,2,3,8,9,11\sim14}$	$T_1[V_L,3V_T]$ $(\neq T_1[Z_L,3Z_T])$	MI+MD
	$\mathcal{L}_{4,5}$	$T_1[V_L,3V_T]$	MD
	$\mathcal{L}_{6,7,10}$	$T_1[V_L,3V_T]$ $(\neq T_1[W_L,3W_T])$ [g]	MD
	$\mathcal{L}_{2\sim5,8,9,11,12,14}$	$B_1^{(1)}\simeq T_1[2\pi,V_T,v]$	MD
	$\mathcal{L}_{\rm MI}$	$B_0^{(2)}\simeq T_0[2V_T,2v]$ [c,h]	MI
$O\left((g^2,g^4)\frac{f_\pi^2}{\Lambda^2}\right)$	$\mathcal{L}^{(2)\prime}$	$T_1[2V_L,2V_T], B_1^{(0)}\simeq T_1[3\pi,v]$ [c]	MD
	$\mathcal{L}_1$	$T_1[2W_L,2W_T]$ [i]	MD
	$\mathcal{L}_{\rm MI,1\sim5,8,9,11\sim14}$	$T_1[4W_T]$	MI+MD
	$\mathcal{L}_{\rm MI,1\sim9,11\sim14}$	$T_1[4V_T]$ $(\neq T_1[4W_T],T_1[4Z_T])$	MI+MD
	$\mathcal{L}_{\rm MI,1,4,5,6,7,10}$	$T_1[4Z_T]$	MI+MD
	$\mathcal{L}_{1,2,8,13,14}$	$B_1^{(0)}\simeq T_1[3\pi,v]$ [c,j]	MD
	$\mathcal{L}_{\rm MI,1\sim9,11\sim14}$	$B_1^{(0)}\simeq T_1[2\pi,2v]$ [c,k]	MI+MD
	$\mathcal{L}_{\rm MI,4,5,6,7,10}$	$B_1^{(0)}\simeq T_1[2\pi,2v] (\neq T_1[2\pi^\pm,2v^\pm])$ [g]	MI+MD
	$\mathcal{L}_{\rm MI,1\sim5,8,9,11\sim14}$	$B_1^{(2)}\simeq T_1[\pi^\pm,2W_T,v^\pm]$	MI+MD
	$\mathcal{L}_{\rm MI,1\sim9,11\sim14}$	$B_1^{(2)}\not\simeq T_1[\pi^\pm,2W_T,v^\pm], T_1[\pi^0,2Z_T,v^0]$	MI+MD
	$\mathcal{L}_{\rm MI,4,5,6,7,10}$	$B_1^{(2)}\simeq T_1[\pi^0,2Z_T,v^0]$	MI+MD

Table VI. Global classification of sensitivities to probing direct and indirect EWSB information from effective operators at the level of S-matrix elements (B).

Required Precision	Relevant Operators	Relevant Amplitudes	MI or MD [b] ?
$O(g^2)$	$\mathcal{L}_{\rm MI}$ $(\equiv \mathcal{L}_{\rm G} + \mathcal{L}_{\rm F} + \mathcal{L}^{(2)})$	$T_0[q\bar{q}; V_L V_L]$, $T_0[q\bar{q}; V_T V_T]$	MI
$O\left(g^2\frac{E^2}{\Lambda^2},\ g^3\frac{f_\pi}{E}\right)$	$\mathcal{L}_{2,3,9}$ $\mathcal{L}_{3,11,12}$ $\mathcal{L}_{\rm MI}$ $\mathcal{L}_{\rm MI}$ $\mathcal{L}_{\rm MI}$	$T_1[q\bar{q}; W_L W_L]$ $T_1[q\bar{q}; W_L Z_L]$ $T_0[q\bar{q}; V_L V_T]$ $T_1[q\bar{q}; V_L V_L]$ $B_0^{(1)} \simeq T_0[q\bar{q}; V_T, v]$	MD MD MI MI MI
$O\left(g^3\frac{E f_\pi}{\Lambda^2},\ g^4\frac{f_\pi^2}{E^2}\right)$	$\mathcal{L}_{1,2,3,8,9,11\sim14}$ $\mathcal{L}_{\rm MI}$ $\mathcal{L}_{\rm MI}$	$T_1[q\bar{q}; V_L V_T]$ $T_1[q\bar{q}; V_L V_T]$ $B_0^{(0)} \simeq T_0[q\bar{q}; 2v]$ [c]	MD MI MI
$O\left((g^2, g^4)\frac{f_\pi^2}{\Lambda^2}\right)$	$\mathcal{L}^{(2)\prime}$ $\mathcal{L}_{1,2,3,8,9,11\sim14}$ $\mathcal{L}_{\rm MI}$	$T_1[q\bar{q}; V_L V_L]$ $T_1[q\bar{q}; V_T V_T]$, $B_1^{(0)} \simeq T_1[q\bar{q}; \pi, v]$ $T_1[q\bar{q}; V_T V_T]$, $B_1^{(0)} \simeq T_1[q\bar{q}; \pi, v]$	MD MD MI

[a] The contributions from $\mathcal{L}_{1,2,13}$ are always associated with a factor of $\sin^2\theta_W$, unless specified otherwise. $\mathcal{L}_{4,5,6,7,10}$ do not contribute to the processes considered in this table. Also, for contributions to the B-term in a given V_L-amplitude, we list them separately with the B-term specified.

[b] MI = model-independent, MD = model-dependent.

[c] Here, $B_0^{(0)}$ is dominated by $T_0[q\bar{q}; 2v]$ since $T_0[q\bar{q}; \pi, v]$ contains a suppressing factor $\sin^2\theta_W$ as can be deduced from $T_0[q\bar{q}; \pi V_T]$ (cf. Table 3a) times the factor $v^\mu = O\left(\frac{M_W}{E}\right)$.

Table VII. Probing the EWSB Sector at High Energy Colliders: A Global Classification for the NLO Bosonic Operators

(Notations: $\surd$ = Leading contributions, $\triangle$ = Sub-leading contributions, and $\perp$ = Low-energy contributions. Notes: †Here, $\mathcal{L}_{13}$ or $\mathcal{L}_{14}$ does not contribute at $O(1/\Lambda^2)$. ‡At LHC(14), $W^+W^+ \to W^+W^+$ should also be included.)

Operators	$\mathcal{L}^{(2)\prime}$	$\mathcal{L}_{1,13}$	$\mathcal{L}_2$	$\mathcal{L}_3$	$\mathcal{L}_{4,5}$	$\mathcal{L}_{6,7}$	$\mathcal{L}_{8,14}$	$\mathcal{L}_9$	$\mathcal{L}_{10}$	$\mathcal{L}_{11,12}$	$T_1 \parallel B$	Processes
LEP-I (S,T,U)	$\perp$	$\perp$ †					$\perp$ †				$g^4\frac{f_\pi^2}{\Lambda^2}$	$e^-e^+ \to Z \to f\bar{f}$
LEP-II	$\perp$	$\perp$	$\perp$	$\perp$			$\perp$	$\perp$		$\perp$	$g^4\frac{f_\pi^2}{\Lambda^2}$	$e^-e^+ \to W^-W^+$
LC(0.5)/LHC(14)			$\surd$	$\surd$				$\surd$			$g^2\frac{E^2}{\Lambda^2} \parallel g^2\frac{M_W^2}{E^2}$	$f\bar{f} \to W^-W^+/(LL)$
		$\triangle$	$\triangle$	$\triangle$			$\triangle$	$\triangle$		$\triangle$	$g^3\frac{Ef_\pi}{\Lambda^2} \parallel g^2\frac{M_W}{E}$	$f\bar{f} \to W^-W^+/(LT)$
LC(1.5)/LHC(14)				$\surd$	$\surd$	$\surd$		$\surd$		$\surd$	$g^2\frac{1}{f_\pi}\frac{E^2}{\Lambda^2} \parallel g^3\frac{M_W}{E^2}$	$f\bar{f} \to W^-W^+Z/(LLL)$
		$\triangle$	$\triangle$	$\triangle$	$\triangle$	$\triangle$	$\triangle$	$\triangle$		$\triangle$	$g^3\frac{E}{\Lambda^2} \parallel g^3\frac{M_W^2}{E^3}$	$f\bar{f} \to W^-W^+Z/(LLT)$
				$\surd$	$\surd$	$\surd$			$\surd$		$g^2\frac{1}{f_\pi}\frac{E^2}{\Lambda^2} \parallel g^3\frac{M_W}{\Lambda^2}$	$f\bar{f} \to ZZZ/(LLL)$
					$\triangle$	$\triangle$			$\triangle$		$g^3\frac{E}{\Lambda^2} \parallel g^3\frac{f_\pi}{\Lambda^2}\frac{M_W}{E}$	$f\bar{f} \to ZZZ/(LLT)$
					$\surd$						$\frac{E^2}{f_\pi^2}\frac{E^2}{\Lambda^2} \parallel g^2$	$W^-W^\pm \to W^-W^\pm/(LLLL)$ ‡
				$\triangle$	$\triangle$			$\triangle$		$\triangle$	$g\frac{E}{f_\pi}\frac{E^2}{\Lambda^2} \parallel g^2\frac{M_W}{E}$	$W^-W^\pm \to W^-W^\pm/(LLLT)$ ‡
					$\surd$	$\surd$					$\frac{E^2}{f_\pi^2}\frac{E^2}{\Lambda^2} \parallel g^2$	$W^-W^+ \to ZZ$ & perm./$(LLLL)$
			$\triangle$	$\triangle$	$\triangle$	$\triangle$		$\triangle$		$\triangle$	$g\frac{E}{f_\pi}\frac{E^2}{\Lambda^2} \parallel g^2\frac{M_W}{E}$	$W^-W^+ \to ZZ$ & perm./$(LLLT)$
					$\surd$	$\surd$			$\surd$		$\frac{E^2}{f_\pi^2}\frac{E^2}{\Lambda^2} \parallel g^2\frac{E^2}{\Lambda^2}$	$ZZ \to ZZ/(LLLL)$
				$\triangle$	$\triangle$	$\triangle$			$\triangle$		$g\frac{E}{f_\pi}\frac{E^2}{\Lambda^2} \parallel g^2\frac{M_WE}{\Lambda^2}$	$ZZ \to ZZ/(LLLT)$
LHC(14)				$\surd$						$\surd$	$g^2\frac{E^2}{\Lambda^2} \parallel g^2\frac{M_W^2}{E^2}$	$q\bar{q}' \to W^\pm Z/(LL)$
		$\triangle$	$\triangle$	$\triangle$			$\triangle$	$\triangle$		$\triangle$	$g^3\frac{Ef_\pi}{\Lambda^2} \parallel g^2\frac{M_W}{E}$	$q\bar{q}' \to W^\pm Z/(LT)$
				$\surd$	$\surd$			$\surd$		$\surd$	$g^2\frac{1}{f_\pi}\frac{E^2}{\Lambda^2} \parallel g^3\frac{M_W}{E^2}$	$q\bar{q}' \to W^-W^+W^\pm/(LLL)$
			$\triangle$	$\triangle$	$\triangle$		$\triangle$	$\triangle$		$\triangle$	$g^3\frac{E}{\Lambda^2} \parallel g^3\frac{M_W^2}{E^3}$	$q\bar{q}' \to W^-W^+W^\pm/(LLT)$
				$\surd$	$\surd$	$\surd$				$\surd$	$g^2\frac{1}{f_\pi}\frac{E^2}{\Lambda^2} \parallel g^3\frac{M_W}{E^2}$	$q\bar{q}' \to W^\pm ZZ/(LLL)$
		$\triangle$	$\triangle$	$\triangle$	$\triangle$	$\triangle$	$\triangle$	$\triangle$		$\triangle$	$g^3\frac{E}{\Lambda^2} \parallel g^3\frac{M_W^2}{E^3}$	$q\bar{q}' \to W^\pm ZZ/(LLT)$
LC($e^-\gamma$)		$\surd$	$\surd$	$\surd$			$\surd$	$\surd$		$\surd$	$eg^2\frac{E}{\Lambda^2} \parallel eg^2\frac{M_W^2}{E^3}$	$e^-\gamma \to \nu_e W^-Z, e^-WW/(LL)$
LC($\gamma\gamma$)		$\surd$	$\surd$	$\surd$			$\surd$	$\surd$			$e^2\frac{E^2}{\Lambda^2} \parallel e^2\frac{M_W^2}{E^2}$	$\gamma\gamma \to W^-W^+/(LL)$
		$\triangle$	$\triangle$	$\triangle$			$\triangle$	$\triangle$			$e^2g\frac{Ef_\pi}{\Lambda^2} \parallel e^2\frac{M_W}{E}$	$\gamma\gamma \to W^-W^+/(LT)$

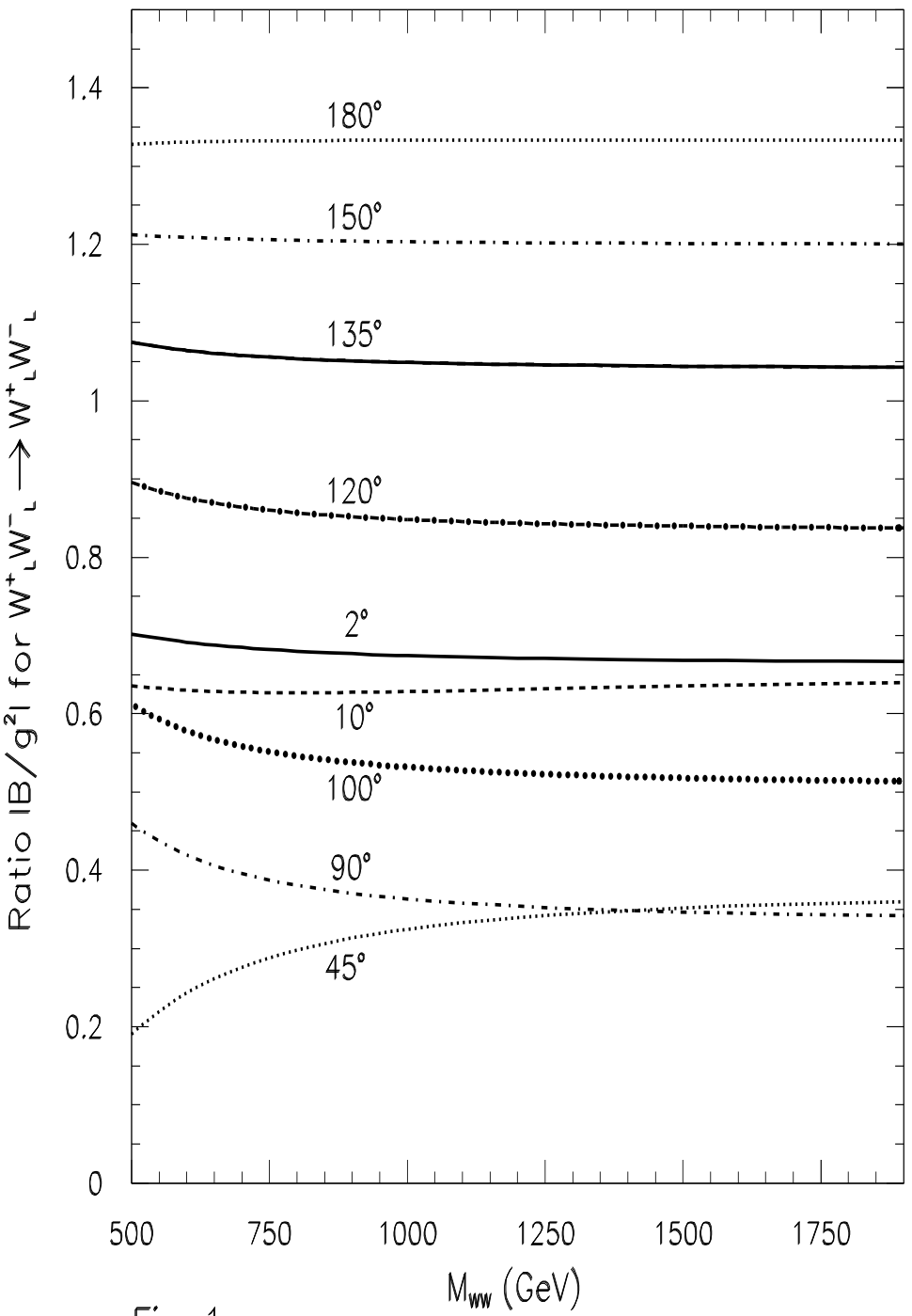
1.4
1.2
1
0.8
0.6
0.4
0.2
0
180°
150°
135°
120°
2°
10°
100°
90°
45°
500
750
1000
1250
1500
1750
M_{ww} (GeV)
Ratio IB/g^2I for $W^+_L W^-_L \longrightarrow W^+_L W^-_L$

Fig. 1a.

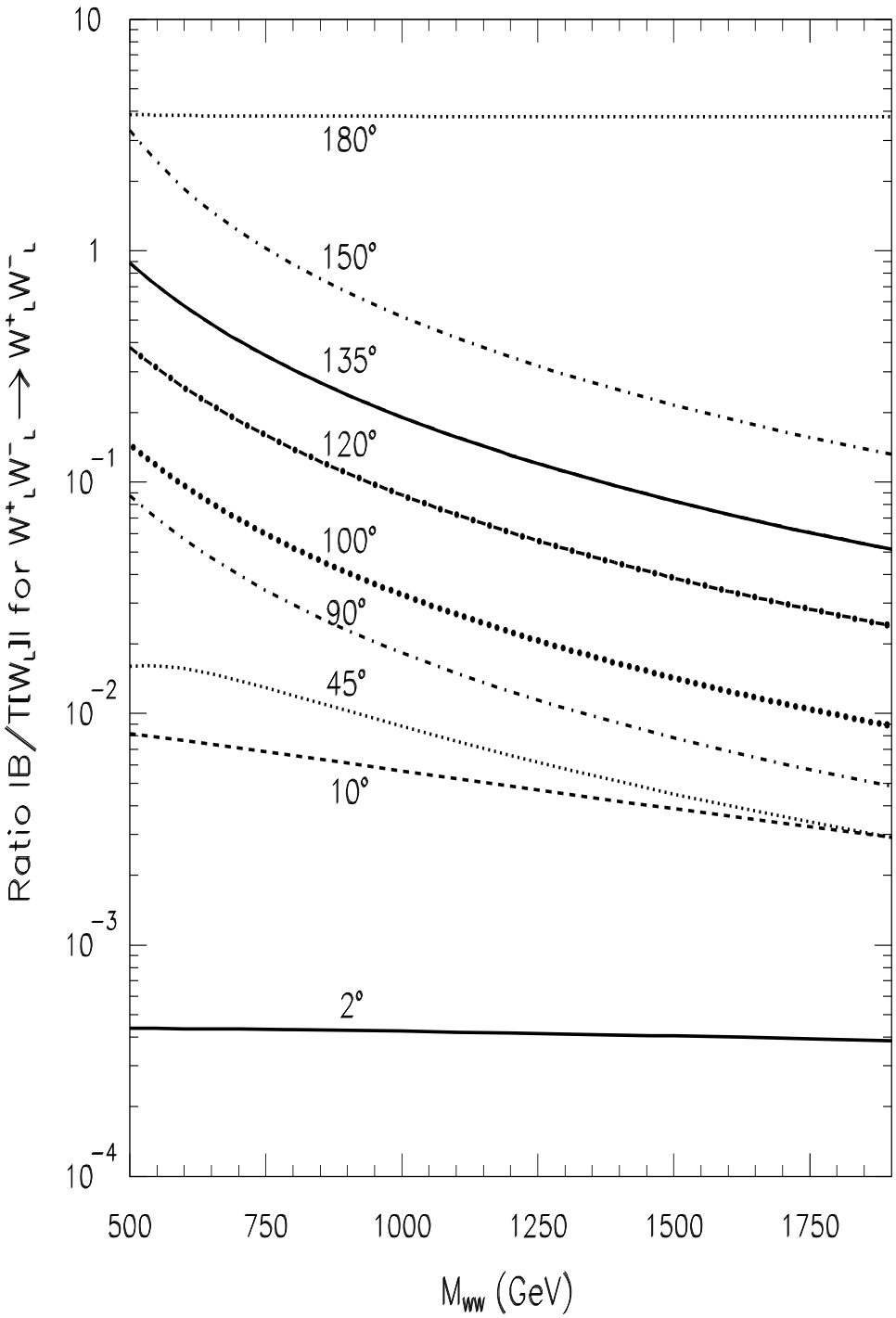
10
1
10^{-1}
10^{-2}
10^{-3}
10^{-4}
180°
150°
135°
120°
100°
90°
45°
10°
2°
500
750
1000
1250
1500
1750
M_{WW} (GeV)
Ratio IB/T[W_L]I for $W^+_L W^-_L \rightarrow W^+_L W^-_L$

Fig. 1b.

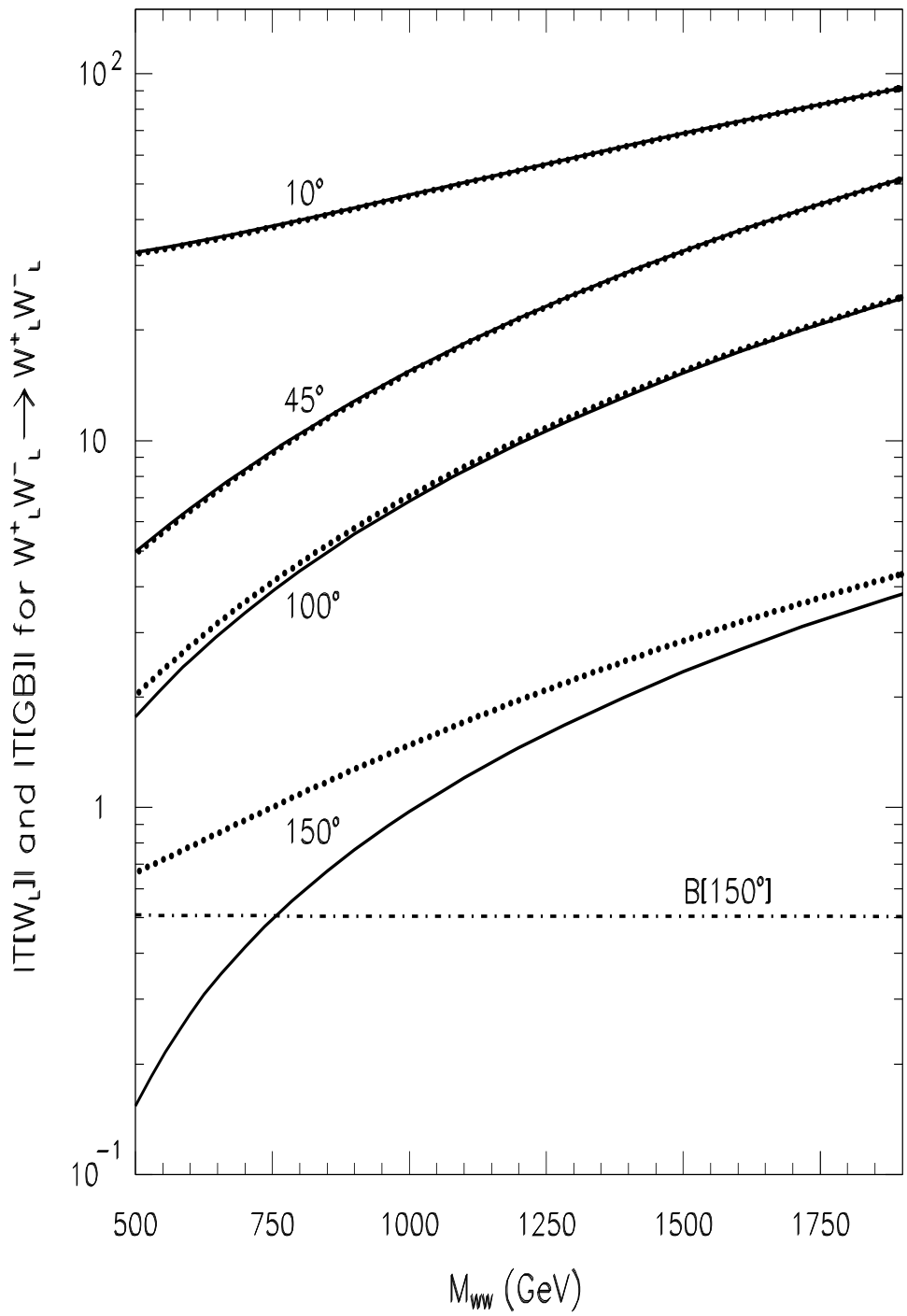
10^2
10
1
10^{-1}
10°
45°
100°
150°
B[150°]
500
750
1000
1250
1500
1750
M_{WW} (GeV)
$|T[W_L]|$ and $|T[GB]|$ for $W^+_L W^-_L \longrightarrow W^+_L W^-_L$

Fig. 1c.

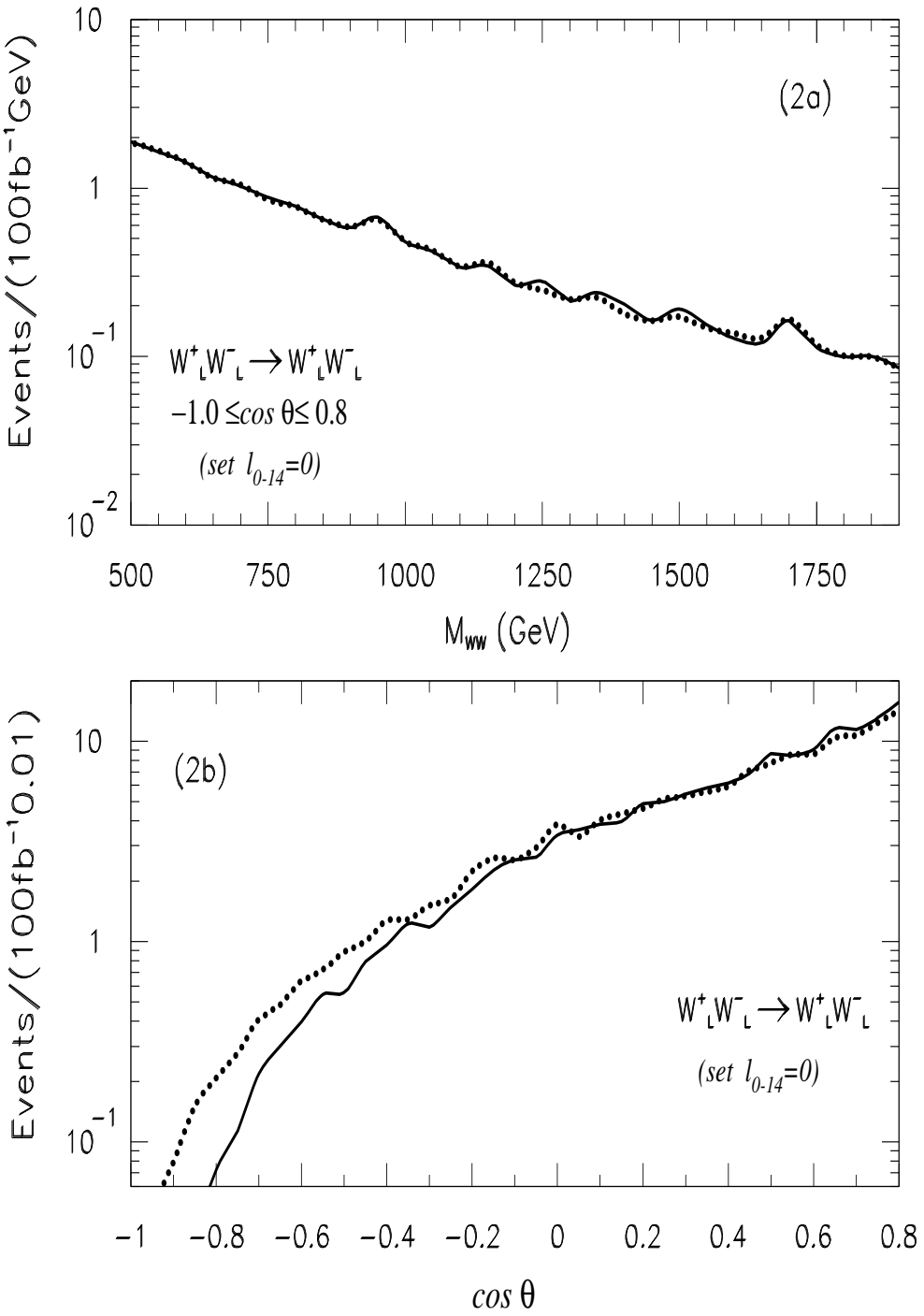

Figs. 2a and 2b.

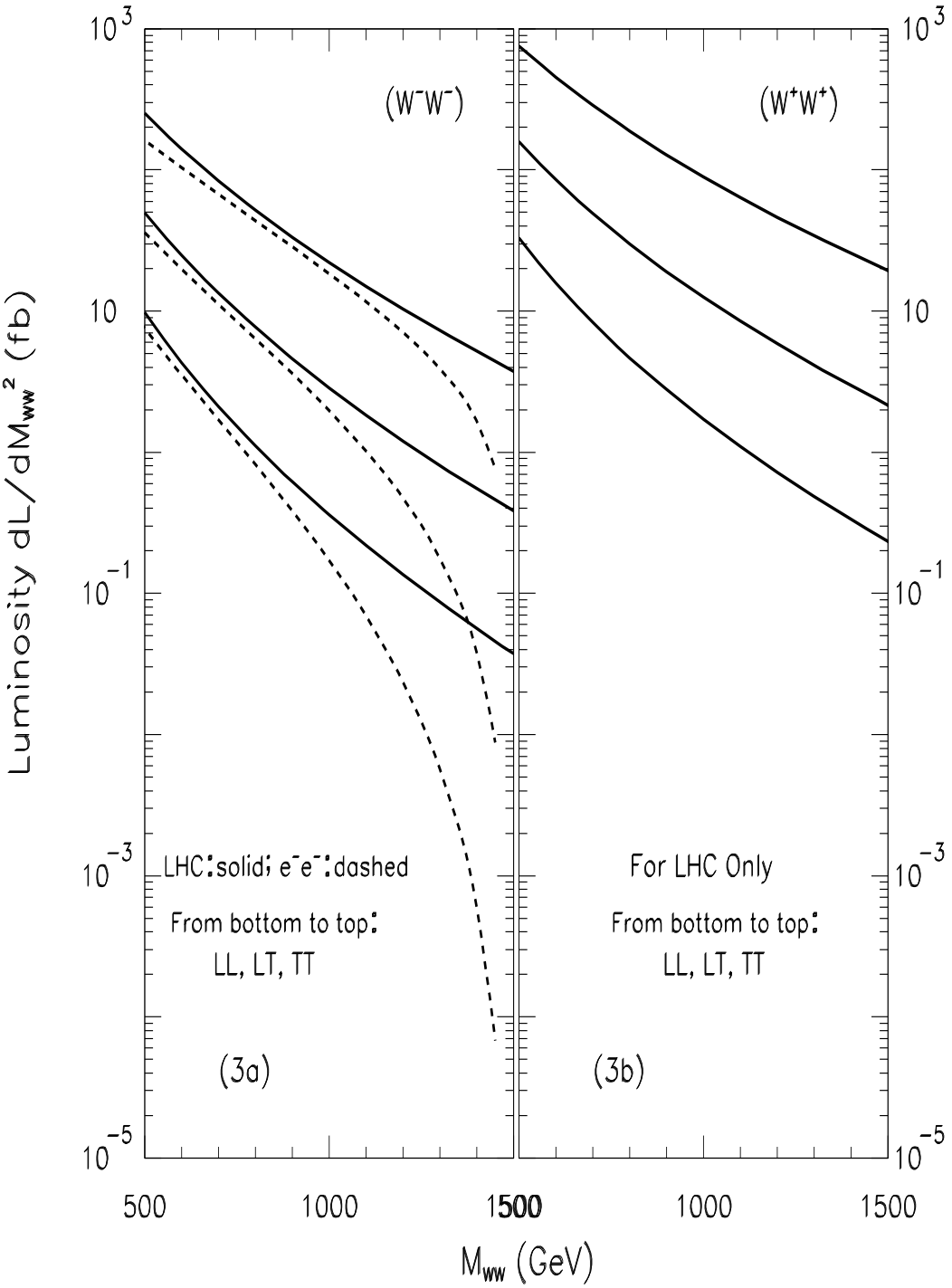

Figs.3a and 3b.

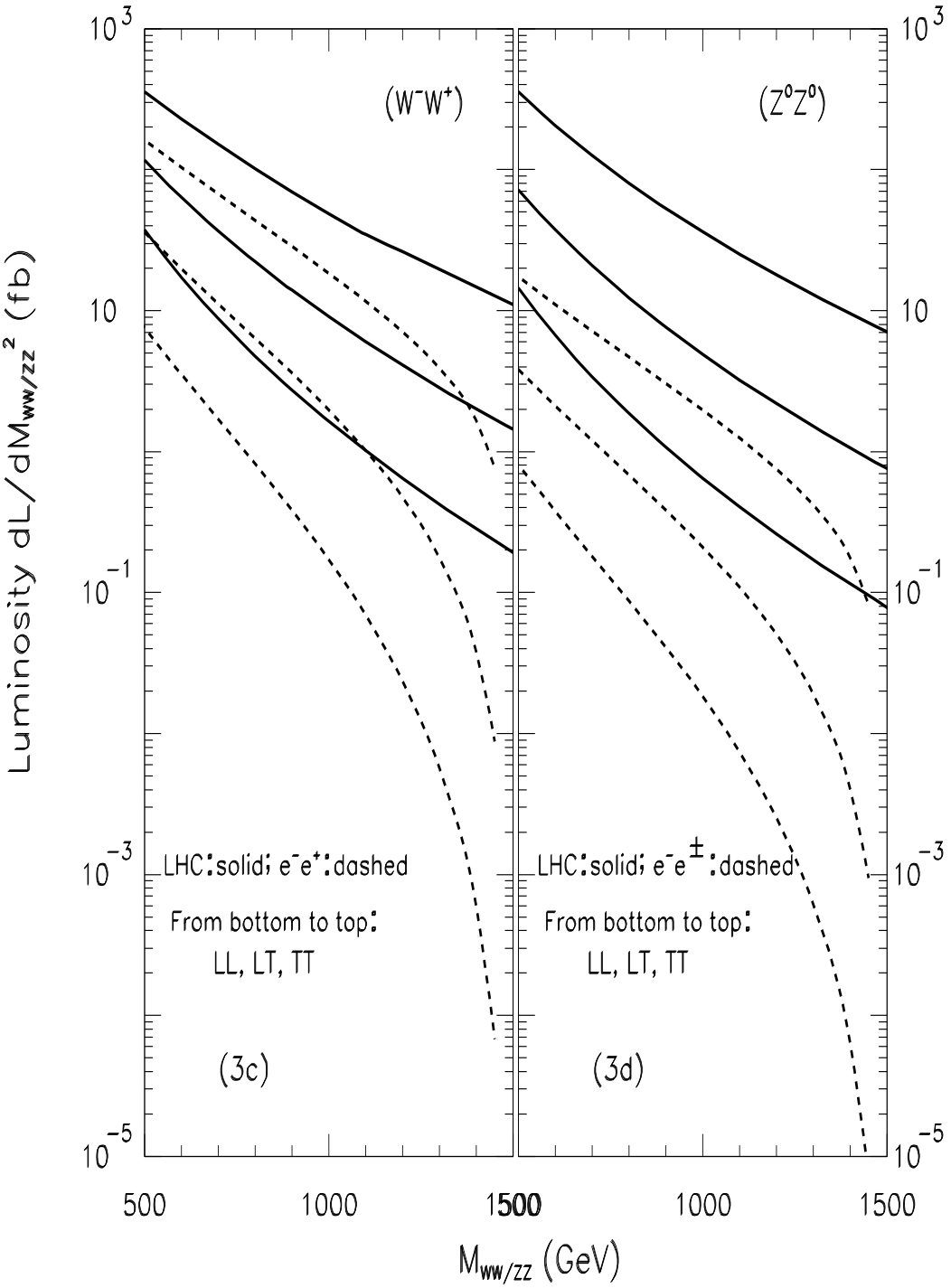

Figs. 3c and 3d.

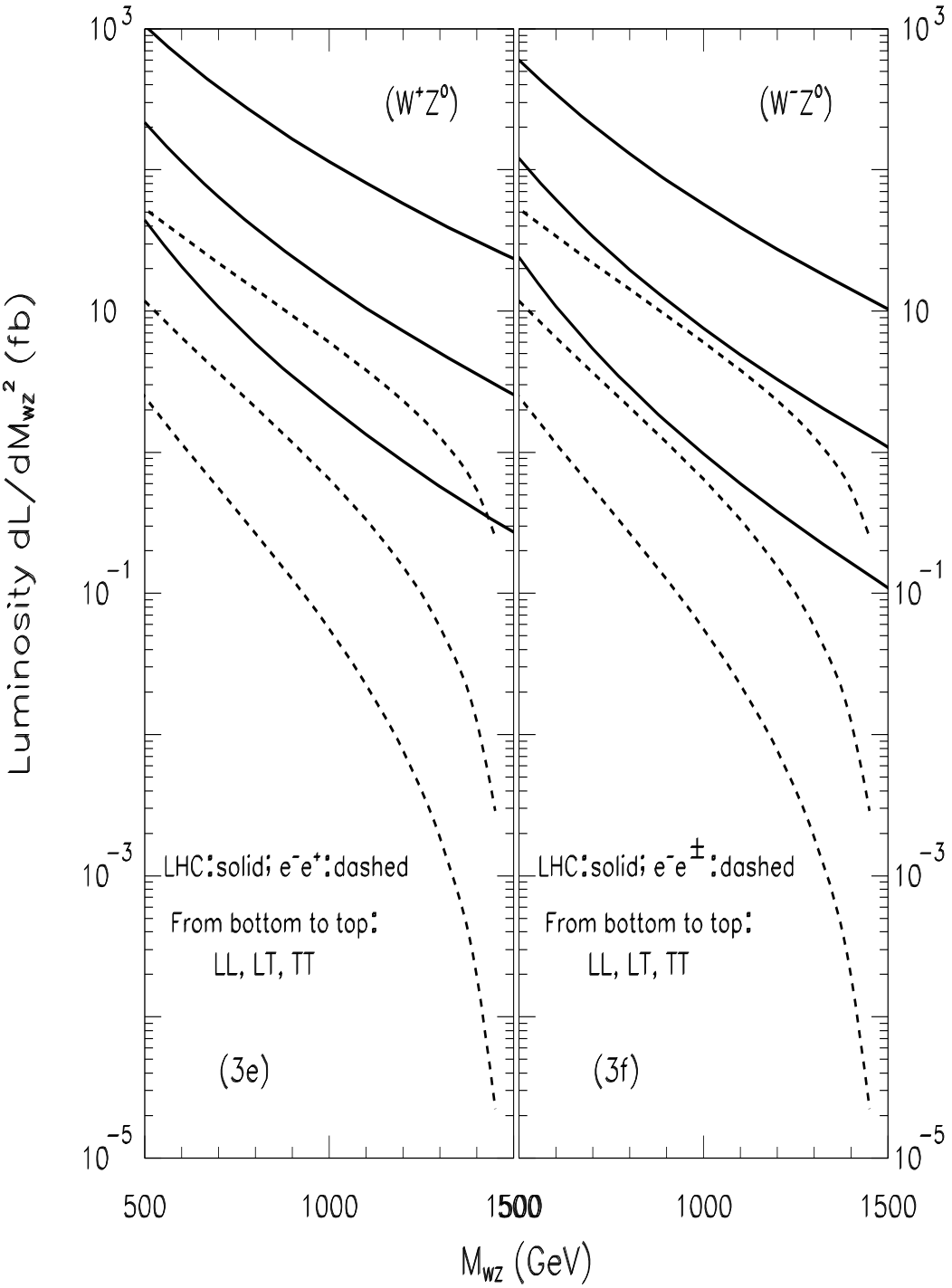

Figs. 3e and 3f.

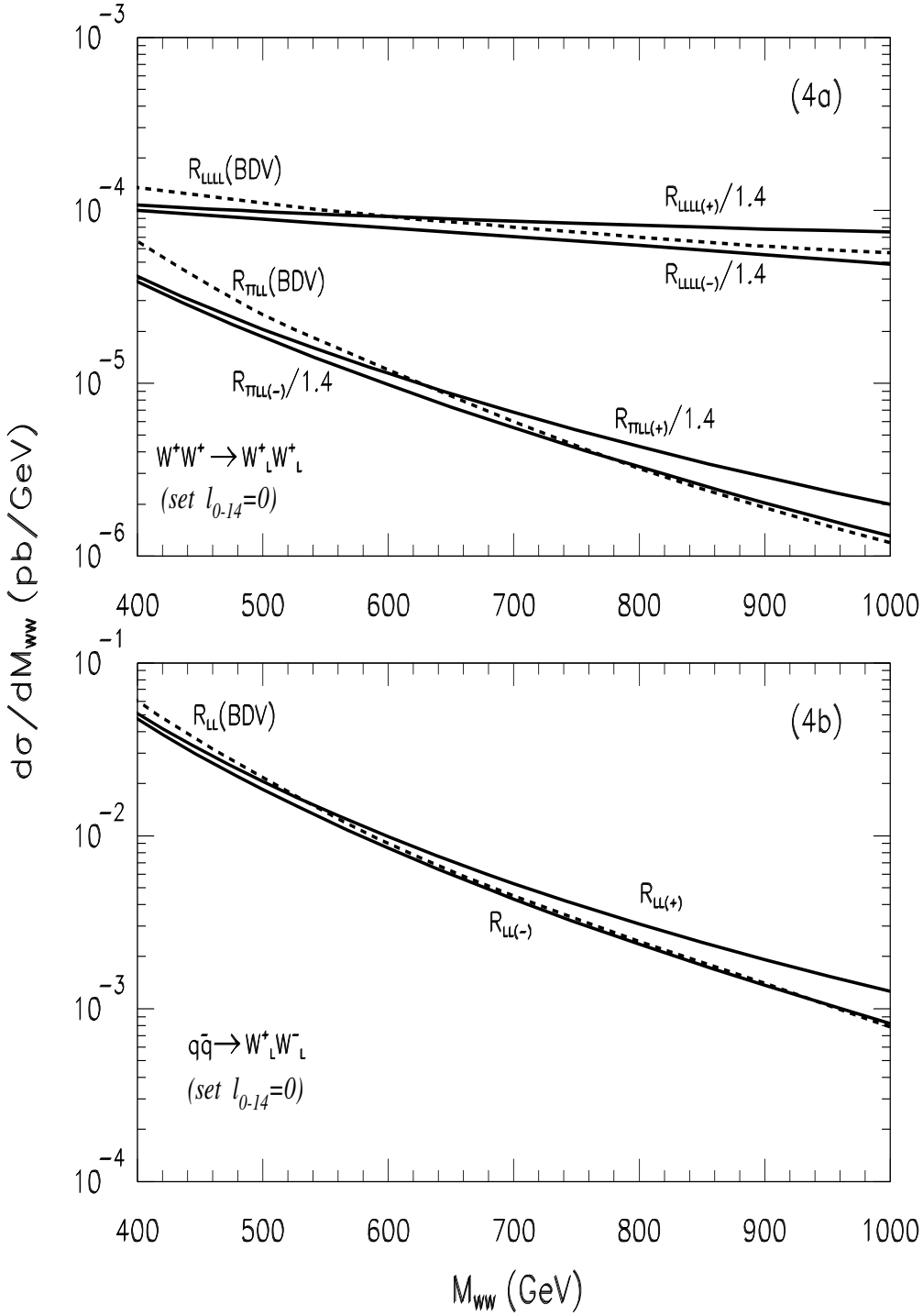
(4a)
R_{LLLL}(BDV)
$R_{LLLL(+)}/1.4$
$R_{LLLL(-)}/1.4$
$R_{\pi LL}$(BDV)
$R_{\pi LL(-)}/1.4$
$R_{\pi LL(+)}/1.4$
$W^+W^+ \to W^+_L W^+_L$
(set $l_{0\text{-}14}$=0)
(4b)
R_{LL}(BDV)
$R_{LL(+)}$
$R_{LL(-)}$
$q\bar{q} \to W^+_L W^-_L$
(set $l_{0\text{-}14}$=0)
$d\sigma/dM_{WW}$ (pb/GeV)
M_{WW} (GeV)

Fig. 4.

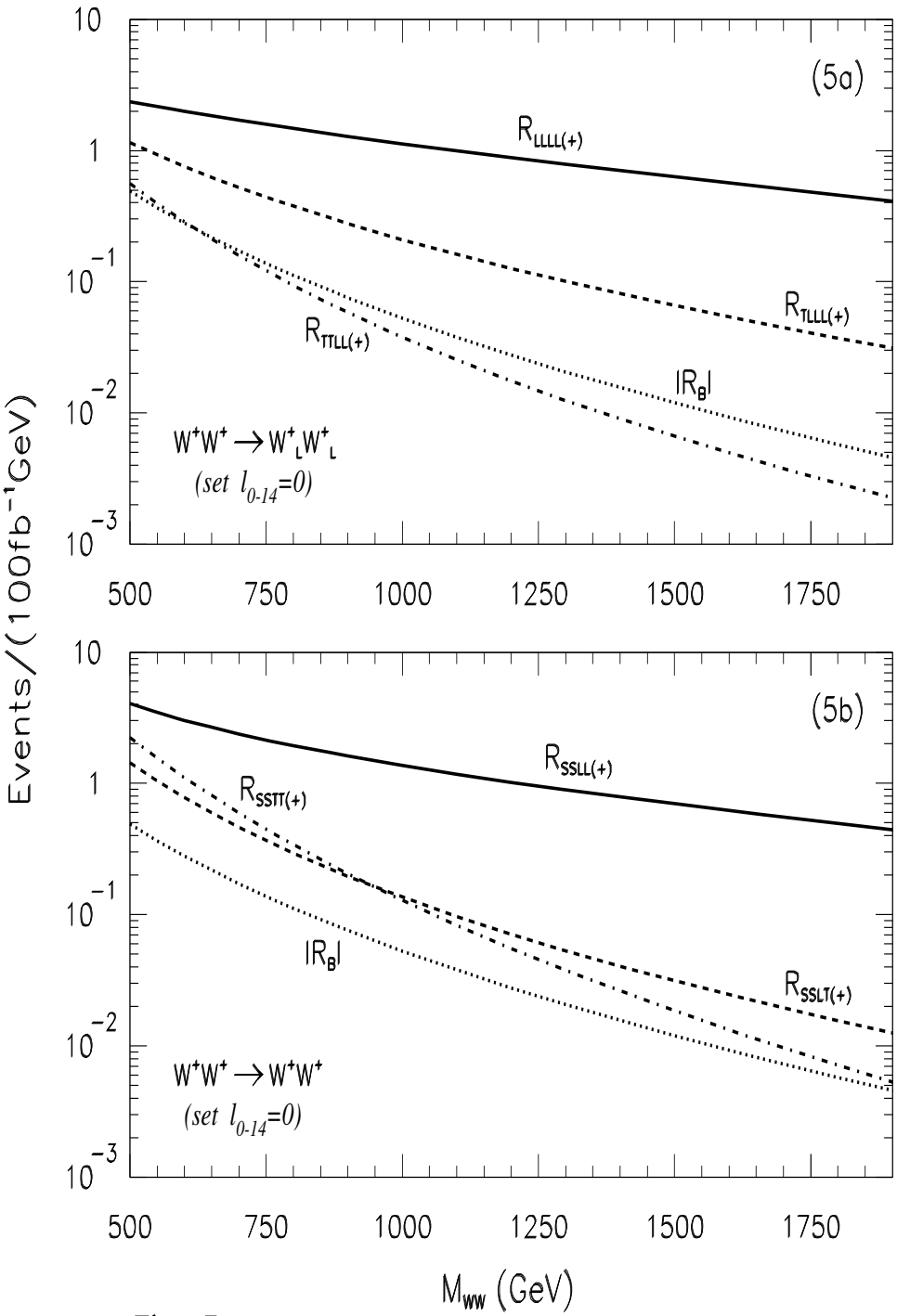
(5a)
$R_{LLLL(+)}$
$R_{TLLL(+)}$
$R_{TTLL(+)}$
$|R_B|$
$W^+W^+ \to W^+_L W^+_L$
(set $l_{0\text{-}14}$=0)
(5b)
$R_{SSLL(+)}$
$R_{SSTT(+)}$
$R_{SSLT(+)}$
$|R_B|$
$W^+W^+ \to W^+W^+$
(set $l_{0\text{-}14}$=0)
Events/(100fb^{-1}GeV)
M_{WW} (GeV)

Fig. 5.

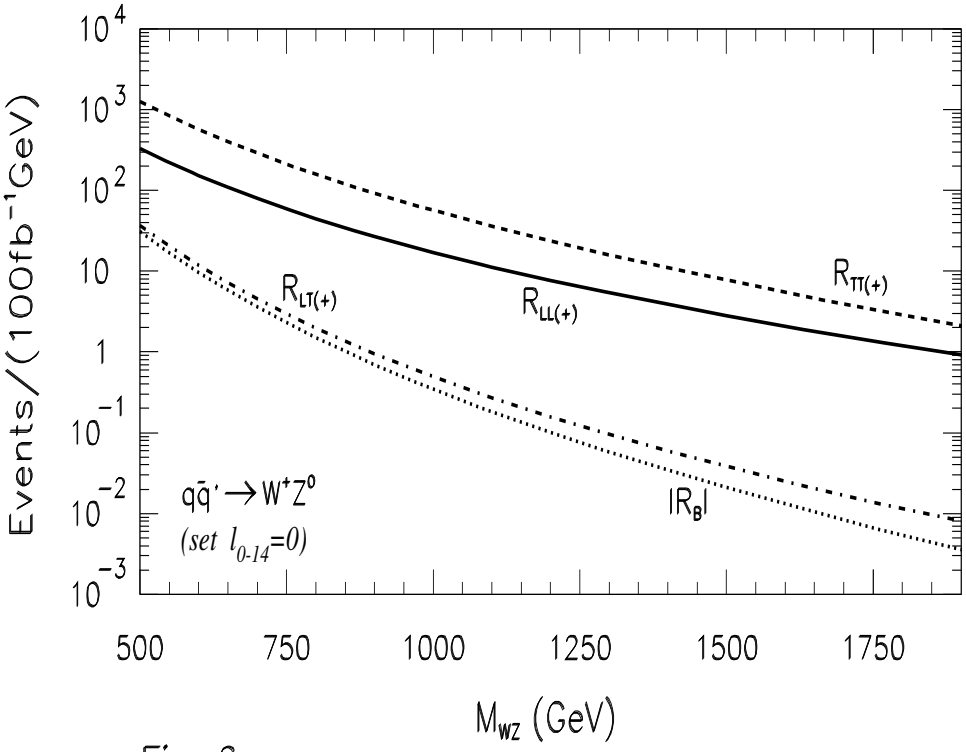
Events/(100fb^{-1}GeV)
10^4
10^3
10^2
10
1
10^{-1}
10^{-2}
10^{-3}
500
750
1000
1250
1500
1750
M_{WZ} (GeV)
$R_{TT(+)}$
$R_{LL(+)}$
$R_{LT(+)}$
$|R_B|$
$q\bar{q}' \to W^+Z^0$
(set $l_{0\text{-}14}$=0)

Fig. 6.

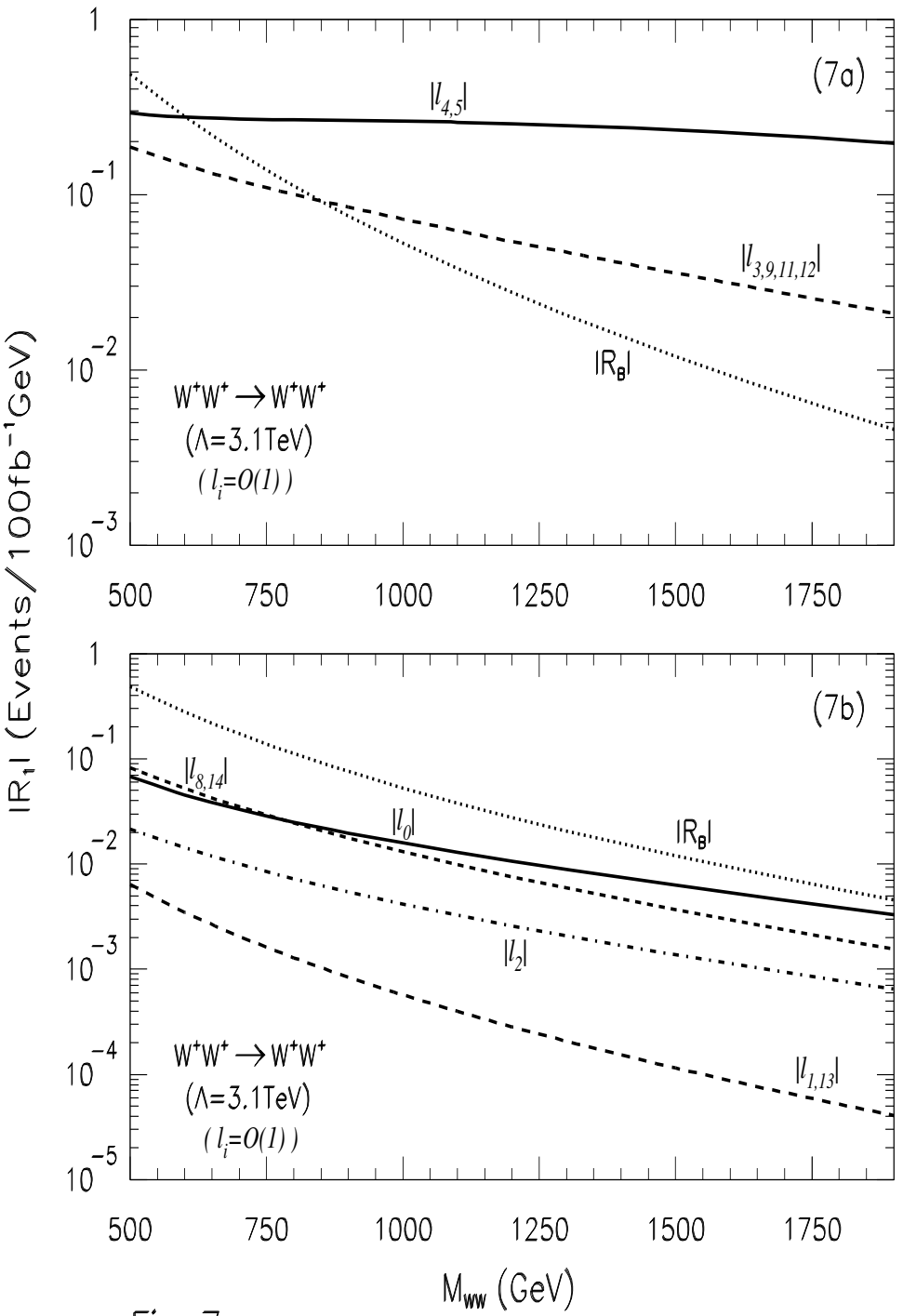
(7a)
$|l_{4,5}|$
$|l_{3,9,11,12}|$
$|R_B|$
$W^+W^+ \rightarrow W^+W^+$
$(\Lambda=3.1\text{TeV})$
$(l_i=O(1))$
(7b)
$|l_{8,14}|$
$|l_0|$
$|R_B|$
$|l_2|$
$|l_{1,13}|$
$W^+W^+ \rightarrow W^+W^+$
$(\Lambda=3.1\text{TeV})$
$(l_i=O(1))$
$|R_i|$ (Events/100fb^{-1}GeV)
M_{WW} (GeV)

Fig. 7.

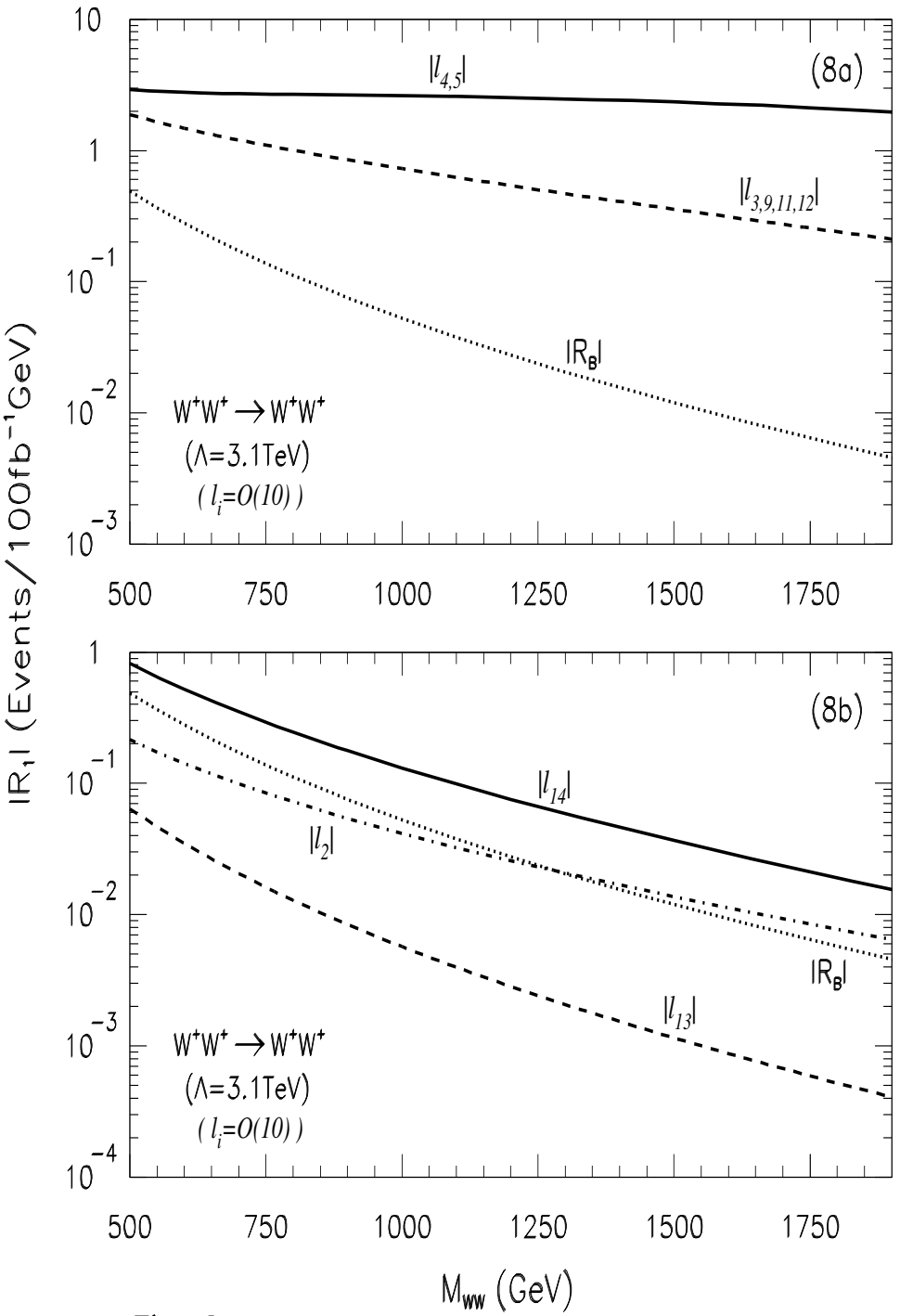
(8a)
$|l_{4,5}|$
$|l_{3,9,11,12}|$
$|R_B|$
$W^+W^+ \to W^+W^+$
$(\Lambda=3.1\text{TeV})$
$(\ l_i=O(10)\ )$
(8b)
$|l_{14}|$
$|l_2|$
$|R_B|$
$|l_{13}|$
$W^+W^+ \to W^+W^+$
$(\Lambda=3.1\text{TeV})$
$(\ l_i=O(10)\ )$
$|R_1|$ (Events/100fb^{-1}GeV)
M_{WW} (GeV)

Fig. 8.

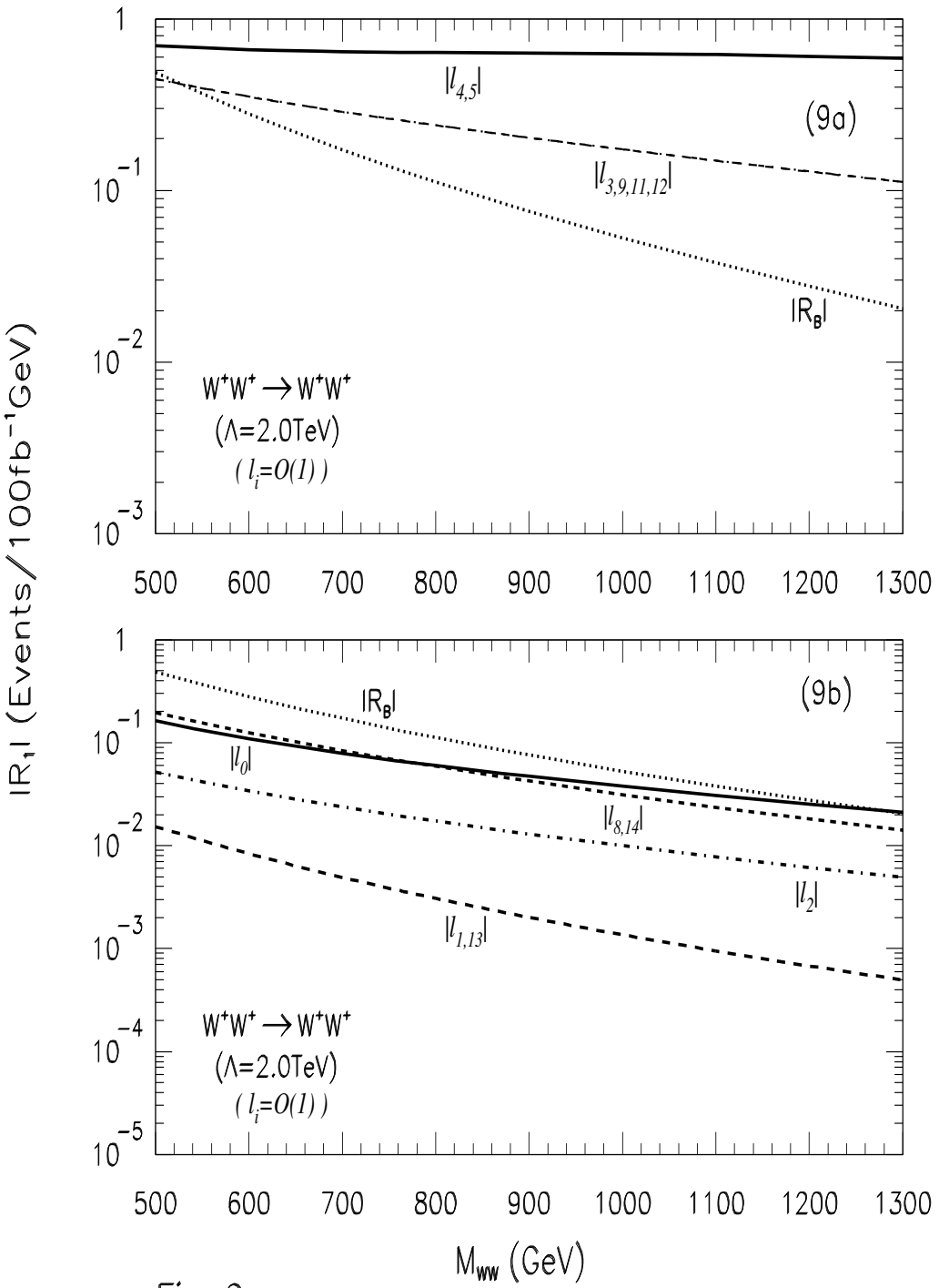
1
10^{-1}
10^{-2}
10^{-3}
$|l_{4,5}|$
(9a)
$|l_{3,9,11,12}|$
$|R_B|$
$W^+W^+ \rightarrow W^+W^+$
(Λ=2.0TeV)
(l_i=O(1))
500 600 700 800 900 1000 1100 1200 1300
1
10^{-1}
10^{-2}
10^{-3}
10^{-4}
10^{-5}
$|R_B|$
(9b)
$|l_0|$
$|l_{8,14}|$
$|l_2|$
$|l_{1,13}|$
$W^+W^+ \rightarrow W^+W^+$
(Λ=2.0TeV)
(l_i=O(1))
500 600 700 800 900 1000 1100 1200 1300
$|R_1|$ (Events/100fb^{-1}GeV)
M_{WW} (GeV)

Fig. 9.

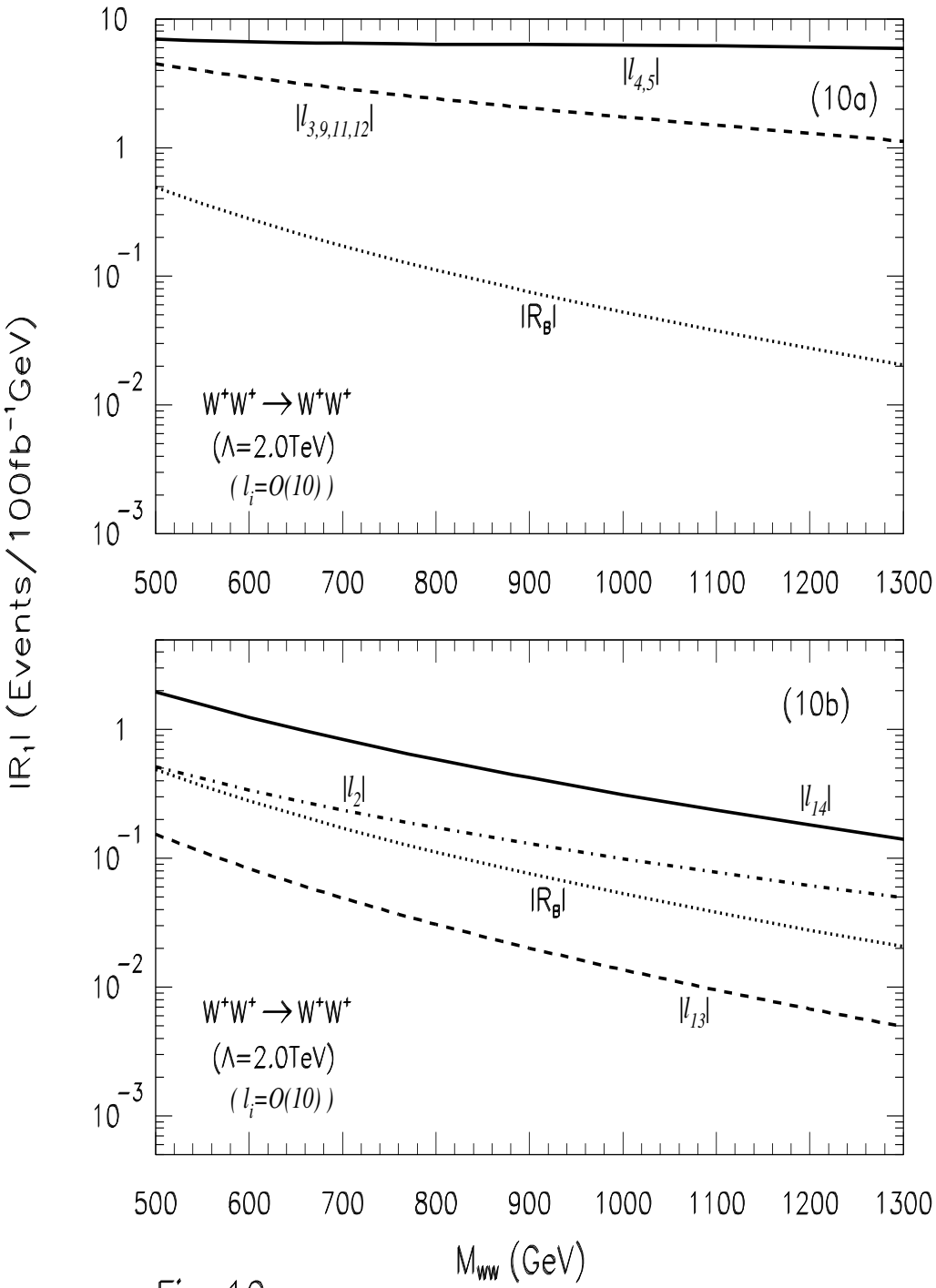
10
1
10^{-1}
10^{-2}
10^{-3}
$|l_{4,5}|$
(10a)
$|l_{3,9,11,12}|$
$|R_B|$
$W^+W^+ \to W^+W^+$
(Λ=2.0TeV)
(l_i=O(10))
500 600 700 800 900 1000 1100 1200 1300
(10b)
$|l_2|$
$|l_{14}|$
$|R_B|$
$|l_{13}|$
$W^+W^+ \to W^+W^+$
(Λ=2.0TeV)
(l_i=O(10))
$|R_i|$ (Events/100fb^{-1}GeV)
M_{WW} (GeV)

Fig. 10.

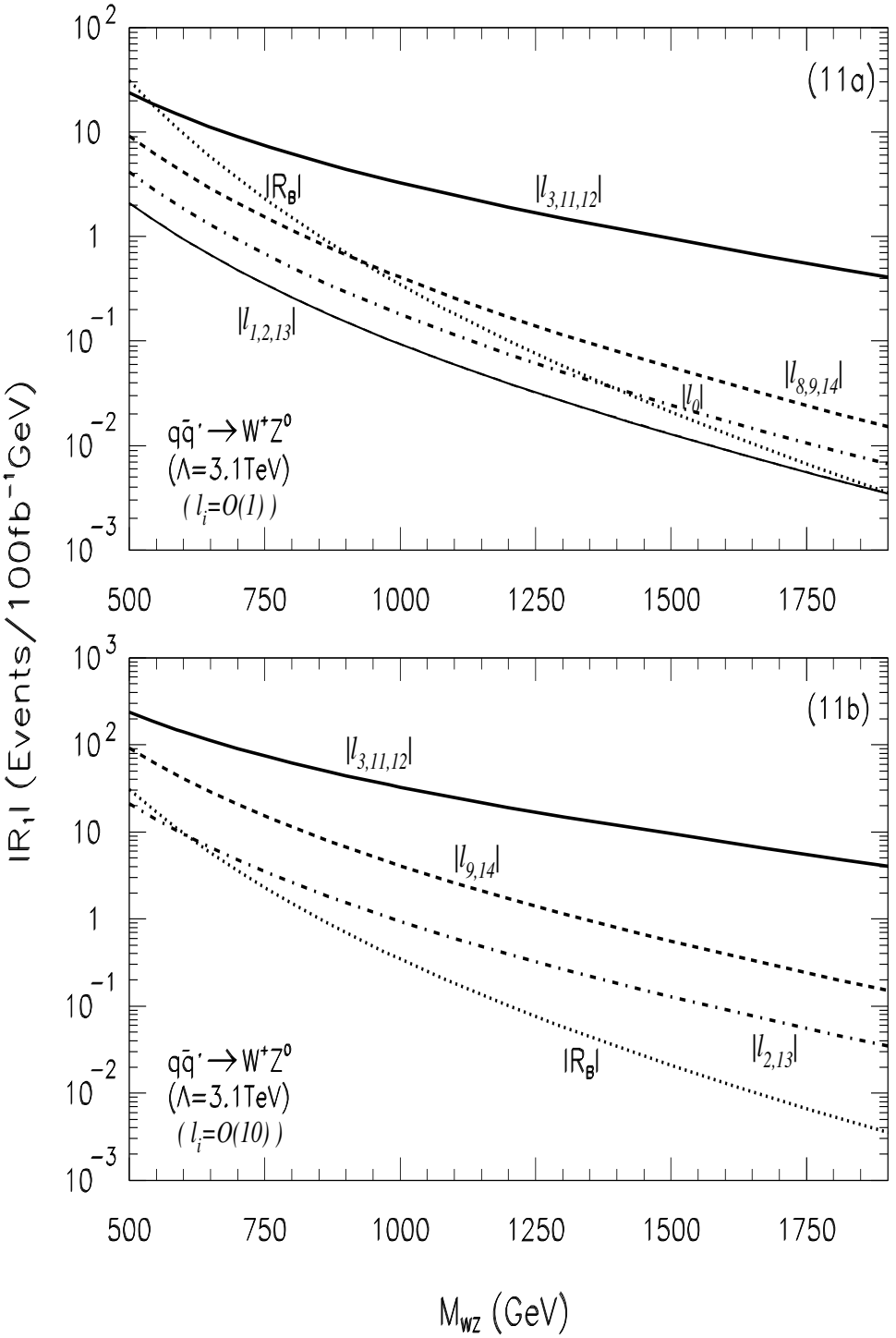
(11a)
$|R_B|$
$|l_{3,11,12}|$
$|l_{1,2,13}|$
$|l_{8,9,14}|$
$|l_0|$
$q\bar{q}' \to W^+Z^0$
$(\Lambda=3.1\text{TeV})$
$(l_i=O(1))$
(11b)
$|l_{3,11,12}|$
$|l_{9,14}|$
$|l_{2,13}|$
$|R_B|$
$q\bar{q}' \to W^+Z^0$
$(\Lambda=3.1\text{TeV})$
$(l_i=O(10))$
$|R_1|$ (Events/100fb^{-1}GeV)
M_{WZ} (GeV)

Fig. 11.

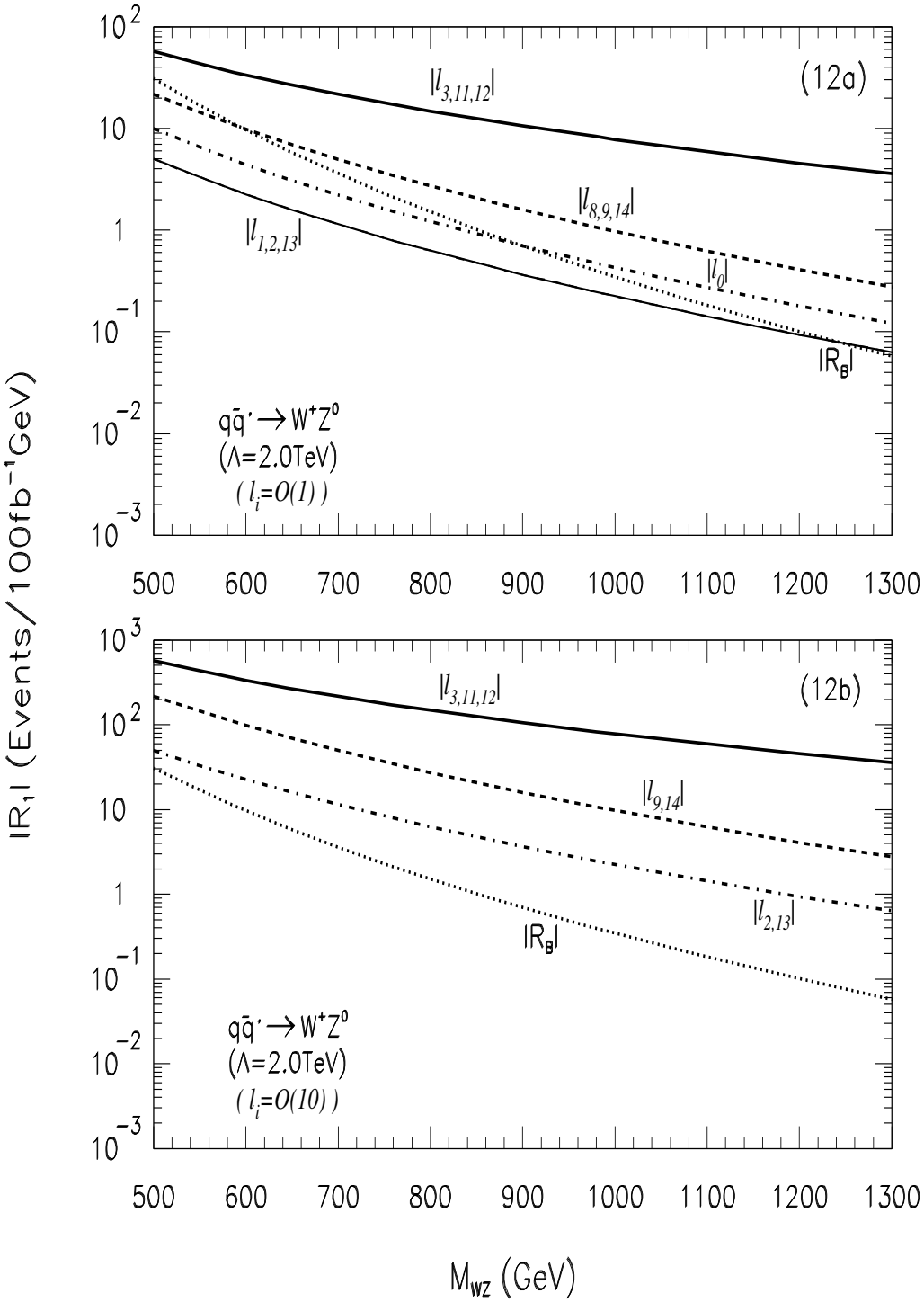
(12a)
$|l_{3,11,12}|$
$|l_{8,9,14}|$
$|l_{1,2,13}|$
$|l_0|$
$|R_B|$
$q\bar{q}' \to W^+Z^0$
$(\Lambda=2.0\text{TeV})$
$(l_i=O(1))$
(12b)
$|l_{3,11,12}|$
$|l_{9,14}|$
$|l_{2,13}|$
$|R_B|$
$q\bar{q}' \to W^+Z^0$
$(\Lambda=2.0\text{TeV})$
$(l_i=O(10))$
$|R_1|$ (Events/100fb^{-1}GeV)
M_{WZ} (GeV)

Fig. 12.